九州大学学術情報リポジトリ
Kyushu University Institutional Repository

SLOPE FAILURE HAZARD ASSESSMENT CONSIDERATION WITH SOIL DEPTH AND RAINFALL INFILTRATION

ヘンドラ, パチリ

https://doi.org/10.15017/1654851

出版情報：九州大学, 2015, 博士（工学）, 課程博士
バージョン：
権利関係：全文ファイル公表済

SLOPE FAILURE HAZARD ASSESSMENT CONSIDERATION WITH SOIL DEPTH AND RAINFALL INFILTRATION

HENDRA PACHRI

SLOPE FAILURE HAZARD ASSESSMENT CONSIDERATION WITH SOIL DEPTH AND RAINFALL INFILTRATION

A Thesis Submitted

In Partial Fulfillment of the Requirements

For the Degree of

Doctor of Engineering

By

HENDRA PACHRI

九州大学

to the

DEPARTMENT OF CIVIL AND STRUCTURAL ENGINEERING

GRADUATE SCHOOL OF ENGINEERING

KYUSHU UNIVERSITY

Fukuoka, Japan

January 6th, 2015

DEPARTMENT OF CIVIL AND STRUCTURAL ENGINEERING
GRADUATE SCHOOL OF ENGINEERING
KYUSHU UNIVERSITY
Fukuoka, Japan

CERTIFICATE

The undersigned hereby certify that they have read and recommended to the Graduate School of Engineering for the acceptance of this thesis entitled, "***Slope Failure Hazard Assessment Consideration with Soil Depth and Rainfall Infiltration***" by **Hendra Pachri** in partial fulfillment of the requirements for the degree of **Doctor of Engineering**.

Dated: January 6, 2015

Thesis Supervisor:

Prof. Yasuhiro Mitani, Dr. Eng.

Examining Committee:

Prof. Guangqi CHEN, Dr Sc.

Prof. Hideki Shimada, Dr Eng

TABLE OF CONTETS

Acknowledgement……ix
Abstract……..xi
CHAPTER 1: Introduction……..1
1.1 Background…….….1
1.1.1 Slope failures hazard assessment…….……4
1.1.2 GIS in Landslides Hazard Assessment…….…….…..……..5
1.1.3 Influence factor of slope failure hazard assessment…….……7
1.2 Research purpose…….…….9
1.3 Overview of this thesis……...……11
Reference
CHAPTER 2: Overview of Slope failure hazard assessment approaches….….15
2.1 Slope failure inventory based probabilistic approach……..…..16
2.2 Statistical approach…….….……..17
2.3 Deterministic approach…….….……18
2.3.1 One-dimensional model……..……..18
2. 3.2 Two-dimensional model……..…….18
2.3.3 Three-dimensional model……..……20
2.4 Application of GIS in landslide hazards assessment……..……21
2.4.1 GIS grid-based data model……..……..22
2.4.2 GIS-based Three-dimensional method of limit equilibrium Methods…….……..…….23
2.4.3 Verification of methods…….…..……..27
2.5 Influence factor in the 3D Slope stability analysis…….27
2.5.1 Soil depth…….….……27
2.5.2 Geotechnical aspects……....29
2.5.3 Rainfall…….……30
2.6 Summary……31
References
CHAPTER 3: Development of soil depth estimation in the catchment area….36
3.1 Introduction…….….36
3.2 Methodology…….……37
3.2.1 Concept of soil depth modelling……37
3.2.2 Data preparation…….…..37
3.2.3 Process based model to simulate of soil depth……..……38

3.2.4 ^{10}Be concentration analysis…….…….…….38
3.3 Case studies to a mountainous area…….….40
3.3.1 Soil depth investigation…….……40
3.3.2 Soil depth simulation…….……40
3.4 Validation of model…….……..40
3.5. Soil Depth Distribution…….….44
3.6 Conclusion……..47
References
CHAPTER 4: GIS-based 3D Analysis Method for Rainfall-induced Slope stability…….51
4.1 Introduction……51
4.2 GIS-based three-dimensional method of limit equilibrium method….. 54
4.2.1 Techniques for algorithms of GIS-based 3D model…….55
4.2.2 Validation of GIS-based 3D model…….……..58
4.3 Monte-Carlo simulation and evaluation of 3D stability…….…….58
4.3.1 Method of Monte-Carlo simulation……..…..58
4.3.2 Random variable for identifying 3 critical slip surface……..……59
4.3.3 identifying 3D critical slip surface with computational process....61
4.4 Slope-unit based regional slope stability evaluation…….…….62
4.5 Spatio-temporal estimation of shallow landslide hazard……..……...64
4.2.1 Homogeneous layer……..…….64
4.2.2 Multi layer……..……..…….64
4.2.3 Effect of rainfall……..…..…..66
4.5 Verification of results……..……77
4.6 Conclusions…….79
References
CHAPTER 5: GIS-based slope failure hazard analysis and prediction in Sangun Mountainous, Fukuoka Prefecture, Japan……82
5.1 Introduction……82
5.2 Study area and slope failure historical……83
5.3 Data preparation…….….84
5.3.1 GIS data creation…….……..84
5.3.2 Rainfall data…….….87
5.3.3 Slope units creation…….…..87
5.3.4 Geotechnical and infiltration parameters……..……88
5.4 Simulation process…….…….89

5.5 Results……..……90
5.5.1 Homogeneous layer……..……..90
5.5.2 Multi layer……..……..…..94
5.5.3 Rainfall effect……..….…..97
5.6 Discussions……..……..108
5.6.1 Slope failures characteristic in the catchment……..…108
5.6.2 Slope failure probability analysis by using a 3D slope stability tool on Sangun mountainous……..…110
5.6.3 Validation of slope failure probability……112
5.7 Conclusion……..…115
References
CHAPTER 6: Conclusions …….118
6.1. Conclusions…….118
6.2. Future work…….120

LIST OF FIGURES

Fig.1.1 Statistic about the occurrence of large landslides hazards in the world……..2
Fig.2.1 Method of landslides hazad assessment (P.leotti and R.Chowdhury,1999)……15
Fig.2.2 1D (infinite) slope and plane slip surface……18
Fig.2.3 Main section of 2D model with overlying soil mass subdivided into vertical Slices……19
Fig.2.4 Column-unit based 3D model……21
Fig.2.5 A slope failures mass and its abstracted GIS layers……24
Fig.2.6 3D view of landslide body and one grid-column……24
Fig.2.7 The model for the simply column-based 3D model……25
Fig.3.1 Sangun basin boundary and small studied catchment in the upstream part Which have been selected for soil depth investigations……..41
Fig.3.2 Spatial distribution of soil depth based on simulation of the soil production Rate (P_0)……..43
Fig.3.3 Root Mean Square Error (RMSE) values on validation. (a) N value=30; and (b) N value=50……44
Fig.3.4 Graph of distribution of soil depth based on soil production rate (P_0) valued during simulation……44
Fig.3.5 Soil depth distribution of the upper catchment of Sangun mountainous area…46
Fig.3.6 Relationship between of soil depth and topographic parameters in the Sangun mountainous. (a) Slope angle; and (b) A topographic curvature ($\nabla^2 Z$)……47
Fig.4.1 Getting the Z value of slip surface……56
Fig.4.2 The mechanism of GIS raster-based 3D model……57
Fig.4.3 Computational processes for min-3D safety factor……...57
Fig.4.4 Flow chart for getting slope unit by DEM……63
Fig.4.5 Interface of 3DSLOPE GIS for slope stability simulation (Xie, 2003)……64
Fig.4.6 Diagrammatic representation of effects of soil depth (h) on slope……65
Fig.4.7 Computational processes for min-3D safety factor of soil depth effect in

The slope stability analysis……66
Fig.4.8 Flowchart of infiltrated depth calculating during duration T of rainfall……70
Fig.4.9 The computational procedures for estimation of rainfall induced slope stability……71
Fig.4.10 Relationships between shear strength versus degree of saturation for two Soil samples (modified from Fredlund et al., 1996 in Montrasio et.al., 2008).73
Fig.4.11 Model1: slip surface form between the wetting front and the groundwater table……..74
Fig.4.12 Model2: slip surface forms between the ground surface and the wetting front……..75
Fig.4.13 Model3: slip surface forms under the groundwater table and the Unsaturated zone exists……..75
Fig.4.14 Model4: slip surface forms under the groundwater table……..76
Fig.4.15 An interface of system 3D slope GIS combining with hydrological model……..77
Fig.5.1 Sangun basin boundary (a) and small studied catchment in the upstream part (b) which have been selected for study area……84
Fig. 5.2. Morphology aspect in the 3D Slope stability analysis. (a) Elevation data (m); (b) Slope angle (º); and (c) Slope aspect……86
Fig. 5.3 Rainfall intensity in the Sangun Catchment area……86
Fig. 5.4 Distribution of Slope units in the study area……87
Fig. 5.5 Distribution of Safety factor values of the homogeneous layer based on friction angle (*Φ*) values……..92
Fig. 5.6 Distribution of Safety factor values of the homogeneous layer based on cohesion (*c*) values……..93
Fig. 5.7 Distribution of Safety factor values of the multi layer based on friction angle (*Φ*) value……..…95
Fig. 5.8 Distribution of Safety factor values of the multi layer based on cohesion (*c)* values……..……96
Fig. 5.9 Relationships between the number of slope unit <= 1.0 and a time of rainfall intensity based on cohesion values (c) =1 kN/m^2 and ; Ks=0.323 cm/h,

θ i=0.052, θ s=0.223, Matric suction = 8.8 cm,GWL= 5m……98
Fig. 5.10 Distribution of Safety factor values of the multi layer with rainfall effect and cohesion values (c) = 1 kN/m^2 ; Ks=0.323 cm/h, θ i=0.052, θ s=0.223, Ms=8.8 cm……..99
Fig. 5.11 Relationships between the number of slope unit <= 1.0 and a time of rainfall intensity based on cohesion values (c) =1 kN/m^{2}and ; Ks=0.323 cm/h, θ i=0.052, θ s=0.223, Matric suction = 8.8 cm, GWl=0m……100
Fig. 5.12 Distribution of Safety factor values of the multi layer with rainfall effect and cohesion values (c) = 1 kN/m^2 ; Ks=0.323 cm/h, θ i=0.052, θ s=0.223, Matric suction = 8.8 cm, GWl=0m……101
Fig. 5.13 Relationships between the number of slope unit <= 1.0 and a time of rainfall intensity based on cohesion values (c) =1 kN/m^{2}and ; Ks=0.669 cm/h, θ i=0.047, θ s=0.247, Matric suction =23.5cm, GWl=0m……102
Fig. 5.14 Distribution of Safety factor values of the multi layer with rainfall effect and cohesion values (c) = 1 kN/m^2 ; Ks=0.669 cm/h, θ i=0.047, θ s=0.247, Matric suction = 23.5 cm, GWl=0m……103
Fig. 5.15 Relationships between the number of slope unit <= 1.0 and a time of rainfall intensity based on cohesion values (c) =1 kN/m^{2}and ; Ks=0.980 cm/h, θ i=0.045, θ s=0.243, Matric suction =11.3 cm, GWl=0m……104
Fig. 5.16 Distribution of Safety factor values of the multi layer with rainfall effect and cohesion values (c) = 1 kN/m^2 ; Ks=0.980 cm/h, θ i=0.045, θ s=0.243, Matric suction = 23.5 cm, GWl=0m……105
Fig. 5.17 Relationships between the number of slope unit <= 1.0 and a time of rainfall intensity based on cohesion values (c) =1 kN/m^{2}and ; Ks=2.796 cm/h, θ i=0.039, θ s=0.285, Matric suction =6.0 cm, GWl=0m……106
Fig. 5.18 Distribution of Safety factor values of the multi layer with rainfall effect and cohesion values (c) = 1 kN/m^2 ; Ks=2.796 cm/h, θ i=0.039, θ s=0.285, Matric suction = 6 cm, GWl=0m……107
Fig. 5.19 Slope failure characteristic in the Sangun basin……..109
Fig 5.20 Relationships of cohesion (c), friction angle (Φ) values and number

of slope failures (%) based on the factor of safety (FS) of the slope stability simulation. (a) homogeneous layer with cohesion (*c*) values; (b) homogeneous layer with friction angle (*Φ*) values; (c)multi layer with cohesion values; (d) multi layer with friction angle (*Φ*) values……113

Fig. 5.21 Distribution of Safety factor values based on the type of layer. (a) homogeneous layer with cohesion (*c*) values; (b) homogeneous layer with friction angle (*Φ*) values; (c) heterogeneous layer with cohesion values; (d) homogeneous layer with friction angle (*Φ*) values…….110

Fig 5.22. Relationships between number of slope failure (%) that compared the slope failure probability with the number of rainfall time (hours) based on the infiltration parameters, the occurrence of groundwater level during on 3D slope stability simulation……111

LIST OF TABLES

Table 2.1 Usefulness of specific combinations of hazard approaches (Van Westen et al. 2006)……16

Table 3.1. Soil depth (m) measurement in the upstream part of Sangun catchment, Fukuoka Prefecture (2015)…….42.

Table 3.2. Soil depth distribution in the upper part of Sangun basin based on the simulation for N value = 30……..45

Table 4.1. The data components of system 3D slope GIS combined with infiltration model…….……..78

Table 5.1. Strength properties of soil in study area……..88

Table 5.2. Parameters λ and A for different types of soil……..88

Table 5.3. Changes in Soil properties by considering the organic materials in the surface (Tatsuro Sato, 2013)…….……..89

Table 5.4. Number of slope unit which safety factor <=1.0 based on cohesion (*c*) and friction angle (*Φ*) values for homogeneous layer…….89

Table 5.5. Number of slope unit which safety factor <=1.0 based on cohesion (*c*) and friction angle (*Φ*) values for multi layer (Soil depth effect)…….94

ACKNOWLEDGEMENT

The completion of my doctoral thesis is probably the most challenge of my doctor course. It would not have been possible to write this thesis without the help and support of the kind people around me, to only some of whom it is possible to give particular mention here.

First of all, I especially want to thank my advisor, Prof. Yasuhiro Mitani, for his guidance during my research and study at Kyushu University. His wisdom, perpetual energy and enthusiasm in research had motivated me. In addition, he was always accessible and willing to help me in my daily life. As a result, research life became smooth and rewarding for me.

I should be grateful to my gratitude Assistant professors Hiro Ikemi. He once gave me an opportunity to go to Tono Geoscience Center, Japan Atomic Energy Agency (JAEA) to further my research. During my doctoral course, he has given my many helps on the research of slope stability analysis.

I would like to thank and appreciate Prof. Guangqi Chen and Prof. Hideki Shimada for detailed checking of my doctoral thesis and for providing the valuable suggestions for revision.

Certainly, special thanks should be given to the members of Environmental Geotechnology Laboratory. The environment of the laboratory is so harmonious that I really enjoy my life in Japan.

Also, I would express my special thanks to my family. I can never thank enough to my mother and father for their unselfish nurturing and endless care. It is their continuous support and encouragement that let me concentrate on and complete this study.

Last, but not the least, I should thank my friends in Japan and elsewhere for their support and encouragement. I gained a lot from them, through their personal and scholarly interactions.

ABSTRACT

Landslides and debris flows are sources of severe natural disasters and societal hazard in mountainous regions throughout the world. Landslide and debris-flow are the main types of slope-mass movements when slopes fail. Therefore, landslide hazard assessment study, which is commonly used for hazard mitigation, should give answers to the three key questions: the magnitude, the location and the occurrence time of the dangerous process. However, so far, there are few reliable methodologies available for giving the answers. As mentioned above, the qualitative analyses are totally subjective and dependent on the experience of the earth scientist, can not assess slope stability quantitatively. Therefore, an easy implementation method of 3D analysis for practical issues is urgently required. Furthermore, 3D deterministic model should be applied to a wide mountainous area for the purpose of landslide hazard assessment with accurate prediction of the magnitude, the location and the occurrence time of the dangerous process. Concerning the occurrence time of slope failure, the trigger factors of the occurrence of landslide, such as soil depth and rainfall, should be taken into account. Therefore, the combining the 3D slope stability analysis with hydrological model ,which considering the cohesion model (Montrasio et al.2008) were conducted to define a correlation between the safety factor of the slope and the rainfall depth. Furthermore, the verification of the slope failure probability has been considered with slope failure in the past. The purpose of slope failure hazard evaluation are: (1) understand the development a GIS-aided methodology to implement the 3D limit equilibrium model in natural slope failure assessment; (2) to assess the soil depth by process based model as one of factor controlling the occurrence and distribution of shallow slope failure; (3) combine the 3D slope stability model with a infiltration model to evaluate the variation of slope stability during rainfall event; and (4) to predict and assess the stability of slopes under soil depth influenced and rainfall infiltration effect in Sangun mountainus area by combine the 3D slope stability model with a infiltration model.

In Chapter 1, some background knowledge about landslide hazard are described. Finally, the objective of this thesis is proposed. Three widely used landslide hazard assessment approaches: landslide inventory based probabilistic approach, statistical approach and deterministic approach are reviewed in Chapter 2. All these approaches are considered valid in certain contexts. Most of deterministic models are based on limit equilibrium approach for a one-, two-, or three-dimensional model. For natural slopes,

3D model is preferred because it considers the spatial distributions of slip body, stratum, and groundwater table. Moreover, the effect of rainfall in the slope stability analysis has to be considered.

In Chapter 3, a process based model analysis to simulate soil depths of mountainous area are introduced. The soil depth model simulations were carried out by utilizing Geographic Information System (GIS) function. Soil depth is one of the most important parameters for controlling shallow landslides. The easiest and most accurate way to measure soil depth is through field measurements. For large-scale areas, especially in mountainous areas, this method is not cost effective or practical as some places are not accessible. To overcome this difficulty, a process based model analysis is used to evaluate soil depths. The effectiveness of this method has been tested by applying it to Sangun mountainous area in Japan. The result shows a consistency between predicted soil depths and samples from field investigation. In the simulation, the third of soil production rate (*Po*) values, such as 0.019, 0.022, and 0.025 cm/yr had been used. Results from the simulation analysis indicated that topographic variables, soil production rate (*Po*), and a soil production time (year) provide the reasonable model for distribution of soil depth. Therefore, the soil depth ranged from 0.51 to 1m has the largest area of soil distribution.

In Chapter 4, the methodology of GIS-based 3D analysis for rainfall infiltration effect has been provided. Firstly, the homogeneous layer is considering to assume that the varying of the uncertainty of geotechnical parameter is important in the slope stability to get the best performance. Furthermore, I concern in the soil depth and rainfall effect in the analysis. Therefore, the combining of GIS-based 3D model and hydrological model are presented. Such as, saturation degree and matric suction of the soil texture has been used in the hydrological model. Furthermore, this model provide the effect of rainfall intensity on the slope failure probability.

In Chapter 5, aiming to apply 3D deterministic model with combining of hydrological model to a wide natural area for predicting the location of slope failure with soil depth and rainfall, a slope-unit-based evaluation method is given. The 3D Slope Stability Analysis for homogeneous and multi layers based on verification of the results will be conducted by considering the inventory slope failure in the past. As results, due to the cohesion (*c*) values gave the similar values in homogeneous and multi layers, therefore the cohesion value equal 1 kN/m2 gave a very reasonable performance compare to similar cohesion values performed by other cohesion values (47.27% for homogeneous layer and 72.73% for multi layer). Furthermore, the friction value of 25^0 is a reasonable performance in the both homogeneous and multi layers about 76.36%.

Furthermore, the effect of rainfall, there are five cases; (1) infiltration parameter for soil as weathered granitic rock and the occurrence of groundwater level (5m); (2) infiltration parameter for soil as weathered granitic rock and groundwater level (0m); (3) infiltration parameter for soil as weathered granitic rock +organic materials (10%) and groundwater level (0m); (4) infiltration parameter for soil as weathered granitic rock + organic materials (20%) and groundwater level (0m); and (5) infiltration parameter for soil as weathered granitic rock + organic materials (30%) and groundwater level (0m)

As results, the validation has been conducted in all cases. Therefore, the assuming of the groundwater level is 0m have been changed (case 2 to case 5). Furthermore, the result shows 89.09% the number of slope failure after 20h is good performance in the case 3.

In Chapter 6, conclusions of this thesis are summerized.

CHAPTER I

INTRODUCTION

1.1 Background

Landslides and debris flows are sources of severe natural disasters and societal hazard in mountainous regions throughout the world. Landslide and debris-flow are the main types of slope-mass movements when slopes fail. Slope failures have caused untold numbers of casualties and huge economic losses. In many countries, economic losses due to landslides and debris-flows are great and apparently are growing as development expands into unstable hillside areas under the pressures of expanding populations. Japan is blessed with rich natural environment. Such an environment, however, presents severe natural conditions. The mountainous and hilly areas make up 70% of the total land area of Japan. With a large number of steep terrains and geological weakness, the Japanese islands are vulnerable to slope-related (landslides and debris-flows) disasters caused by weather conditions like typhoons and localized torrential rain. Slope-related disasters caused by localized torrential downpours, earthquakes, volcanic eruptions, etc. occur frequently every year, and slope-related disasters account for about a half of the dead and missing by natural disasters.

The occurrence of large landslides hazards in the world (Fig. 1.1) based on the international disaster database produced by the Centre for Research on the Epidemiology of Disasters (http://www.emdat.be/) had been summarized (Jia.N, 2012). In the figure shows that in spite of improvements in recognition, prediction and mitigation measure, the oocurrence of landslides is increasing.

Physical scientists define a natural hazard either as the probability that a reasonably stable condition may change abruptly (Scheidegger, 1994), or as the probability of occurrence of a potentially damaging phenomenon within a given area and in a given period of time (Varnes, 1984). The latter remains the most widely accepted definitions for natural hazard and for maps portraying its distribution over a region. In many countries, the economic losses and casualties due to landslides are greater than commonly recognized and generate a yearly loss of property larger than that from any other natural disaster, including earthquakes, floods and windstorms.

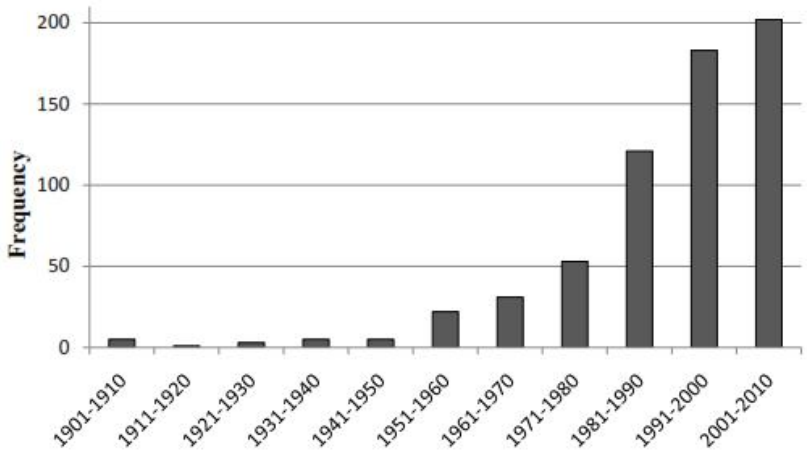

Fig.1.1 Statistics about the occurrence of large disasters hazards in the world

To address the landslide problem, governmental agencies need to develop a better understanding of landslide hazard and to make rational decisions on allocation of funds for management of landslide risk. However, it is widely accepted that the landslide problem is dominated by uncertainty. This uncertainty arises at all stages in the resolution of the problem, from site characterization to material property evaluation to analysis and design and consequence assessment (Morgenstern, 1997). Otherwise, most of countries, especially third world countries, have difficulty meeting the high costs of controlling natural hazards through major engineering works and rational land-use planning. Industrialized societies are increasingly reluctant to invest money in structural measures that can reduce natural risks. Hence, the new issue is to implement warning systems and land utilization regulations aimed at minimizing the loss of lives and property without investing in long-term, costly projects of ground stabilization.

Government and research institutions worldwide have long attempted to assess landslide hazards and risks and to portray its spatial distribution in maps. Within this framework, earth sciences, and geomorphology in particular, may play a relevant role in assessing areas at high landslide hazard and in helping to mitigate the associated risks, providing a valuable aid to a sustainable progress. Tools for handling and analyzing spatial data, *i.e.* Geographical Information System (GIS), may facilitate the application of quantitative techniques in landslides hazard assessment and mapping.

Landslide hazard evaluations are concerned with identifying critical

geological, material, environmental, and economic parameters that will affect the project, as well as understanding the nature, magnitude, and frequency of potential slope problems. A number of methods have now been developed. As example, Japan has sustained many recurring disasters in granitic areas following heavy rains, resulting in a total of nearly 1500 casualties over the last 70 years, including 20 in Hiroshima in 1999 and 11 in Yamaguchi in 2009 (Chigira et.al, 2011). All the proposed methods are based upon a few, widely accepted principles or assumptions (Varnes, 1984; Carrara *et al.*, 1991; Hutchinson, 1995), namely:

(a) Slope failures leave discernible morphological features; most of them can be recognized, classified, and mapped either in the field or through remote sensing, chiefly aerial photographs;

(b) Landslide is controlled by mechanical laws that can be determined empirically, statistically or in deterministic approach. Conditions that cause landslides directly or indirectly linked to slope failure, can be collected and used to build predictive models of landslide occurrence;

(c) The past and present are keys to the future. The principle, which follows from uniformitarianism, implies that slope failures in the future will be likely to occur under the conditions which led to past and present instability;

(d) Landslide occurrence in space or time, can be inferred from heuristic investigations, computed through the analysis of environmental information, or inferred from physical models. Therefore, a territory can be zoned into hazard classes ranked according to different probabilities.

Ideally, evaluation of landslide hazard and its mapping should derive from all of these assumptions. Failure to comply with them will limit the applicability of any hazard assessment, regardless of the methodology used or the goal of the investigation.

In the studies concerned about the mountainous area such as landslide hazard mapping, one important problem is the suitable selection of a study object, or mapping unit. Mapping units are portions of the land surface which contains a set of ground conditions which differ from the adjacent units across definable boundaries, and are assigned a unique hazard value, so they are the minimum meaningful spatial units in the analysis. At the scale of the analysis, a mapping unit represents domain that maximizes internal homogeneity and between-units heterogeneity. Various methods have been proposed to partition the landscape for landslide hazard assessment and mapping (Meijerink, 1988; Carrara *et al.*, 1995).

Selection of an appropriate mapping unit depends upon a number of factors, namely: the type of landslide phenomena to be studied; the scale of the investigation; the quality, resolution, scale and type of the thematic information required; the availability of the adequate information management and analysis tools; and the method used for evaluating the slope instability. Each technique for dividing the territory has advantages and limitations that can be enhanced or reduced choosing the appropriate hazard evaluation method. To evaluate the occurrence of slope failure in the future, the development of methods is important in this study.

1.1.1 Slope failures hazards assessment

Regarding landslide and debris-flow hazard assessment, many review articles exist, such as Hansen (1984), Varnes (1984), Einstein (1988, 1997), Anbalagan (1992), Fell and Hartford (1997), Hungr (1997), Leroi (1997), Chau et al. (2004), and Glade (2005). Landslide and debris-flow hazard mapping is very useful in estimating, managing and mitigating landslide hazard for a region. Ideally, a reliable debris flow hazard map should carry appropriate weights from historical landslide events, from geomorphological analysis, and from mechanical or dynamical analysis of slides, falls, and flows of the earth mass. Since all three aspects of hazard analysis involve a large amount of factual, geological and simulated data, the use of computer or information technology is crucial to the success of such analysis. Since the mid 1980s, Geographical Information Systems (GIS) have become a very popular technology for analyzing natural hazards, including landslides (Coppock, 1995, Carrasco, 2003). Some of these GIS-based hazard analyses focus on earthquake-induced landslides (e.g. Luzi et al. 2000), and some on rainfall-induced landslides (e.g. Miller and Sias, 1998). GIS analysis has also been proposed to produce rockfall hazard maps (e.g. Cancelli and Crosta, 1994). However, the reliability of the hazard analysis does not depend on which GIS software or platform is used but on what analysis method is employed (Carrara et al., 1999; Guzzetti et al., 2000). Therefore, various methods of analysis have been proposed by many different authors (e.g. Carrara et al., 1991; Dikau et al., 1996; Leroi, 1997; Guzzetti et al., 1999; Carrara et al., 1999; Guzetti et al., 2000; Dai and Lee, 2001, 2002a, b; Chau et al., 2004). One main limitation for all these analyses is that dynamics of debris flows or landslides has not been included in the hazard mapping.

While landslides have a significant impact, their importance is often under- estimated as the landslide damage is considered simply as a result of the triggering processes and thus is included in reports of other phenomena such as earthquakes, flood *etc.* (Schuster 1996). Actually, landslides are various types of gravitational mass movements of the Earth's surface that pose the earth-system risk; they are triggered by earthquakes, rainfall, volcanic eruptions and human activities. Landslides are multiple hazards, involving typhoons/hurricanes, earthquakes, and volcanic eruptions, and sometimes causing tsunamis. Therefore, landslide disaster reduction requires cooperation of a wide variety of natural, social, and cultural sciences.

Each year the importance of assessing, preparing for and mitigating the potential effects of natural hazards, including landslides, increases. In recent years, the assessment of landslide hazard has become a topic of major interests for both geoscientists and engineering professionals as well as for local communities and administrations in many parts of the world. The aims of landslide hazard evaluation are (Abramson 2002):

- To understand the development and form of natural slopes and the processes responsible for different natural features.
- To assess the possibility of landslides involving natural or existing engineered slopes.
- To assess the stability of slopes under short-term and long-term conditions.
- To analyze landslides and to understand failure mechanisms and the influence of environmental factors.
- To enable the redesign of failed slopes and the planning and design of preventive and remedial measures, where necessary.

1.1.2 GIS in Landslides Hazard Assessment

Currently, there are a large number of researches that analyze landslide hazards using GIS. These applications could be either statistic (Ayalew and Yamagishi 2005; Dai and Lee 2003; Ramani et al. 2011) or deterministic (Safaei et al. 2011; Van Westen and Terlien 1996; Xie et al. 2003). However it is found that most researchers are concentrated in using a statistic method to quantify the relationship between slope failure and influential factors while GIS performs regional data preparation and processing; only a few researches, using infinite slope model which allows for calculation of a safety factor for each pixel

individually to evaluate the stability of a specific-site slope, have been conducted into the integration of GIS and the deterministic model (Anbalagan 1992; Dai et al. 2002; Van Westen 1993). Although many engineers are familiar with GIS technology, they remain unaware of its analytical power and potential for wide and varied use. Since GIS enables more complex analysis of multiple data than can normally be achieved using conventional techniques, it is expected to incorporate a sophisticated engineering model into GIS (Qiu 2007).

In recent years, GIS with their excellent data format and spatial data processing ability, have attracted great attention in landslide and debris-flow disaster assessment. This is not only because the collection, manipulation, visualization and analysis of the environmental data on landslide and debris flow hazard can be accomplished much more efficiently and cost effectively in GIS, but also a GIS has the grid-based raster data which can be as the mesh of finite difference method. Esaki and Wang (2000) gave a try to use the grid cell as the column of the limit equilibrium method of slope stability analysis. Combining the GIS grid-based data with a column-based 3D slope stability analysis model, Xie et al. (2003, 2004a, 2004b, 2006) developed and improved a GIS-based 3D slope stability analysis and landslide hazard assessment. Wang et al. (2006) developed a two-dimensional depth-averaged numerical model to simulate the rainfall-induced debris flow. And as raster grid networks in GIS can be used as the finite difference mesh, the continuity and momentum equations are solved numerically using the finite difference method.

Analysis of landslide hazard requires evaluation of the relationships between various terrain conditions and landslide occurrences. GIS allows for the storage and manipulation of information concerning the different terrain factors as distinct data layers and provides many spatial analyse that are effective for landslide analysis. Thus, it is an excellent tool for landslide hazards mapping.

The advantages of GIS for assessing landslide hazards include the following:

- With the strong spatial data modelling and display abilities of GIS, it is easy and efficient to build and display a slope model under GIS environment. As example, a slope can be represented as a set of spatially distributed structures, such as surface elevation, strata, discontinuity layer, and groundwater table, among others.
- A much larger variety of hazard analysis functions becomes attainable. These functions include map overlay, reclassification, and some other

spatial analyse incorporating logical, interpolated, conditional, zonal, and neighbourhood operations. Because of the speed of calculation, complex functions requiring a large number of map overlays and table calculations become feasible (Soeters and Van Westen 1996).

- The input maps derived from field observations can be updated rapidly when new data are collected. Also, after completion of the project, the data can be used by others in an effective manner in the course of a landslide hazard assessment project (Soeters and Van Westen 1996).
- Currently, some main GIS software (e.g. ArcGIS or MapInfo) provides program kit for users. It is easy and convenient to customize specific modules for landslide hazard analysis under GIS environment.
- GIS can handle various data sources, such as CAD, database, GPS points, and aerial photos.

1.1.3 Influence factors of slope failure hazard assessment

Interpretation of future landslide occurrence requires an understanding of conditions and processes controlling landslides in the study area. Three physical factors-past history, slope steepness, and bedrock-are the minimum components necessary to assess landslide hazards. It is also desirable to add a hydrologic factor to reflect the important role which ground water often plays in the occurrence of landslides. An indication of this factor is usually obtained indirectly by looking at vegetation, slope orientation, or precipitation zones. All of these factors are capable of being mapped. Specific combinations of these factors associated with differing degrees of landslide hazards. The identification of the extension of these combinations over the area being assessed results in a landslide hazard map.

For landsliding, a conceptual confusion arises from the use of the same term, *landslide*, to address the natural phenomena. The wide spectrum of landslide phenomena and the complexity and variability of their interactions with the environment (both natural and human) make the acceptance of a single definition of landslide hazard unsuitable. A landslide is a mass downward movement of either rock or unconsolidated material. The movement is caused by gravity acting upon materials that are in an unstable state of equilibrium. Movement may be initiated by any change in conditions that upsets the temporary conditions. Three general types of landslides are most commonly encountered in civil engineering

works. They are movements involving surficial material, movements involving deep-seated soft soils, and movements involving rock strata. The conditions favoring movements are (1) changes in groundwater conditions; (2) presence of clay or shale that softens when wet; (3) structure; and (4) topography. Very large, fast-moving landslides (*e.g.* rock avalanches) are probably the most destructive and hazardous mass movements. Slow-moving, deep-seated failures rarely claim lives, but can cause high property damage. Fast-moving soil-slip-debris slows triggered by intense rainfalls are extremely destructive, causing widespread damage and casualties. Each type of slope movement poses a different threat and may require a separate assessment, based on distinct definitions of landslide hazard.

The former probability of the occurrence is mainly caused by the uncertainty of geotechnical parameters or geotechnical models. Due to a limited number of ground investigation boreholes, a limited number of shear strength and other geotechnical tests and the fact that no method of measurement is perfect, one major source of the uncertainty of parameters is the temporal variability of important parameters such as pore water pressure within a slope at different locations or depths and especially along a potential slip surface. Modeling uncertainties may relate to minor geological details and to assumptions inherent in concepts such as limit equilibrium. Neglecting the process of progressive failure in simulating slope performance also introduces an important uncertainty.

Hazard is often expressed as an annual probability of occurrence of an event such as slope failure; therefore the frequency of occurrence on a temporal basis must be considered. Alternatively, data concerning the frequency of failure events related to triggering agents may be considered, e.g. the return period of a rainstorm of a certain intensity and duration can be related to slope performance. Alternatively, frequency based on the concept of antecedent rainfall percentage exceedance time may be considered.

The recognition of uncertainties and frequency has led to the development of methods of analysis within a probabilistic framework while maintaining the basic geotechnical models. A number of approaches have been developed in recent years, which do not have a direct counterpart within a deterministic framework. These include methods for the assessment of the probability of a geotechnical system consisting of a number of elements or a number of possible modes of failure or both (Chowdhury, 1998; Dai *et al.*, 2002).

Probability of occurrence can be determined either directly from landslide record or indirectly by establishing the landslide-triggering threshold of the initiating agent and analyzing agent behavior. Since performance indicators of the deterministic method such as safety factor do not take into consideration the probability of landslide occurrence, to convert safety factor maps into failure probability maps use is made of the probability of the triggering event (time probability), as well as the variance of the input data (variable probability: the probability that the safety factor, based on the distributions of the input data, will be <=1). For the latter either Monte Carlo simulations (Hammond *et al.*, 1992) or mathematical error propagation methods (Burrough, 1986) can be used.

The stability of steep slopes in fine-grained soils is generally related to soil suction. Rainfall infiltration induces variation of pressure heads and a decrease in soil suction and consequently a decrease in shear strength and an increase in soil weight, causing slope failure (Fredlung and Rahardjo 1993; Wieczorek 1996).

1.2 Research purpose

Landslide hazard is defined as the probability of occurrence of a potentially damaging phenomenon within a given area and in a given period of time by Varnes (1984). The definition incorporates the concepts of *magnitude*, *geographical location* and *occurrence time*. The first refers to the "dimension" or "intensity" of the natural phenomenon which conditions its behavior and destructive power; the second implies the ability to identify the place where the phenomenon may occur; the third refers to the temporal prediction of the event. Therefore, landslide hazard assessment study, which is commonly used for hazard mitigation, should give answers to the three key questions: the magnitude, the location and the occurrence time of the dangerous process.

However, so far, there are few reliable methodologies available for giving the answers. As mentioned above, the qualitative analyses are totally subjective and dependent on the experience of the earth scientist, can not assess slope stability quantitatively. Due to lack of the concrete mechanics of the physical processes involved, the statistical approaches, being a kind of the quantitative method, are also difficult to identify the detailed items of landslides. In contrast, the deterministic models are based on physical laws of conservation of mass, energy or momentum, have ability to make the problems clear.

Once the slope geometry and subsoil conditions have been determined, the stability of a slope may be assessed using the deterministic methodologies. Most of them are based on the limiting equilibrium approach for a two-dimensional (2D) model. The results of the 2D analysis are usually conservative, and although more expensive, three-dimensional (3D) analysis tends to increase the accuracy of the result. Furthermore, it is well known that a 3D situation may become important in cases that the geometry of the slope and slip surface varies significantly in the lateral direction, the material properties are highly anisotropic, or the slope is locally loaded (Chang, 2002).

However, the applications of 3D stability models are generally limited to site-specific slopes, seldom been used for regional slope due to the difficulties in processing and managing a vast amount of complex information of natural slope and in creating 3D data for topography, strata, ground water through limited investigations. Even for site-specific slopes, practical application of 3D methods is still lacking. Currently, there are several computer programs commercially available for 3D slope stability analysis: 3D-PCSTABLE (Thomaz and Lovell, 1988), CLARA (Hungr, 1988), TSLOPE3 (Pyke, 1911), *etc.* The applicability and limitation of these computer programs have been reported by Stark and Eid (1998).

Therefore, an easy implementation method of 3D analysis for practical issues is urgently required. Also, 3D deterministic model should be applied to a wide mountainous area for the purpose of landslide hazard assessment with accurate prediction of the magnitude, the location and the occurrence time of the dangerous process. Concerning the occurrence time of slope failure, the trigger factors of the occurrence of landslide, such as soil depth and rainfall, should be taken into account.

In the present, some new technologies are essential. GIS, as a relatively new software tool for geotechnical engineers, has capabilities that range from convenient data storage to complex spatial analysis and graphical presentation. Combining the conventional geotechnical methodologies with GIS will significantly enhance the slope stability analysis. As the earlier study of this topic, Xie *et al.* (2003) proposed a GIS-based 3D slope stability analysis model which is derived from the Hovland's model (1977) in order to calculate the 3D safety factor within GIS, and further used this model for locating the critical slip surface in a large area by means of minimizing the 3D safety factor.

However, it is not enough if the model is only considered by geotechnical parameter, such as cohesion value and friction angle . Therefore, to extend the applicability of the deterministic model to regional scale, this thesis proposes a set of GIS integrated models to systematically evaluate landslide hazard at regional scale. It considers the influences of soil depth and rainfall infiltration, and is applied to assess stabilities of a natural slope. In this study, the combining the 3D slope stability analysis with hydrological model ,which considering the cohesion model (Montrasio *et al.*2008) to define a correlation between the safety factor of the slope and the rainfall depth.

Furthermore, the verification of the slope failure probability is important, and this study has been considered with slope failure in the past. Moreover, landslides often transform into debris flows at mountainous areas. To evaluate the consequence and the risk of landslide hazard to human society, the evidence of slope failure in the past is also used to evaluate inundation areas of debris flows triggered by landslides in the short time.

The purpose of slope failure hazard evaluation are: (1) understand the development a GIS-aided methodology to implement the 3D limit equilibrium model in natural slope failure assessment; (2) to assess the soil depth by process based model as one of factor controlling the occurrence and distribution of shallow slope failure; (3) combine the 3D slope stability model with a infiltration model to evaluate the variation of slope stability during rainfall event; and (4) to predict and assess the stability of slopes under soil depth influenced and rainfall infiltration effect in Sangun mountainous area by combine the 3D slope stability model with a infiltration model.

1.3 Overview of this thesis

For the above purpose, the following contents are included in this thesis:

Chapter 1 describes some background knowledge about landslide hazard. Then, it introduces the landslide hazard assessment. Finally, the objective of this thesis is proposed.

Chapter 2 reviews three widely used landslide hazard assessment approaches: Landslide inventory based probabilistic approach, statistical approach and deterministic approach. All these approaches are considered valid in certain contexts. Deterministic approach is used in this study because it provides the best quantitative information for landslide hazard assessment. Most of deterministic

models are based on the limit equilibrium approach for a one-, two-, or three-dimensional model. For natural slopes, 3D model is preferred because it considers the spatial distributions of slip body, stratum and groundwater table. Furthermore, the influence factor in the 3D slope stability analysis will be presented.

Chapter 3 introduces a proses based model analysis to simulate soil depths of mountainous area. The methods of simulating the distribution of soil depth by spatial. Soil depth is one of the most important parameters for controlling landslides. The easiest and most accurate way to measure soil depth is through field measurements. For large-scale areas, especially in mountainous areas, this method is not cost effective or practical as some places are not accessible. To overcome this difficulty, a process based model analysis is used to evaluate soil depths. All the terrain attributes that control soil depth are selected as influential factors. The effectiveness of this method has been tested by applying it to Sangun Mountainous of Japan. The result shows a consistency between predicted soil depths and samples from field investigation.

Chapter 4 provides the methodology of GIS-based 3D Slope stability analysis. We are concerned in the homogeneous and multi layers. Soil depth and rainfall effect are considered in the analysis. Landslides often take place in mountainous areas after intense rainfall. As the rainfall begins to infiltrate the slope, shear strength of the soil is reduced.

In **Chapter 5**, aiming to apply 3D deterministic model to a wide natural area for predicting the location of slope failure with soil depth and rainfall, a slope-unit-based evaluation method is given. The concept and the identifying method of the slope unit are explained. A probabilistic analysis that is used for zonation mapping is also presented. The 3D slope stability analysis for homogeneous and heterogeneous layers based on verification of the results will be conducted by considering the inventory slope failure in the past, which is presented in **Chapter 5**. And, finally, conclusions of this thesis are given in **Chapter 6**.

References

Abramson, L. W. (2002). "General slope stability concepts." Slope Stability and Stabilization Methods, L. W. Abramson, T. S. Lee, S. Sharma, and G. M. Boyce, eds., Wiley, Hoboken, NJ, 1-56.

Anbalagan, R. (1992). "Terrain Evaluation and Landslide Hazard Zonation for Environmental Regeneration and Land-Use Planning in Mountainous Terrain. " *Landslides, Vols 1 and 2*, 861-868.

Ayalew, L., and Yamagishi, H. (2005). "The application of GIS-based logistic regression for landslide susceptibility mapping in the Kakuda-Yahiko Mountains, Central Japan." *Geomorphology*, 65(1-2), 15-31.

Chigira M, Mohamad Z, Sian LC, Komoo I (2011). Landslides in weathered granitic rocks in Japan and Malaysia. Bulletin of the Geological Society of Malaysia 57, 1-6.

Chang, M. (2002). A 3D slope stability analysis method assuming parallel lines of intersection and differential straining of block contacts. Canadian Geotechnical Journal, 9: 799–811.

Chen, R.H. and Chameau, J.L. (1983). Three-dimensional limit equilibrium analysis of slopes. Geotechnique, 32(1): 31–40.

Chowdhury, R.N. (1998). Evolving geotechnical reliability assessment strategies towards.Invited expert paper, Special Volume on year 20th Geotechnics, AIT, Bangkok.

Dai, F. C., and Lee, C. F. (2003). "A spatiotemporal probabilistic modelling of storm-induced shallow landsliding using aerial photographs and logistic regression." *Earth Surface Processes and Landforms*, 28(5), 527-545.

Fredlung DG, Rahardjo H (1993) Soil mechanics for unsaturated soils. Wiley, New York.

Hovland, H.J. (1977). Three-dimensional slope stability analysis method. Journal of the Geotechnical Engineering Division, ASCE, 103(GT9): 971–986.

Hungr, O. (1988). CLARA: slope stability analysis in two or three dimensions. O. Hungr Geotechnical Research, Inc., Vancouver, B.C., Canada.

Leroi, E. (1996). Landslide hazard-risk maps at different scales: objectives, tools and developments. Proc. VII Int. Symp. Landslides, Trondheim, 1: 35–52.

Montrasio L, and R.Valentino (2008). A model for triggering mechanisms of

shallow landslides. Natural Hazards Earth System Sciences., 8. 1149-1159.

Morgenstern, N.R. (1997). Toward landslide risk assessment in practice. Landslide Risk Assessment, Cruden, D., Fell, R. (Eds.), Balkema, Rotterdam, pp.15–23.

Pyke, R. (1911). TSLOPE3: users guide. Taga Engineering Systems and Software, Lafeyette, Calif.

Ramani, S. E., Pitchaimani, K., and Gnanamanickam, V. R. (2011). "GIS based landslide susceptibility mapping of Tevankarai Ar sub-watershed, Kodaikkanal, India using binary logistic regression analysis." *Journal of Mountain Science*, 8(4), 505-517.

Safaei, M., Omar, H., Huat, B. K., Yousof, Z. B. M., and Ghiasi, V. (2011). "Deterministic rainfall induced landslide approaches, advantage and limitation." *Electronic Journal of Geotechnical Engineering*, 16 1619-1650.

Scheidegger, A.E. (1994). Hazards: singularities in geomorphic systems. Geomorphology, 10: 19–25.

Thomaz, J.E. and Lovell, C.W. (1988). Three-dimensional slope stability analysis with random generation of surfaces. Proceedings of 5th International Symposium on Landslides, 1:777–781.

Varnes, D. J. (1978). "Slope movement types and processes." Landslide: Analysis and Control, Special Report 176., R. L. Schuster and R. J. Krizek, eds., Transportation Research Board, National Research Council, National Academy Press, Washington, DC, 11-33.

Xie, M. W., Esaki, T., Zhou, G. Y., and Mitani, Y. (2003). "Geographic information systems-based three-dimensional critical slope stability analysis and landslide hazard assessment." *Journal of Geotechnical and Geoenvironmental Engineering*, 129(12), 1109-1118.

Van Westen, C. J. (1993). "Application of Geographic Information System to landslide hazard zonation." ITC, Enschede, The Netherlands.

Van Westen, C. J., and Terlien, M. T. J. (1996). "An approach towards deterministic landslide hazard analysis in GIS. A case study from Manizales (Colombia)." *Earth Surface Processes and Landforms*, 21(9), 853-868.

CHAPTER 2

OVERVIEW OF SLOPE FAILURES HAZARD ASSESSMENT APPROACHES

Overviews and classification of landslide hazard assessment approaches can be found in Aleotti and Chowdhury (1999), Carrara et al. (1999), Guzzetti et al.(1999) and Van Westen et al. (2006). There are a number of methods of landslide hazard assessment that have been developed as summarized in Fig. 2.1 (P.Aleotti and R. Chowdhury, 1999).

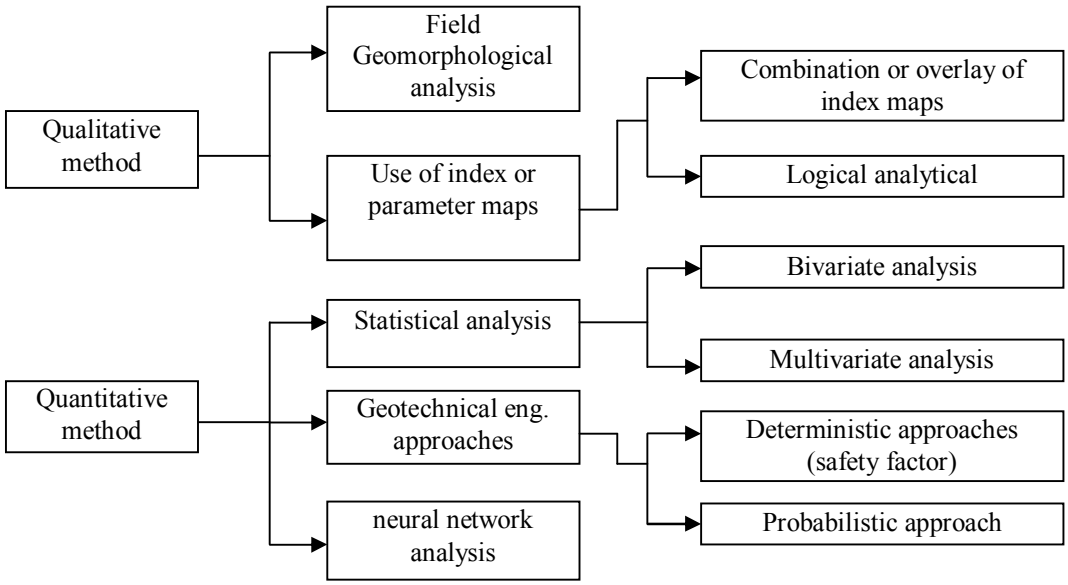

Fig.2.1. Methods of landslide hazard assessment (P.Aleotti and R.Chowdhury, 1999)

Broadly speaking, these approaches may be either qualitative or quantitative.Van Westen et al. (2006) gave an indication of the usefulness of particular hazard approaches based on the level of quantification, given that they are carried out over relatively large areas at medium scales (1:10,000-1:50,000) using GIS-based methods for risk zonation (Table 2.1).

The numbers in Table 2.1 have the following explanations:

- 0: The hazard method is not appropriate for the risk method.
- 1: Moderately useful combination. The hazard method is less appropriate for the risk method.
- 2: Highly useful combination. The hazard method could be the best method

for risk assessment, but this depends on the availability of data (e.g.,historical landslide records)

- 3: Most useful combinations, which will result in the best risk assessment given the available input data.

Table 2.1 Usefulness of specific combinations of hazard approaches (Van Westen et al. 2006)

Hazard approaches	Qualitative	Semi-quantitative	Quantitative
Inventory-based probabilistic approach	2	2	2
Heuristic/Geomorphological direct mapping/expert-based approach	3	3	0
Statistical approach (bivariate or multivariate)	3	2	2
Deterministic approach	0	1	3

2.1 Slope failure inventory based probabilistic approach

Landslide inventory maps are commonly prepared by collecting historical information on landslide events from field investigation and satellite images. National landslide inventory databases have been developed in several countries that suffer greatly from landslide hazards, for instance, Italy (Guzzetti 2000), China (Liand Wang 1992), U.S. (Harp and Jibson 1995; Killey et al. 1984) and Japan (The Japan Landslide Society 2012). They are elementary forms of susceptibility mapping and are generally the best methods for quantitative risk assessment because they emphasize the location and extent of recorded landslides.

However, the generation of landslide inventory maps and databases are tedious procedures. Landslides have to be mapped and described one by one, and each one might have different characteristics. In most countries, there is no single agency that has the responsibility for maintaining a landslide database. Even when such a map exists, it seldom gives adequate information on the type and characteristics of the slope failure. One way to overcome this problem is to complement the historic information with landslide interpretations from aerial photographs or satellite images. This would allow landslide inventory maps for fixed periods, related to the available imagery. However, for most of the mapped

landslides the exact date of occurrence remains unknown, thus making it difficult to correlate the landslide with a triggering event, especially as different landslide types have different meteorological triggers (Van Westen et al. 2006).

2.2 Statistical approach

Statistical approaches were developed to overcome the relatively high level of subjectivity related to expert evaluation which is used in heuristic approach (Fallet al. 2006). They involve the statistical assessment of combinations of factors that have caused landslides in the past. Quantitative or semi-quantitative estimates are then performed in areas not affected by landslides, but where the same conditions exist (Dai et al. 2002). Statistical methods are generally considered the most appropriate method for landslide susceptibility mapping at regional scales because they are objective, reproducible and easily updatable (Naranjo et al. 1994). They are usually integrated with GIS platform, as most of terrain indicator factors can be derived from DEMs of GIS.

Bivariate statistical analyses involve the idea of comparing a landslide inventory map with maps of landslide-influencing parameters in order to rank the corresponding classes according to their roles in landslide formation. Ranking is normally carried out using landslide densities (Lee et al. 2002). Multivariate statistical analyses of important causal factors controlling landslide occurrence may indicate the relative contribution of each of these factors to the degree of hazard within a defined land unit. A variety of multivariate statistical approaches emerged from the 1980s (Baeza 2001; Carrara 1983; Santacana et al. 2003) and remain important and widely used tools.

There are three drawbacks in statistical approaches:

- Indicator factors are selected by an expert or personal opinion and in most cases, they are simplified by taking only those that can be relatively easily mapped in an area or derived from a DEM.
- This method assumes that landslides happen under the same combination of conditions throughout the study area and through time, whereas in reality the environmental factors change continuously.
- Very few studies develop separate statistical models for different landslide types and most merge all active landslides together in one group which is used to generate statistical relations. Statistical landslide susceptibility assessment hardly ever takes the triggering factors into account.

2.3 Deterministic approaches

Deterministic, or physically based, approaches are based on physical laws of conservation of mass, energy or momentum. The main physical properties are quantified and applied to specific slope stability models. The input parameters include geometrical data, data on the shear strength parameters (cohesion and angle of internal friction), and information on pore water pressure. These parameters can be determined in the field or in the laboratory. Deterministic approaches provide the best quantitative information on landslide hazard which can be used directly in the design of engineering works or in the quantification of risk (Van Westen et al. 2006).

2.3.1 One-dimensional model

One-dimensional (1D) model, or infinite slope model, assumes that the slope is extended infinitely in all directions and sliding is assumed to occur along a plane parallel to the face of the slope (Taylor 1948) (Fig. 2.2). 1D model may be justified for shallow slope failure and also in some parts of a study area involving deep-seated failure. Such calculations can easily be performed in a GIS by calculating the stability of each individual pixel, and ignoring the influence of its neighbouring pixels (Van Westen et al. 1997). In a GIS environment only the 1D model with the slip plane parallel to the surface can be used efficiently for larger areas, as landslide models on the catchment scale, with complex or curved slip surfaces, are difficult to implement.

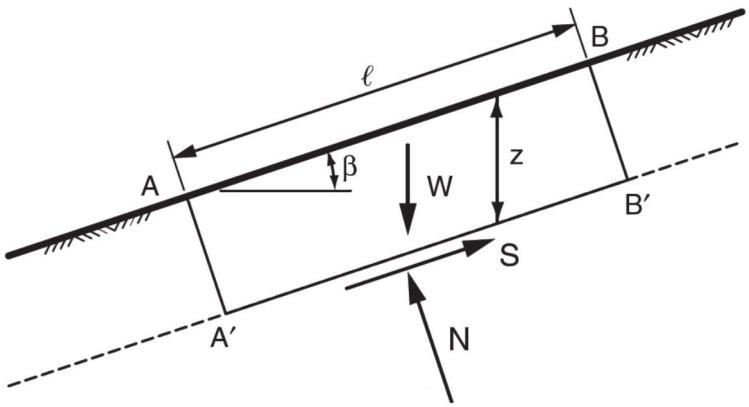

Fig. 2.2 1D (infinite) slope and plane slip surface

2. 3.2 Two-dimensional models

Two-dimensional (2D) model is called the method of slices. It studies the stability of the main section along slip direction (Fig. 2.3). The soil mass above

the slip surface is subdivided into a number of vertical slices. Some methods of slices assume a circular slip surface while others assume an arbitrary (noncircular) slip surface.

Methods that assume a circular slip surface consider the equilibrium of moments about the center of all slices. In contrast, the procedures that assume an arbitrary shape for the slip surface usually consider equilibrium in terms of individual slices. 2D model is widely used for artificial slope stability analysis because of artificial slope, the section maps along the lateral direction are almost the same, thus the slip body can be considered as infinitely sketched in the perpendicular direction of the main section.

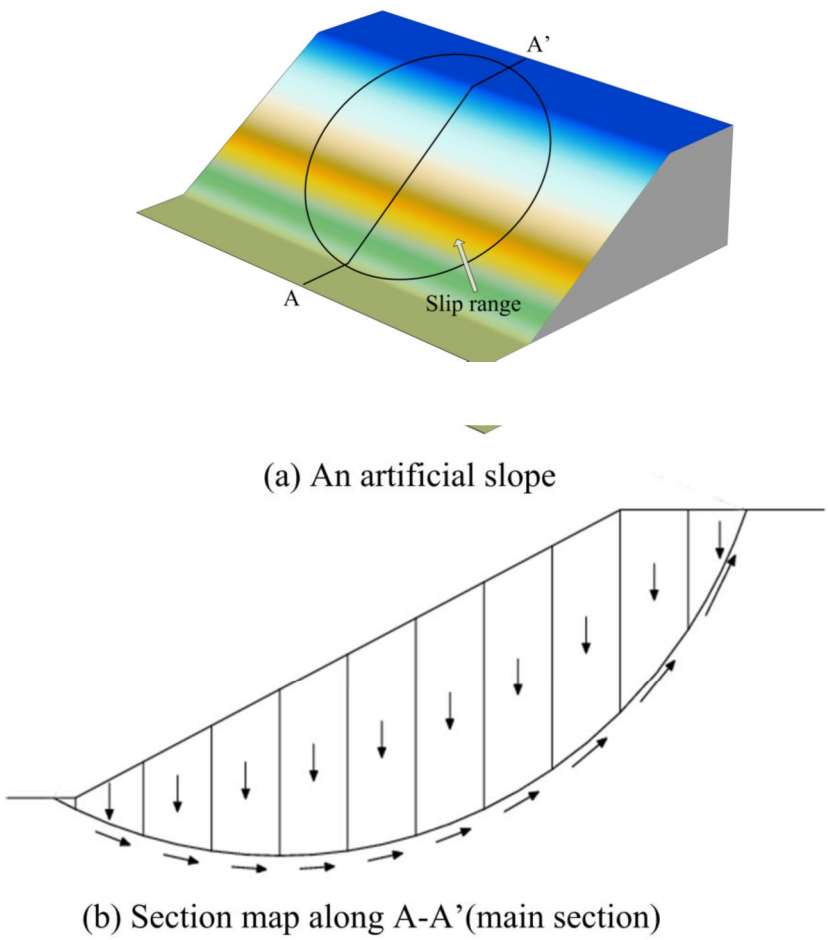

Fig. 2.3 Main section of 2D model with overlying soil mass subdivided into vertical slices

Various 2D methods have been made and employed in practice. Of all these 2D models, ordinary method of slices, Simplified bishop method, simplified Janbu method and Sarma method are widely adopted. 2D methods have become the most common methods due to their ability to accommodate complex geometries and variable soil and water pressure. However, 2D model is difficult to be integrated with GIS environment because its study object is section map, which is different from planar or three-dimensional (3D) map of GIS software.

2.3.3 Three-dimensional model

As mentioned above, 2D methods yield good results for artificial slope. For natural slope, the geometry of slip body, stratum and groundwater table are in 3D spatial distribution, which vary in space even along a short distance. But in 2D model, the slip body is assumed as infinitely stretched in the perpendicular direction of the main section. Therefore, the spatial distribution of slip body cannot be considered in 2D model. Moreover, the safety factor of 2D model is conservative because the shear resistance along the two sides of slip mass, end effects and lateral non-homogeneity are neglected. 3D model is thus preferred in the natural slope stability analysis.

A large number of 3D slope stability methods have been proposed since the late 1960s (Hovland 1977; Hungr 1987; Hungr et al. 1989; Lam and Fredlund 1993;Leshchisky and Huang 1992). Most of 3D methods are based on the column unit (Fig.2.4) and can be considered as a direct extension of corresponding 2D methods. For example, the 3D Janbu method keeps the same assumption with a 2D simplified Janbu method and extends the slide unit into the column unit. Because the entire slope related GIS data can be represented as grid-based data, it is possible that these column-based3D methods can be used for 3D stability analysis by using the GIS grid-based data.

In the next chapter, three 3D column-unit based 3D methods will be expanded. Their integration with GIS will be described in detail as well (Chapter 4).

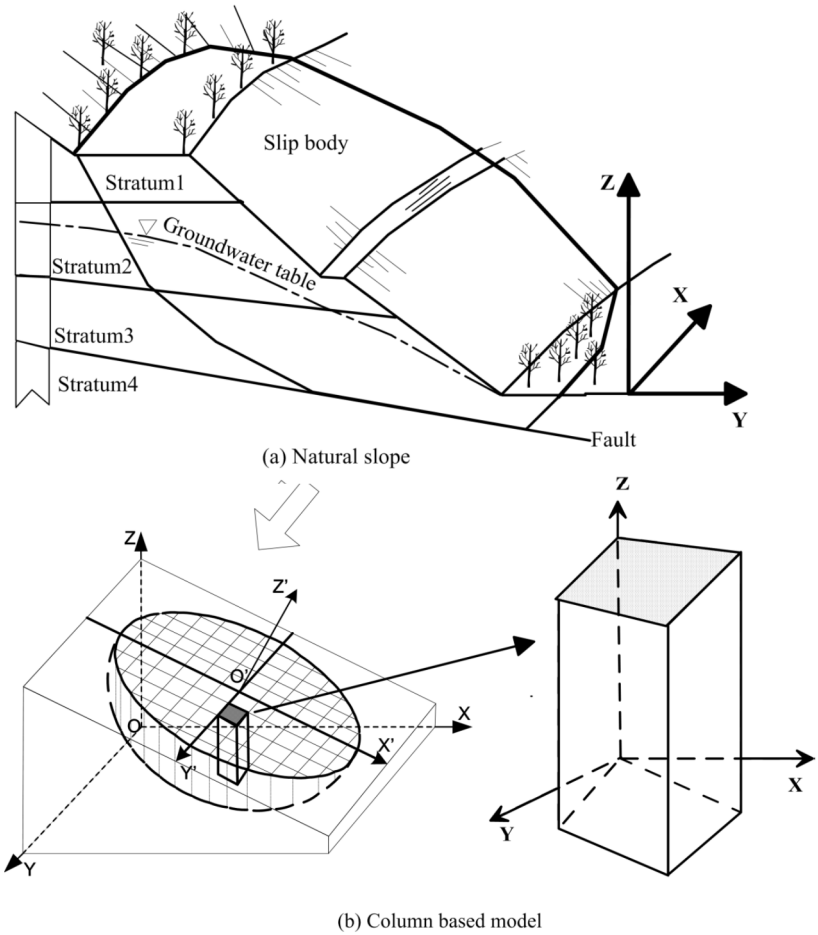

Fig. 2.4 Column-unit based 3D model

2.4 Application of GIS in landslide hazard assessment

From a survey of recent applications of GIS to slope stability analysis, it is found that most researchers have concentrated on using a statistical method to quantify the relationship between slope failure and influential factors, whereas GIS performs regional data preparation and processing. Very little research has been conducted into the integration of GIS and the deterministic model for slope stability (Carrara, 1983, 1995; Anbalagan, 1992; Van Westen and Terlien, 1996; Van Westen et al., 1997; Aleotti and Chowdhury, 1999; Dai and Lee, 2001).

The deterministic methods can be performed within or outside GIS. If the calculations are performed outside GIS, the system is only used as a spatial database for storing, displaying, and updating the input data. Data conversion can be a major problem because most programs have their own data format and data structure. Another disadvantage of using external models is the representation of

the results of the model calculations, in which the spatial data cannot be directly used and the results are not spatially distributed as in a GIS. To overcome the problem of data conversion, deterministic model calculations can be performed within a GIS component.

Coincidentally, most 3D limit equilibrium methods for slope stability analysis use column-based method in which the failure mass is divided into a number of small soil columns. Combining the grid-columns that derived from the overlay of GIS raster layers and the soil and rock columns that derived from discretization of the sliding mass, Xie et al. (2003a; 2003b; 2004a; 2004b; 2005; 2006a; 2006b) has developed and improved the GIS-based 3D limit equilibrium models for slope stability analysis.

2.4.1 GIS grid-based data model

Representation models describe slope-related objects such as strata, faults, groundwater, sliding surface, and ground surface, and these data models are easily and effectively managed by 3D slope models. Representation models created in GIS use a set of data layers. These data layers contain either raster or vector data. Vector GIS comprises three different geometry data types: points, lines and polygons. Each element can be described by many additional characteristics that are archived in the database comprising all GIS data. A raster GIS comprises raster layers where each layer represents certain information whose value forms the pixel value and is represented by the color of the pixel. All attributes are visualized in the form of raster layers, represented by a rectangular mesh or grid. Cells from various layers are stacked vertically and as such can describe numerous attributes at each location, while the raster data model uses single grid cells to represent single units with the same attributes. Ordinarily, the grid data format, with the same cell heights and cell widths, is used to represent slope-related data and information such as ground elevations, strata, faults, weak discontinuities, groundwater, and the cohesion and friction angles of soil or rock.
Based on the Mohr-Coulomb criterion, the 3D safety factor of a slope failure mass can be calculated from the available shear strength and the required shear strength present along the slip surface:

$$SF_{3d}=\frac{\tau available}{\tau required} \tag{2.1}$$

Equation (2-1) can then be mathematically calculated using an integration

formula:

$$SF_{3d}=\frac{\iint fR(x,y)dxdy}{\iint fs(x,y)dxdy} \quad (2.2)$$

where, $fR(x,y)$ is the available shear strength function and $fs(x,y)$ is the required shear strength slip surface. Because the functions of sliding force, normal stress and even the water pore pressure along on the slip surface cannot be clearly obtained, this integration formula is always calculated by an approximation using a different formula:

$$SF_{3d}=\frac{\sum_x\sum_y f_R(x_i,y_i)}{\sum_x\sum_y f_S(x_i,y_i)} \quad (2.3)$$

It is already known that the slope-related data can be expressed using the grid-based GIS data (raster data form). With this in mind, a grid-based 3D model can be used for calculation of the slope safety factor if a column-based 3D model is used. For a genuine slope failure mass, as shown in Fig. 2.5, using the functions of GIS spatial analysis, all input data involved in the 3D safety factor calculation can be made available for each grid cell, while all slope-related data are in the grid-based form. By inputting these data into a deterministic model of slope stability, a value for the safety factor can be calculated. A 3D grid-column, corresponding to each grid cell, is used to represent all the strata data, ground surface, and slip surface that represents all the geomorphologic and geological engineering information included in each 3D grid-column unit (Fig. 2.6). It is now generally accepted that all GIS using the spatial analyst function. This grid data model is used for slope stability in this study.

2.4.2 GIS-based three-dimensional method of limit equilibrium methods

The column-based method has been widely used for developing 3D models of slope stability analysis. Based on the force equilibrium or moment equilibrium equations, various limit equilibrium solutions have been proposed.

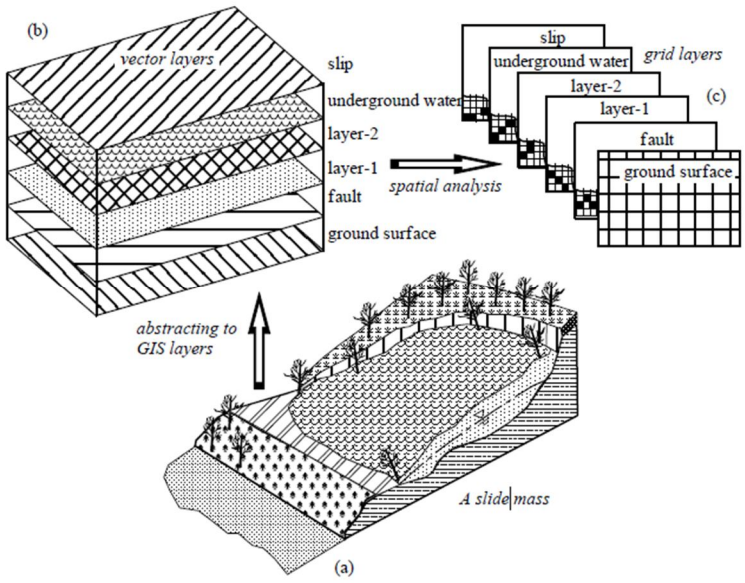

Fig. 2.5 A slope failure mass and its abstracted GIS layers.

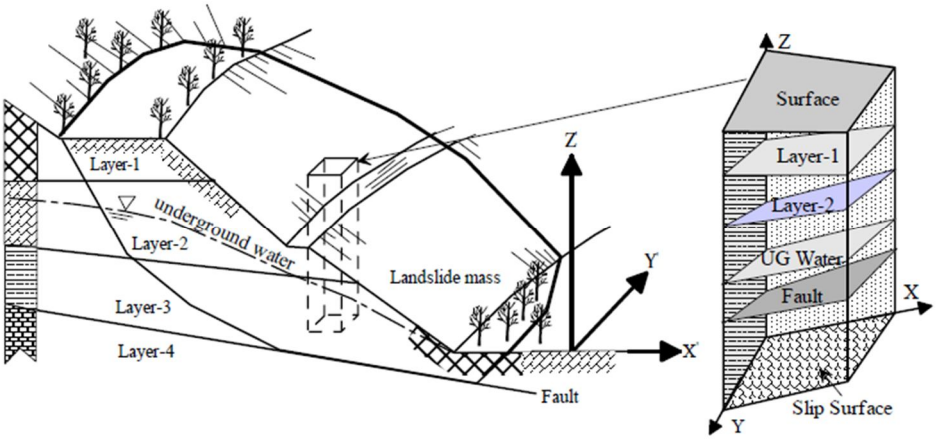

Fig. 2.6 3D views of landslide body and one grid-column.

The vast nature of the slope-related data and the degree of complication of the 3D slope problem algorithms means that each method of achieving a 3D limit equilibrium is based on different data formats and computational implementations; consequently, each individually developed 3D model (and even its related software) remain difficult to use for engineers. The users and engineers seldom have the opportunity to conduct a comparative study using different 3D models. A common data format and platform for assessing 3D slope stability is

therefore a very welcome aspect. The following four columns-based 3D models are developed to the GIS-based models in terms of 3D slope stability analysis, with all models based on a common data format and platform.

a. Hovland's column-based model

In this model, the stability of a landslide is related to geological information, geomorphologic aspects, geomechanical parameters and hydraulic conditions. The discretization of the study range to the small soil (or rock) column, as shown in Fig.2.7, allows all of the slope-related data to be illustrated, as shown in the 3D view of one column in Fig.2.6. Assuming that the vertical sides of each pixel column are frictionless, the equation for the 3D safety factor can be deduced.

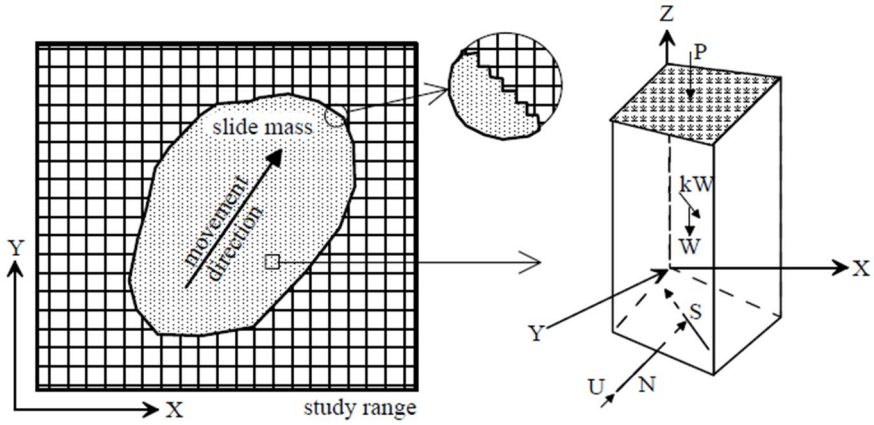

Fig. 2.7 The model for the simply column-based 3D model.

The equation of Hovland's model can be expressed using resistant and sliding forces along the slip surface:

$$SF_{3d} = \frac{\sum_J \sum_I \{c'A + [(W+P)\cos\theta - U]\tan\phi'\}}{\sum_J \sum_I [(W+P)\sin\theta_{Avr} + kW] - E} \tag{2.4}$$

Where SF_{3d} is the 3D slope safety factor, W is the weight of one column, A is the area of the slip surface, c' is the effective cohesion, ϕ is the effective friction angle, θ is the dip (the normal angle of the slip surface), J,I are the row and column numbers of the grid in the range of slope failure (in this study a polygon feature will be used to confine the boundary of the slide mass), P is the pore pressure acting on the slip surface of each column, k is the vertical force acting on each column (the distributed force of the upper load), k is the horizontal earthquake acceleration factor, and E is the result for all the horizontal

components of the applied point loads; the reinforcement force can be considered in this force because all forces refer to the slip surface and consideration of earthquakes and horizontal loads becomes problematic.

Without GIS, performing a 3D safety factor calculation based on this column-based model would be a tedious and time-consuming task, and data renewal or a multi-case study would be inconvenient. However, within the GIS system, using the GIS spatial analysis function, the slope stability-related data of the entire study area can be represented in the term of the GIS vector layers, as shown in Fig. 2.5. For each layer, a grid-based layer can be obtained using the GIS spatial analysis function, and the grid size (cell size) can be set at the required precision.

When calculating the 3D safety factor of a slope by equation (2-4), the following equations are necessary:

W is the weight of each grid-column, which can be calculated with reference to Fig. 2.3:

$$W=d^2\sum_{i=1}^{n} hi\gamma i \qquad (2\text{-}5)$$

where, d is the grid size of the grid-column, i=1,…., n is the stratum number, and hi, γi, is the height and unit weight, respectively, of each stratum.

P is the vertical force acting on each column, which can be calculated using the vertical stress p, while the vertical load produced by building load can be considered in p,

$$P=d^2p \qquad (2\text{-}6)$$

U is the pore pressure acting on the slip surface of each column, which is calculated using the pore stress along the slip surface: u

$$U= Au \qquad (2\text{-}7)$$

By now, it is clear that using the slope-related GIS grid layers and the cohesion and friction angles of the slip surface alone (these two parameters can also be represented by the grid layers, in which the spatial distribution of the parameter uncertainty can be addressed), the 3D safety factor can be calculated using equation (2-4). If not explicitly stated otherwise, the notation in the following section is the same as that used in this model. The four 3D slope models addressed in this paper are based on the unified data format, according to the GIS dataset.

b. Revised Hovland's model

This model is based on the same assumption as that used in Hovland's model. The basic algorithm is based on previous research, in which the external and seismic loads were the subjects of evaluation. Using the grid database concerning the surfaces, strata, groundwater, faults and slip surfaces, and a GIS grid-based equation, all the resistant and sliding forces refer to the possible sliding direction, but not necessarily the *Y* axis direction that was used in Hovland's model.

$$SF_{3d} = \frac{\sum_J \sum_I \{c'A + [(W+P)\cos\theta - U]\tan\phi'\}\cos\theta_{Avr}}{\sum_J \sum_I [(W+P)\sin\theta_{Avr}\cos\theta_{Avr} + kW] - E} \tag{2.8}$$

The calculation involved in converting the coordinate system to a sliding direction ('*X*) is represented by the following equation:

$$\begin{Bmatrix} x' \\ y' \end{Bmatrix} = \begin{bmatrix} \cos(AvrAsp-90) & -\sin(AvrAsp-90) \\ \sin(AvrAsp-90) & \cos(AvrAsp-90) \end{bmatrix} \begin{Bmatrix} x \\ y \end{Bmatrix} \tag{2.9}$$

In the Bishop and Janbu 3D extension models, the safety factor (SF_{3d}) is implicit in the equilibrium equations; the SF_{3d} is therefore calculated using an iterative procedure.

Here, the Newton iterative method is used to solve the SF_{3d}. For the root of $SF_{3d}=f(SF_{3d})$, the approximate root after *k* times iteration is

$SF_{3d}^{(k+1)}=SF_{3d}^{(k)}-(f(SF_{3d}^{(k)}) - SF_{3d}^{(k)})/(f'(SF_{3d}^{(k)})-1)$

2.4.3 Verification of the methods

Combining the GIS grid-based data with four proposed column-based 3D limit equilibrium slope stability analysis models, the new corresponding GIS grid-based 3D deterministic models have been devised for evaluating the slope stability by Xie et al. (2003a, b; 2004a, b; 2005a; 2006a, b). Applications of this method have verified that it is useful and effective, and is very convenient for data preparation and results display (Xie et al., 2005a, b, c).

2.5 Influence factor in the 3D Slope stability analysis

2.5.1 Soil depth

Shallow landslides and debris flows are dangerous phenomena responsible for a large number of casualties and economic losses (Schuster and

Fleming 1986; Crosta 1998; Catani et al. 2005; Montrasio et al. 2009). Many efforts have been made to develop process-based models in order to assess slope stability at basin scale (Guzzetti et al. 1999,2008). However, when trying to predict or model shallow landslides in a distributed way over large areas, one of the main problems is not the stability model itself, but the uncertainty in the spatial variability of the input parameters (Khazai and Sitar 2000; Savage et al. 2004; Guzzetti et al. 2007). There is a large agreement on considering soil thickness as one of the most important factors controlling shallow landsliding (Johnson and Sitar 1990; Wu and Sidle 1995; Van Asch et al. 1999; Dietrich et al. 2008).

Therefore, attention should be paid in choosing the right criterion to enter this parameter in basin scale slope stability models. To enter soil thickness in basin scale models, many authors rely on a straightforward and simplistic solutions such as considering a spatially constant value in the whole studied area (Khazai and Sitar 2000; Savage et al. 2004), using soil thickness classes (Revellino et al. 2008), assigning a constant value for each geological formation encountered on the analyzed site (Savage et al. 2004) or deriving a distributed soil thickness map from a single known topographic attribute such as the elevation (Saulnier et al. 1997) or the slope gradient (De Rose 1996; Salciarini et al. 2006). Soil properties vary spatially even within homogeneous layers as a result of depositional and post depositional processes that cause variation in properties (Lacasse and Nadim, 1996). Nevertheless, most geotechnical analyses adopt a deterministic approach based on single soil parameters applied to each distinct layer. The conventional tools for dealing with ground heterogeneity in the field of geotechnical engineering have been applied under the use of safety factors and by implementing local experience and engineering judgment (Elkateb et al., 2002).

Accordingly, numerous studies have been undertaken in recent years to develop a probabilistic of slope stability that deals with the uncertainties of soil properties in a systematic manner (Alonso, 1976; Vanmarcke, 1977b; Li and Lumb, 1987; Christian et al., 1994; Griffiths and Fenton, 2004). Detailed reviews of these studies can be found in Mostyn and Li (1993), El-Ramly et al. (2002), and Baecher and Christian (2003).

Unfortunately, probabilistic slope stability analysis methods do not consider all of the components of slope design where judgment needs to be utilized and they also do not suggest the level of reliability that should be targeted

(D'Andrea, 2001). However, working within a probabilistic framework does offer the advantage that the reliability of the system can be considered in a logical manner. Thus, probabilistic models can facilitate the development of new perspectives concerning risk and reliability that are outside the scope of conventional deterministic models.

2.5.2 Geotechnical aspects

A landslide starts as a consequence of terrain is not stable, and for this reason it is important in geotechnical practice to ascertain the stability conditions of soils or rocks. Owing to the significance in the prevention of disasters, slope stability has been the subject of much effort. There exist numerous numerical models, textbooks, and computer programs for assessing the stability on different kinds of terrain.

Gravity would tend to flatten out slopes, if it was not for the cohesion and friction forces of rocks and soils. However, the stability conditions may change due to temporary adjustments of equilibrium or because of external perturbations. In this case, a landslide may be triggered. There are numerous books and articles on slope stability. Here only a few basic examples are discussed to illustrate stability problems without any pretense of completeness.

The stability of a slope depends on several factors:

1. The kind of material involved. For example, recent volcaniclastic material may become very unstable and collapse into debris flows and lahars following intense precipitation. In contrast, a hard and compact rock like intact gneiss is normally very stable.
2. The geometry of the material. Layers of rocks dipping toward slope are particularly unstable (Fig. 2.3). The slope angle is another important variable. The Frank landslide in Canada was probably due to instability along a bedding plane (Cruden and Krahn, 1973).
3. The distribution of weight along slope. Loading the top of a slope may have great influence on stability. Likewise, cutting the slope at its base diminishes the buttressing of the lower layers underneath and promotes sliding conditions. This was particularly evident with the Betze-Post mine, where a mass of 3–10Mm^3 of unconsolidated deposits showed a slow creep of some cm/day. Transferring some of the material from the top of the heap to the foot proved of immediate effect in diminishing the creep

rate (Rose and Hungr, 2007).

4. Water is one of the most important instability factors. It decreases cohesion in soils and increases weight and pore water pressure in granular media. The rate at which water seeps into to the slope may also be critical. Some slopes may become unstable if even small amounts of water penetrate fast; others are more sensitive to the amount of water fallen in a long time span.

2.5.3 Rainfall

Rainfall-induced shallow landslides, also called "soil slips", are becoming ever more frequent all over the world and are receiving a rising interest in consequence of the heavy damage they produce. Hazard assessment of shallow landslides represents an important aspect of land management in mountainous areas. The analysis and forecast of temporal and spatial distribution of shallow landslides represent meaningful aspects of land management in mountainous areas. Shallow landslides (soil slips) are characterized by small thickness (0.3–2 m) and small scar areas (Campbell, 1975; Moser and Hohensinn, 1983; Ellen, 1988, Crosta, 1998). They are mainly triggered during intense rainfall events by the rapid growth of pore pressure (Sidle and Swanston, 1982) or by the loss of the component of apparent cohesion (Fredlund, 1987). As a result, a failure surface developments within the soil profile or at the contact with the underlying bedrock.

Through a transformation that can be due to liquefaction and dilatancy (Ellen and Fleming, 1987) the slipped mass evolves in a debris flow, that propagates downward eroding transport channels and increasing the volume of moving mass (Ellen, 1988, Crosta, 1998; Wieczorek et al., 2000). Factors controlling the occurrence and distribution of shallow landslides can be divided into two categories (Wu and Sidle, 1995): the almost-static variables and the dynamic variables. The almost-static variables, like soil properties (thickness, permeability and mechanical characteristics), seepage in the bedrock and topography (elevation, slope, areas of convergence and divergence, etc.), contribute to the definition of the susceptibility of the slopes to failure and they define the spatial distribution of the landslides. The dynamic or transitory variables, like the degree of saturation of the soil and the cohesion due to the presence of the roots and/or to partial saturation, control the triggering of failures

along susceptible slopes. Climatic and hydrological processes and human activities control dynamic variables, and they characterize the temporal pattern of landslides.

The shallow landslide hazard assessment requires an evaluation both of the susceptibility of the territory to fail and of the probability of occurrence of the phenomena in time. Many methods for landslide susceptibility assessment have been proposed, namely: empirical evaluation of susceptibility of slopes to instability on the basis of geomorphological evidences (Brundsen et al., 1975; Humbert, 1977; Kienholz et al., 1978); statistical analysis (bivariate or multivariate) of the factors presumably responsible for landsliding (Brabb et al., 1984; Carrara, 1983; Yin and Yan, 1988; Bonham-Carter, 1990); analysis of the probability of failure with stability models based on stochastic hydrological simulations (Hammond et al., 1992). All these methodologies can be considered valid in certain contexts for some applications. None of them, however, expressly takes into account the dynamic variables of the system as well as their short time and long-time behavior. This variability is considered by physically based mathematical models that explicitly incorporate the dynamic variables. Different models have been developed to describe how landslide triggering depends on dynamic variables as hydrological conditions and land use changes (Montgomery and Dietrich, 1994; Wu and Sidle, 1995; Borga et al., 1998; Pack et al., 1998). These models are based on the coupling of the infinite slope stability analysis with hydrological models able to modulate water table heights in steady or quasi-steady conditions with groundwater flows parallel to the slope. The assumptions of these models are too restrictive under certain conditions. For example, pore water pressure in hillslopes responds very rapidly to transient rainfall, and the pressure redistribution includes a large component normal to slope. In order to overtake these limitations, Iverson (2000) has recently developed a flexible modelling framework, with different approximations of Richards (1931) equation valid for varying periods of time and for different hydrological conditions.

2.6 Summary

The following are the summaries of chapter 2:

- The advantages of 3D limit equilibrium methods are deterministic methods, column-based methods, and easy to use GIS data。

- To overcome the problems related to the combining of infiltration model and 3D slope stability analysis, deterministic model calculations can be performed entirely within the GIS.
- A GIS based methodology to standardize the conventional column based 3D models into a uniform framework.
- A Monte Carlo technique by minimizing the 3D safety factor through an iterative procedure is available in the simulation。
- A methodology of slope unit for realizing application of 3D deterministic model in wide natural slope area is needed to perform of the analysis

References

Aleotti, P., and Chowdhury, R. (1999). "Landslide hazard assessment: summary review and new perspectives." *Bulletin of Engineering Geology and the Environment*, 58(1), 21-44.

Baeza, C. C., J. (2001). "Assessment of shallow landslide susceptibility by means of multivariate statistical techniques." *Earth Surface Processes and Landforms*, 26, 1251- 1263.

Carrara, A. (1983). "Multivariate methods for landslide hazard evaluation." *Mathematical Geol*, 15 (403-426).

Carrara, A., Guzzetti, F., Cardinali, M., and Reichenbach, P. (1999). "Use of GIS technology in the rediction and monitoring of landslide hazard." *Nat Hazards*, 20 (2-3), 117-135.

Casadei M, Dietrich WE, Miller NL (2003) Testing a model for predicting the timing and location of shallow landslide initiation in soil-mantled landscapes. Earth Surf Proc Land 28(9):925–950

Cruden, DM & Krahn,J. 1973. A reexamination of Geology of the Frank Slide. Can. Geotech J. 35: 299-311

Catani, F., Segoni, S., and Falorni, G. (2010). "An empirical geomorphology-based approach to the spatial prediction of soil thickness at catchment scale." *Water Resources Research*, 46(5), art. no. W05508.

Catani F, Casagli N, Ermini L, Righini G, Menduni G (2005) Landslide hazard and risk mapping at catchment scale in the Arno River basin. Landslides 2:329–342

Crosta, G. B., and Agliardi, F. (2002). "How to obtain alert velocity thresholds for large rockslides." *Phys Chem Earth Parts A/B/C*, 27(36), 1557-1565.

Crosta GB (1998) Regionalisation of rainfall thresholds: an aid to landslide hazard evaluation. Environ Geol 35:131–145

Dai, F. C., Lee, C. E., and Ngai, Y. Y. (2002). "Landslide risk assessment and management: an overview." *Engineering Geology*, 64, 65-87.

Fall, M., Azzam, R., and Noubactep, C. (2006). "A multi-method approach to study the stability of natural slopes and landslide susceptibility mapping." *Engineering Geology*, 82(4), 241-263.

Gupta, R. P., and Joshi, B. C. (1989). "Landslide hazard zoning using GIS approach-a case study from the Ramganga catchment, Himalayas."*Engineering Geology*, 28, 119-131.

Guzzetti, F. (2000). "Landslide fatalities and the evaluation of landslide risk in Italy." *Eng Geol*, 58(2), 89-107.

Guzzetti, F., Carrara, A., Cardinali, M., and Reichenbach, P. (1999). " Landslide hazard evaluation: a review of current techniques and their application in a multiscale study, Central Italy." *Geomorphology* 31(1-4), 181-216.

Guzzetti F, Peruccacci S, Rossi M, Stark CP (2007) Rainfall thresholds for the initiation of landslides in central and southern Europe. Meteorol Atmos Phys 98:239–267

Guzzetti F, Peruccacci S, Rossi M, Stark CP (2008) The rainfall intensity-duration control of shallow landslides and debris flows: an update. Landslides 5:3–17

Hammouri, N. A., Husein Malkawi, A. I., and Yamin, M. M. A. (2008). "Stability analysis of slopes using the finite element method and limiting equilibrium approach." *Bulletin of Engineering Geology and the Environment*, 67(4), 471-478.

Schuster RL, Fleming RW (1986) Economic losses and fatalities due to landslides. Am As Eng Geol Bull 23:11–28

Montrasio L, Valentino R, Losi GL (2009) Rainfall-induced shallow landslides: a model for the triggering mechanism of some case studies in Northern Italy. Landslides 6:241–251. doi:10.1007/s10346009-0154-7

Khazai B, Sitar N (2000) Assessment of seismic slope stability using GIS modeling. Geogr Inf Sci 6(2):121–128

Johnson KA, Sitar N (1990) Hydrologic conditions leading to debris-flow initiation. Can Geotech J 27:789–801

Pelletier JD, Rasmussen C (2009) Geomorphically based predictive mapping of soil thickness in upland watersheds. Water Resour Res 45:W09417. doi:10.1029/2008WR007319

Savage WZ, Godt JW, Baum RL (2004) Modelling time-dependent areal slope stability. In: Lacerda WA, Erlich M, Fontoura SAB, Sayao ASF (eds) Landslides: Evaluation and Stabilisation, Proceedings of the 9th International Symposium on Landslides. A.A. Balkema Publishers, London, pp 23–36

Tesfa TK, Tarboton DG, Chandler DG, McNamara JP (2009) Modelling soil depth from topographic and land cover attributes. Water Resour Res 45:W10438. doi:10.1029/2008WR007474

Wu W, Sidle RC (1995) A distributed slope stability model for steep forested basins. Water Resour Res 31(8):2097–2110

Van Asch TWJ, Buma J, Van Beek LPH (1999) A view on some hydrological triggering systems in landslides. Geomorphology 30(1):25–32 (8)

CHAPTER 3

DEVELOPMENT OF SOIL DEPTH ESTIMATION IN THE CATCHMENT AREA

3.1 Introduction

As mentioned in Chapter 2, 3D deterministic models require a large amount of detailed input data, derived from laboratory tests or field measurements, and therefore, it is difficult to apply them over large areas (Van Westen et al. 2006). There is a consensus that soil depth is one of the most important parameters for controlling shallow landslides (Segoni et al. 2011). Soil depth is defined as the depth from the ground level to bedrock. It is a parameter used in determining the safety factor and it also controls the shape of critical slip surfaces. The easiest and most accurate way to measure soil depth is through field measurements. But this is only possible for small and well-monitored test sites. For large-scale areas, especially in mountainous areas, this method is not cost effective or practical as some places are not accessible. Satellite or airborne remote sensing techniques are ineffective, as to date they are only capable of resolving the first few centimeters of soil (Liang, 1997).

The soil thickness on the hillslope, which often coincides with the failure depth, is a critical parameter in performing a slope stability analysis, and it is an important factor, such as to the ratio of the saturated depth to the soil thickness (Ho et.al., 2012). Soil thickness can vary as a function of many different and interplaying factors, such as underlying lithology, climate, gradient, hillslope curvature, upslope contribution area, and vegetation cover, making the distributed estimation of soil thickness challenging and often unreliable (Catani et.al, 2010). The soil is the surficial material mantling the underlying weathered or fresh bedrock and lacking relict rock structure (Dietrich et al., 1995). Currently, there are two alternative methods: (1) the physically-based deterministic method and, (2) statistics-based correlation analysis (Moore et al., 1993 and Gessler et.al., 1995). There are numerous researchers that analyzed the problem of soil thickness prediction (e.g., an empirical geomorphology-based approach, by a process based model, using digital elevation data (Dietrich, et.al, 1995), or a process-based terrain characterization (Park, et.al., 2001)). In this study, we attempt to predict

the soil depth values over a discrete space at a chosen spatial resolution of the both methods of the process-based model and statistical model over complex terrain from topographic. We simulate the soil depth by following the Dietrich model (Dietrich et al., 1995). This is based on topographic Digital Elevation Data (DEM) using airborne laser survey data (LiDAR data) and Geographic Information System (GIS). By assuming (1) that soil production is a function of soil depth, (2) and that soil transport is proportional to the slope and (3) that soil production is in local dynamic equilibrium with the divergence of soil transport, topographic curvature becomes a surrogate for soil production.

3.2. Methodology

3.2.1 Concept of soil depth modeling

In order to create the patch variation in soil depth, we use a stochastic soil production and annual soil transport model, building upon earlier work (Dietrich et al, 1995). The simplest model for soil depth was proposed to explain the general tendency in hilly landscapes for the sharp convex ridges to have thin soil or bedrock outcrop. Their model had explored two general kinds of production laws, one which is a simple exponential decline with thickening soil, i.e, $-\delta e/\delta t = P_0 e^{-mh}$ (in which P_0 and m are empirical constants). In the model, K and ρs were assumed spatially constant with the soil depth described as a complex, bell-shaped function of h, f(h) = -(ðe /ðt):

$$K\nabla^2 z = \delta h/\delta t - \rho r/\rho s\, f(h) \qquad (3.1)$$

3.2.2 Data preparation

To apply Equation (31) to Sangun basin, we need to assign the diffusivity (K) value, the production function, and the bedrock and soil density. In the Sangun mountain, Fukuoka Prefecture, Japan abundant slope failures occurred in 2003.There was no information about an influence on the type of soils on the occurrence. Moreover, in the slope stability analysis, soil thickness is an important input parameter. The diffusivity is not known, therefore, the simulation of soil depth must consider the change of the diffusivity (K) values to get the reasonable value. Here we will use the range 37 – 55 cm^2/yr. The production function is based on of the production rate of cosmogenic nuclides concentration. Moreover, the bedrock and soil density were obtained from the literature. We use a 5 m resolution Digital Elevation Model (DEM) prepared using airborne laser survey data (LiDAR data). An inventory of slope failure has been documented. The

distribution of the slope failure has been conducted by utilizing Geographic Information System (GIS) function.

3.2.3 Process-based model to simulate of soil depth

The soil depth model simulations were carried out by utilizing Geographic Information System (GIS) function. The soil model, in the form is given in Equation (3.1), assumes that over the time period sufficient to influence the soil depth, the dominant hillslope process can be represented by a slope dependent transport law. The diffusivity (K), the bedrock and soil density, and the production function are uncertainty values. Therefore, we needed guidance for initial values from the literature. Dietrich. et. al (1995) explained that diffusivity (K) value was estimated by Reneau (1988) by using Equation (3.1) by dividing a calculated flux of sediment required to infill unchannelled valleys (based on radiocarbon determined deposition rates) by the mean gradient of the adjacent source slopes.

In the following we parameterize the model based on some literature (Dietrich et al., 1995, Reneau et al., 1988). Also, we did not obtain data in Japan that related these parameters. From the range of diffusivity (K) value 37 – 55 cm^2/yr, the mean gradient value has been used. Therefore, here we will use 50 cm^2 / yr. Moreover, for the bedrock and soil density ratio, we will use the value proposed by Dietrich et al data of about 1.7. In this study, we consider the sensitive values of soil production data. And for bedrock and soil density ratio is not described in the study area. Furthermore, the production function is not known, therefore, the initial value will be as from Dietrich et.al data, and we make a range of values get the best results from simulations. The range value of 0.019 cm/yr to 0.025 cm/yr will be used in the simulation. By fitting an exponential function, ($-\delta e/\delta t = P_0 e^{-mh}$), to the thick (no production at 150 cm) and thin soil production rates (0.0042 cm/yr at 30 cm), the P0 =0.019 cm/yr and m = 0.05 (Dietrich et al., 1995) values are obtained. During one simulation, the time step will be set up to 1,000 years and a time limit of 2,000 yr.

3.2.4 Estimation of ^{10}Be concentrations

On such slopes both the soil thickness and the rate of soil production by rock weathering are uniform and the soil creep flux increases with distance from the top of the slope. It then follows (McKean.J.A et al, 1993) that the slope must steepen with distance from the divide; i.e., the slope profile must be convex

upward to provide the necessary transport capacity.

Application for cosmogenic ^{10}Be proceeded in quartz of river sediment could follow that serve as a tool as powerful as the in situ produced cosmogenic nuclides to derive erosion rates and soil residence times from individual soil surface samples or detrital river sediment (Willenbring.J.K et al, 2010). River sediments are eroded at different rates in different source areas (i.e. different sub-catchments) and, therefore, inherit different nuclide concentrations. The mixing of grains through hillslope and fluvial transport processes homogenizes nuclides in the downstream sediment load. Therefore, a handful of sediment collected from a river bed can lead to a profoundly new understanding of the rates of landscape change (Blanckenburg.F, 2005). Recently, several research groups have begun to measure the abundance of nuclides in sediments with the goal of estimating basin-scale rates of denudation (Bierman.P.R et al, 1998).

Samples were treated to isolate 20 to 60 grams of pure quartz from samples. The experimental work required for the measurements of in situ produced nuclides with quartz rich minerals has some chemical aspects (Altmaier.M, et al, 2001). The three major experimental steps classified are (1) separation of purified quartz mineral; (2) BeO preparation for AMS (*Accelerator Mass Spectrometer*) targets; and (3) measurement of the $^{10}Be/^{9}Be$ ratio by AMS. For 10Be analysis, the most important characteristic is the ability to prepare a sample that is free of atmospherically produced ^{10}Be (Bierman, P.R, 1994). Quartz has been shown to be useful because it is resistant to weathering and alteration and can be effectively cleaned of meteoric 10Be by HF etching. The procedures of (1) and (2) are following the method of Kohl and Nishiizumi (1991).

Measurements were performed by the JAEA-AMS-TONO facility at the Tono Geoscience Center of the JAEA (Matsubara et al, 2014). The $^{10}Be/^{9}Be$ ratio was calibrated against the standards (01-5-1) supplied from University of California.

The ^{10}Be concentration calculations were performed following Balco et al. (2008) by converting Be isotope ratio measurements to nuclide concentrations in quartz. The ^{10}Be concentration in quartz is the quantity needed to calculate a production rate. Production rate calculations were performed following Balco et al. (2008) in Savi et al. (2013) using the CRONUS EARTH calculator (ver. 2.2;http://hess.ess.washington.edu/) (Savi.s et al, 2013). Topographic aspects such as latitude, longitude and the mean elevation of the sites in the catchment were

determined from a digital elevation model (DEM) with 5 m resolution.

3.3 Case studies in a mountainous area

3.3.1 Soil depth investigation

We apply these models to a small catchment in the upper Sangun mountain area. The area is mostly underlain by granite rock. During the investigation, the morphometry aspect was considered to collect measurements of soil depth. We have two profile of soil investigation. A Portable Dynamic Cone-Penetrometer Test (CPT) tool was used in the measurements. The CPT is a valuable method of assessing subsurface stratigraphy associated with soft materials, discontinuous lenses, organic materials (peat), potentially liquefiable materials (silt, sands, and granule gravel), and landslides (David, R., 2006). The measurements were carried out at 20 selected points, see Fig. 3.1. The sampling interval was 5 or 10 m, and positions were identified by a GPS.

In order to determine the grade of weathering, the classification of granites presented by Hencher and Martin (Vahed et al, 2009) was selected. This classification makes possible to classify weathering grade according to characterized with a range of rebound values of the N-type of the hammer. The resulting classification of selected parts in Sangun Mountain is given in Table 3.1.

3.3.2 Soil depth simulation

This simulation presents a distribution of soil depth. The variables identified as predictors include topographic variables, soil production rate (P_0), a density of the rock and soil, and diffusivity (K) value. However, the range of soil production rate (P_0) was considered in the simulation such to get a reasonable value of soil depth compared with soil depth indirect measurements.

We use three P_0 values, such as 0.019, 0.022, and 0.025 cm/yr. For the purpose of model validation, the time interval of 1,000 to 2,000 years was used. Fig. 3.2 shows soil depth distribution maps with importance value of the P_0 value, (a) 0.019 cm/yr, (b) 0.022 cm/yr, and (c) 0.025 cm/yr.

3.4 Model Validation

The performance of the process based model can be compared to the field measurements to compute the error between the two data sets. We propose that mean square prediction error close to zero value could indicate a good result from simulation process. Root Mean Square Error (RMSE) (also known as Root Mean Square Deviation) is one of the most widely used statistics in GIS. In a variety of

geostatistical applications, RMSE is one method to evaluate the model performance.

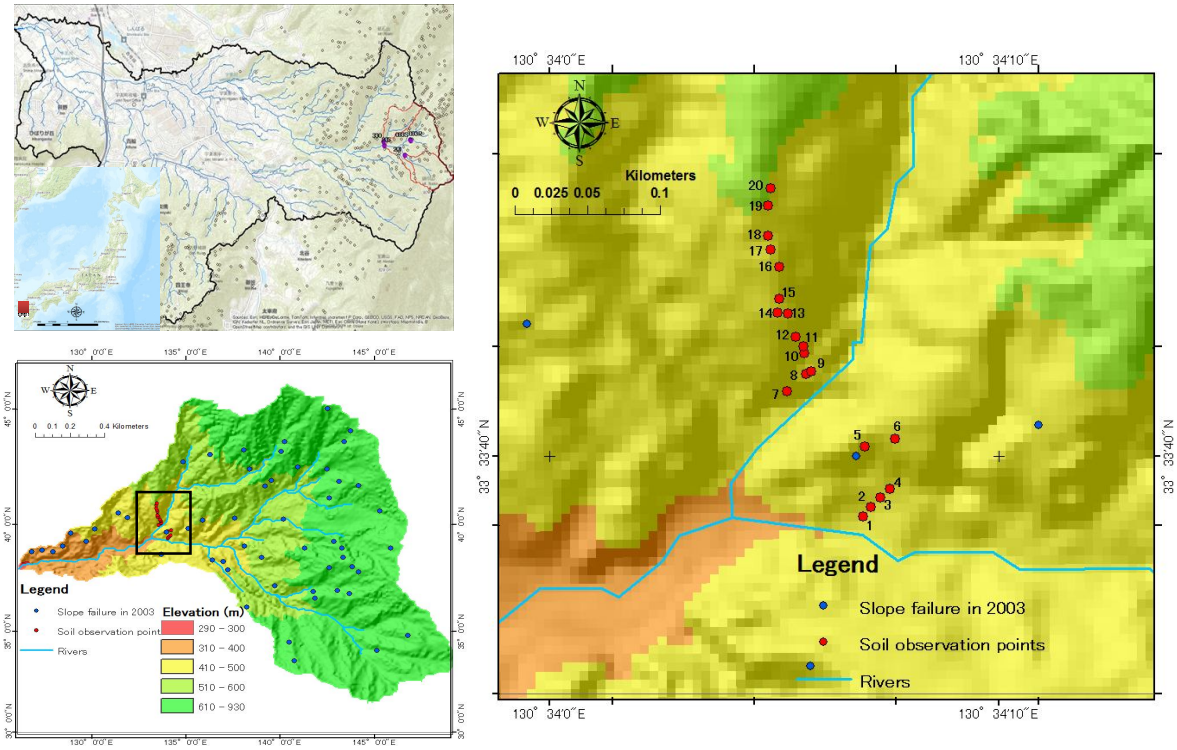

Fig. 3.1.Sangun basin boundary and small studied catchment in the upstream part which have been selected for soil depth investigations.

Root mean square error takes the difference for each soil depth value based on simulation and surveyed value. We can swap the order of subtraction because the next step is to take the square of the difference. RMSE value is calculated by following Equation (3.2):

$$RMSE = \sqrt{\frac{1}{N}\sum_{i=1}^{N}(x_i - y_i)^2} \qquad (3.2)$$

where N: number of observation points; x_i: prediction value; y_i: observation value. The raster file of soil depth was prepared and sampled at the measuring points. Therefore, we estimate the soil characteristic and compared the observed and predicted soil depth values (Table 3.1). The characteristic soil depth was divided into two parts depending on the N value. N value 30 represents the moderately

weathered rock zone, and 50 represents the slightly weathered rock zone.

Table 3.1. Soil depth (m) measurement in the upstream part of Sangun catchment, Fukuoka Prefecture (2015).

N SPT	Soil Depth (m)										Description
(Blow)	S1	S2	S3	S4	S5	S6	S7	S8	S9	S10	
30	1.6	0.5	1.35	1.55	0.35	0.35	0.1	0.25	0.45	0.6	Saprolitic soil zone
50	2.4	0.72	1.44	1.75	0.35	0.35	0.1	0.25	1	0.8	Partially weathered Rockzone

N SPT	Soil Depth (m)										Description
(Blow)	S11	S12	S13	S14	S15	S16	S17	S18	S19	S20	
30	0.55	0.13	0.65	0.9	0.6	0.71	0.95	1.1	1	1.5	Saprolitic soil zone
50	1.18	0.13	0.81	1.4	0.71	0.71	2.21	2.29	1	2.15	Partially weathered Rockzone

The process based model simulates soil depth at 11 times (1,000; 1,100; 1,200; 1,300; 1,400; 1,500; 1,600; 1,700; 1,800; 1,900; and 2,000) and have P_0 values 0.019; 0.022; and 0.025 cm/yr for simulating the influence of soil production rate. Observations were available only for twenty observation points. Fig. 3.3 shows that the model performed very well for simulating soil depth. In the Fig. 3.3a shows the N value 30 which a blue line presents P_0=0.019 cm/yr and time 1,500 year are the better RMSE value (0.306) than other P_0 values.

Furthermore, Fig. 3.3b shows the N value 50 which a red line presents soil P_0= 0.019 cm/yr and time 2,000 year have a low RMSE value (0.570). Therefore, the root-mean-square errors (RMSE) reported in Fig. 3.3 indicate that the RMSE value 0.306 is better than the other values the process based model for predicting soil depth at the point scale in term of these the sample statistical measures.

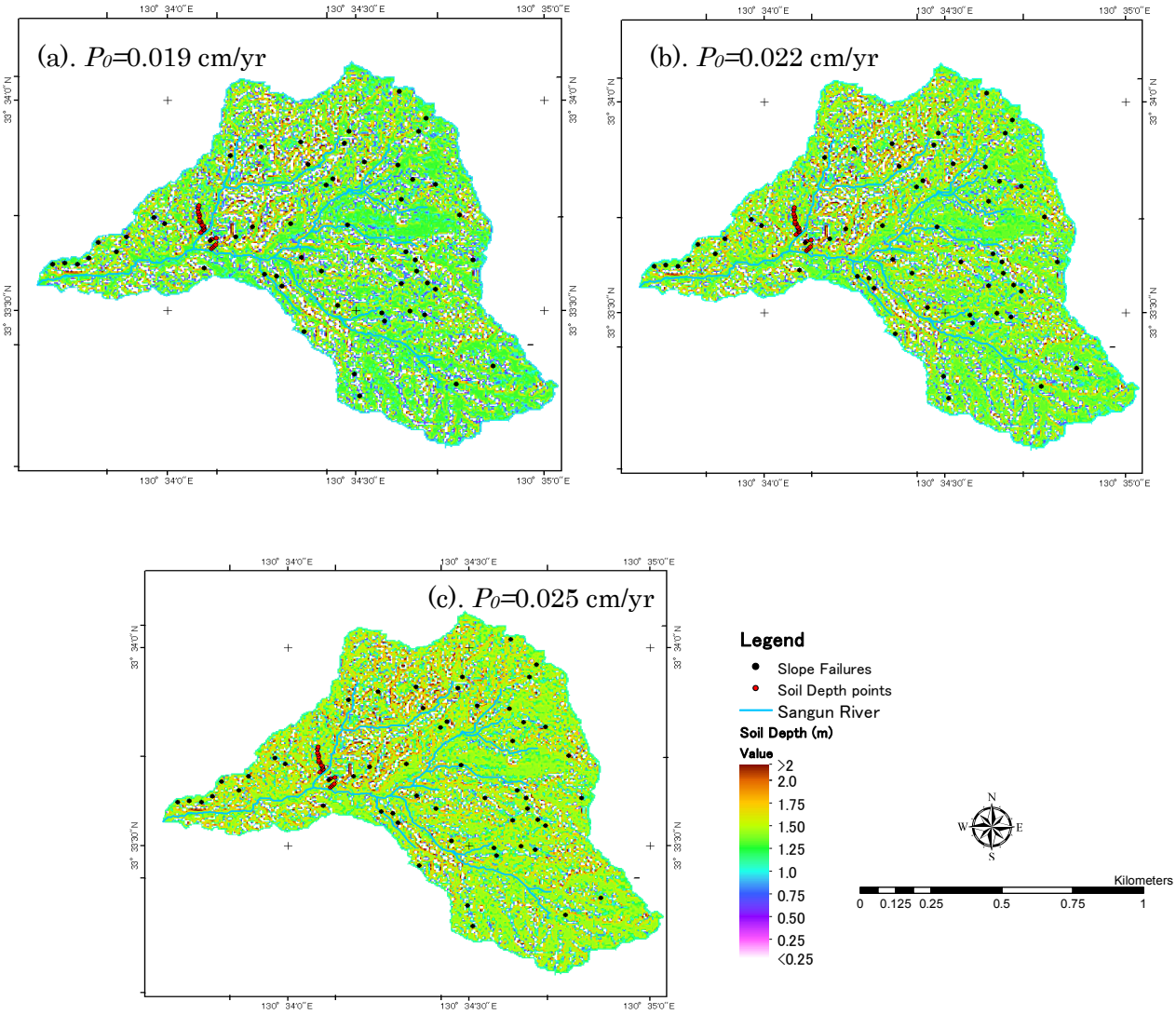

Fig 3.2. Spatial distribution of soil depth based on simulation of the soil production rate (P_0).

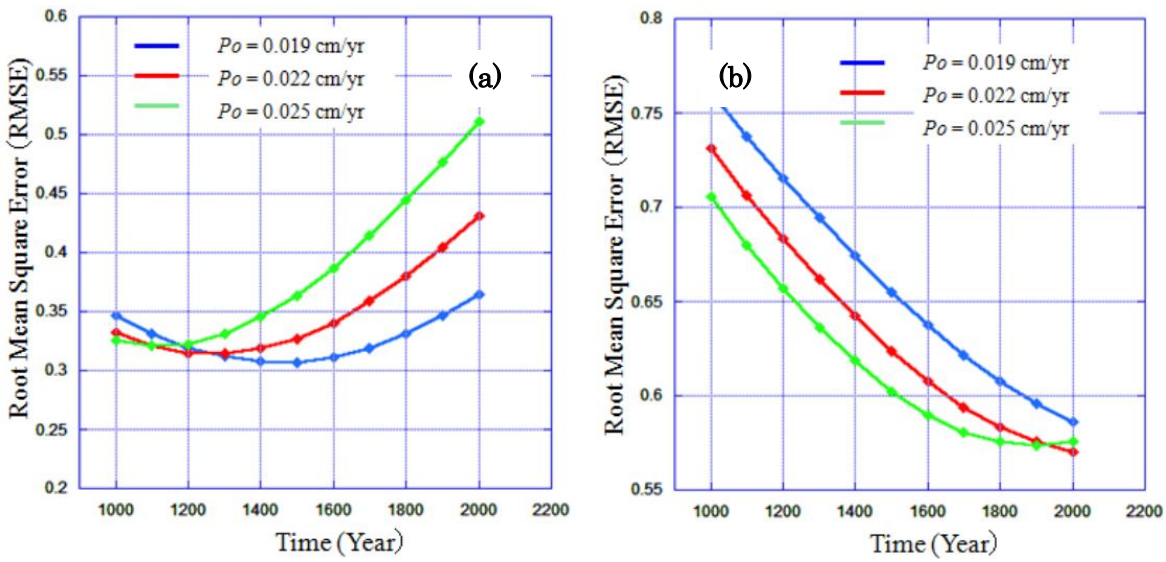

Fig.3.3. Root Mean Square Error (RMSE) values on validation. (a) N value=30; and (b) N value=50.

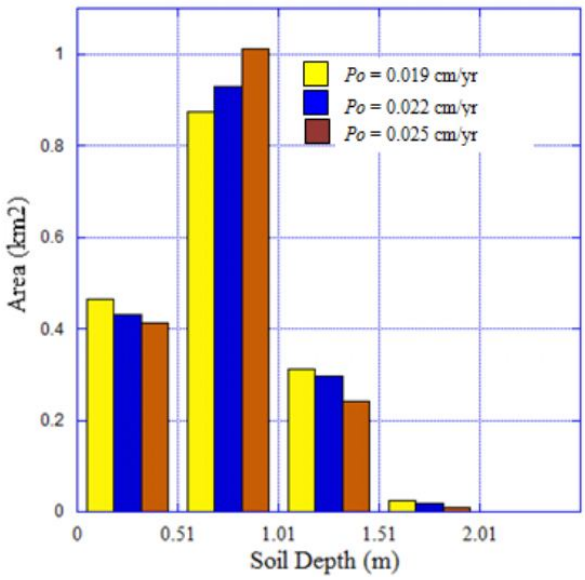

Fig.3.4 Graph of distribution of soil depth based on soil production rate (P_0) values during simulation.

3.5 Soil Depth Distribution

Process-based model (Dietrich et al., 1995) has been used to predict soil depth over a landscape using topographic and, soil production rate and time in the

Sangun mountains. The variables identified as predictors included morphology, soil depth observations, soil production rate (P_0), and production time (t). In this study, the soil production rate (P_0) 0.019 cm/yr, 1500 year, N value 30 (0.1 – 1.6 m) provide the reasonable model for the spatial distribution of soil depth (Fig.3.3a). Table 3.2 shows an amount of soil depth distribution area in the study area that based on the simulation by using the N value 30 (0.1 – 1.6 m) and the variation of the soil production rate (P_0). Soil production function refers to the rate of bedrock weathering into the soil as a function of soil thickness. The relationship between soil production rate (P_0) and the amount of soil depth distribution is not linear.

The soil production rate increases for soil depth 0.51 – 1.00 m. Moreover, the soil depths of 0 -0.5 m, and greater than 1.01 m show the soil production rate (P_0) to decrease. In the soil depth model, the distribution of soil depth shows a trend with a peak centered on the depth range 0.51 – 1.00 m (Fig. 3.4). For P_0= 0.019 cm/ yr, the maximum area of soil depth distribution is 0.875 km^2 the 1,500 years. Secondly, the P_0=0.022 cm/yr shows the peak maximum area is 0.928 km^2 the 1,300 years. And thirdly, the P_0=0.025 cm/yr shows the peak maximum area is 1.011 km^2 on 1,100 years. Furthermore, the area of distribution of soil depth 0.51 – 1.00 m is larger than the other soil depth interval, about 52.23% of the total area.

Table 3.2. Soil depth distribution in the upper part of Sangun basin based on the simulation for N value = 30.

Soil depth (m)	*Po*=0.019 cm/yr		*Po*=0.022 cm/yr		*Po*=0.025 cm/yr	
	Area (km^2)	%	Area (km^2)	%	Area (km^2)	%
0 - 0.5	0.46	27.67	0.43	25.68	0.41	24.56
0.51 - 1.00	0.88	52.23	0.93	55.43	1.01	60.38
1.01- 1.50	0.31	18.56	0.30	17.70	0.24	14.40
1.51 - 2.00	0.02	1.45	0.02	1.12	0.01	0.64
>2.00	0.002	0.09	0.001	0.07	0.00	0.02
Total	1.67	100	1.67	100	1.67	100

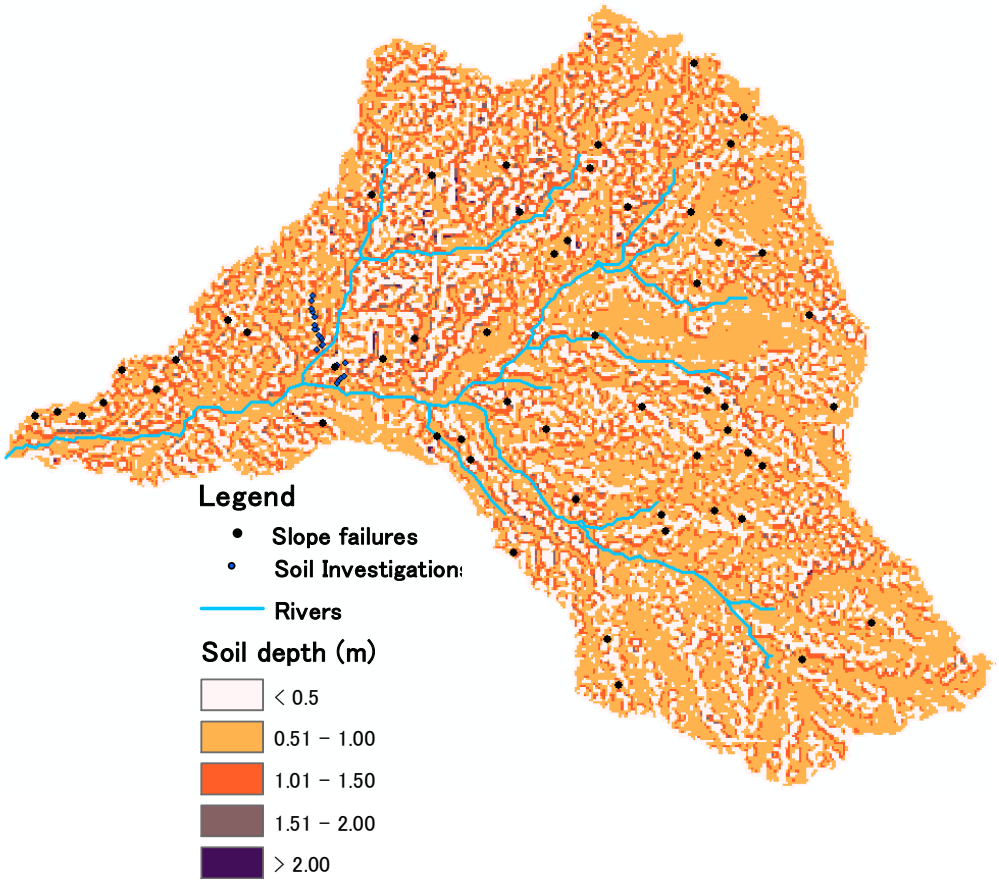

Fig 3.5 Soil depth distribution of the upper catchment of Sangun mountainous area.

Fig 3.6 shows Relationship between of soil depth and topographic parameters in the Sangun mountainous. Where the topography is reasonably well capature in the digital elevation data, this figre represantive the model successfully predicts the extent of thick colluvial deposits in convex area and identifies areaa of significant bedrock of granite. The results also suggest that soil depth tends to a varying value on slopes angle . From this figure, a result in agreement with field observations.

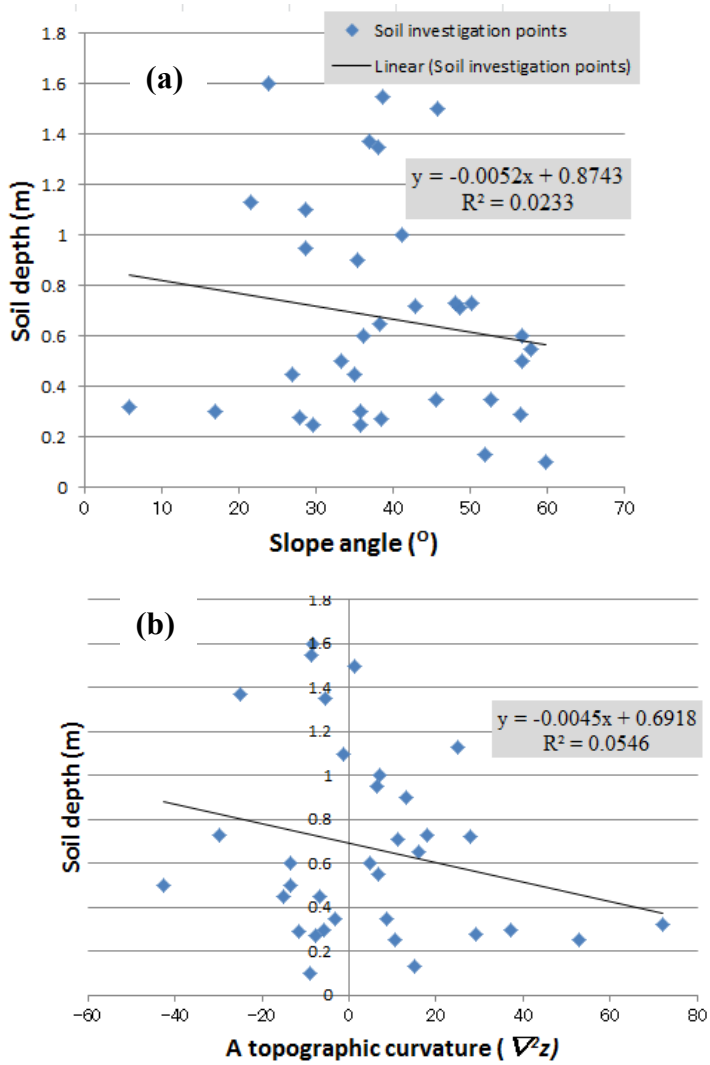

Fig 3.6 Relationship between of soil depth and topographic parameters in the Sangun mountainous. (a) Slope angle; and (b) A topographic curvature ($\nabla^2 Z$).

3.6 Conclusions

In this study, the spatial distribution of soil depth was simulated using a process-based model (Dietrich, et al., 1995), and different soil depth observations to perform a simulation analysis to provide the relationship of slope failure and soil depth distribution in the upper catchment of Sangun mountains. Results from the simulation analysis indicated that topographic variables, soil production rate (P_0), and a soil production time (t) provide the reasonable model for the spatial

distribution of soil depth. The results also showed that the soil depth ranged from 0.51 m to 1 m has the largest area of soil distribution.

Considering the limited number of soil depth observations, this model appears as an important improvement toward solving the need for distributed soil depth information in the process based modeling. In the study area, soil depth in concave area is increasing and convex area is decreased. Soil depth is increased, which the slope angle decreases.

References

Altmaier, M., Klas, W., and Herpers, U. (2001) Surface exposure dating by in-situ produced cosmogenic nuclides: chemical mineral separation of purified quartz. *Radiochim. Acta*, 89, 779-782.

Bierman, P.R. (1994) Using in situ cosmogenic isotopes to estimate rates of landscape evolution: A review from the geomorphic perspective. *Journal of Geophysical Research*, 99, 13885-13896.

Bierman, P.R. et al. (1998) Erosion, Weathering, and Sedimentation. In: Kendall, C., and McDonnell, J.J. (eds.) *Isotope Tracers in Catchment Hydrology*. Elsevier Science. Chapter 19.

Costa, J.E., and Wieczorek, G. F. (1987) Debris flow/avalanches: process, recognition and mitigation. *Geological Society of America, Reviews in Engineering Geology,* 7, Geological Society of America, Boulder, 239pp.

Catani, F., Segoni, S., and Falorni, G. (2010) An empirical geomorphology-based approach to the spatial prediction of soil thickness at cathment scale, *Water Resources Research*, 46, W05508, Doi: 10.1029/2008WR007450.

David, R. (2006) Subsurface Exploration Using the Standard Penetration Test and the Cone Penetrometer Test. *Environmental & Engineering Geoscience,* Vol XII No 2 , 161-179

Dietrich, W. E., Reiss, R., Hus. M. L., and Montgomery, D. R., (1995) A process-based model for colluvial soil depth and shallow landsliding using digital elevation data. *Hydrological Processes,* 9, 383-400

Duzgoren-Aydin, NS., Aydin, A. (2006) Chemical and mineralogical heterogeneities of weathered profiles: implications for landslide investigation. *Nat Hazard Earth Syst* 6:315–322.

Hanamura, et. Al. (2004) Heavy rain Disaster in Kyushu Area on July 2003. *Japan Society of Engineering Geology*, 25, ISSN 0917-2289, 30-31

Ho, J.Y., Tun Lee, K., Chang. T. C., Wang, Z. Y., and Liao, Y. H. (2012). Influences of spatial distribution of soil thickness on shallow landslide prediction. *Enginering Geology,* 124, 38-46.

Matsubara, A., Saito-Kokubu, Y., Nishizawa, A., Miyake, M., Ishimaru, T., and Umeda, K. (2014) Quaternary Geochronology Using Accelerator Mass Spectrometer (AMS): Current Status of the AMS System at the Tono

Geoscience Center. Geochronology, edited by J. van Mourik, pp. 3-30, InTech.

Park, S.J., McSweeney, K., and Lowery.B., (2001) Identification of the spatial distribution of soils using a process-based terrain characterization. *Geoderma,* 103 , 249-272

Savi, S., Norton. K. P., Picotti, V., Brardinoni, F., Akcar, N., Kubik, P.W., Delunel, R., Schlunegger, F. (2013) Effects of sediment mixing on ^{10}Be concentrations in the Zielbach catchment, central-eastern Italian Alps. *Quaternary Geochronology.* DOI. 0.1016/j.quageo.2013.01.006.

Vahed, G, Husaini, O., and Bujang, K. H. (2009) A Study of the Weathering of the Seremban Granite. *Electronic Journal of Geotechnical Engineering,*14 Bund D.

Von Blanckenburg, F. (2005) The control mechanisms of erosion and weathering at basin scale from cosmogenic nuclides in river sediment. *Earth and Planetary Science Letters*, 237, 462-479.

Willenbring, J.K., and Blanckenburg, F.V. (2010) Meteoric cosmogenic Beryllium-10 adsorbed to river sediment and soil. *Applications for Earth-Surface Dynamics. Earth-Science Review*, 98, 105-122.

CHAPTER 4

GIS-BASED 3D ANALYSIS METHOD FOR RAINFALL EFFECT

4.1 Introduction

An important issue in recent climate impact research has been the assessment of the effects of climatic variability and climate change on geomorphic processes and hazards, such as landslides (Collison et al., 2000; Dehn et al., 2000). Slope failures are studied systematically, in order to evaluate the nature of the hazard and the damages to human life, buildings and infrastructures, transportation systems, utilities and lifelines. They are complicated processes, mainly because of the many different causal factors involved in the manifestation of the phenomenon i.e. lithology, geological structures and joints, geomorphologic features, slope angle, relative relief, land use, ground water conditions, climate and seismic activity.

Climate and seismic activity change periodically and they are the two main natural triggering causal factors contributing to landsliding. Slope movements are associated with quick changes in the position of masses both in natural or man-made slope cuts and fills during civil-works, and the driving forces, are body forces such as the gravity and the seismic action. The influence of climate on landslide processes can be considered either as a weathering factor, acting slowly, or as a rapid influencing factor such as rainfall, snow or frost.

Popescu (1994), proposed safety factor (SF) variation as a function of time, for a given slope. Seasonal rainfall and evaporation, is reflected in seasonal variations in the SF. Landslide causative factors can be separated to preparatory causal factors and triggering causal factors. The computed value of SF is a clear and simple distinction between stable and unstable slopes. According to Crozier (1986), it is preferred to characterize existing slopes as stable, marginally stable, and actively unstable.

Slope stability analysis techniques fall into three categories: (1) deterministic methods or limit equilibrium methods, where safety is defined by a single value of safety factor (SF); (2) finite element and finite difference methods, where the stress-strain behavior of soil or rock can be understood; (3) probabilistic methods, where safety is measured by probabilistic terms of risk of failure.When utilizing GIS for implementation of the deterministic method of slope stability,

two options, performing deterministic calculations inside or outside GIS, exist. Performing calculations outside GIS needs to interface a third party solution, usually typified by static file transfer and disparate user interfaces. In this kind of approach, even though external existing models can be used directly without losing time in programming the model algorithms into GIS, unfortunately, it is always wrought with complication caused by data conversion between different hardware platforms, operating systems, database servers, and operational models, both in data input and result presentation.

In this study, a 3D limit equilibrium methods for slope stability analysis use column-based method in which the failure mass is divided into a number of small soil columns. The combination of the grid-columns that derived from the overlay of GIS raster layers and the soil columns that derived from discretization of the sliding mass makes the application of 3D deterministic models possible (Qiu *et al.*, 2006).

The development of geotechnical analysis for slopes of soil and rock has progressed as a consequence of improvement in the knowledge of basic geotechnical concepts and an understanding of the causes, processes and mechanisms associated with slope failures. Pore-water pressure often plays an important role in slope stability and it may determine how the factor of safety varies spatially and over time. The effective stress principle is fundamental to an understanding of the short-term and long term behavior of soil and rock slopes in which pore-water pressure develops as a consequence of water infiltration and seepage. Rainfall-induced slope failures occur generally, but not always, in saturated soils. Such failures are caused by the increase of pore-water pressures to critical values.

Soil thickness is considered as one of the most important factors controlling shallow landsliding (Wu and Sidle, 1995). Soil properties vary spatially even within homogeneous layers as a result of deposition and post depositional processes that cause variation in properties (Lacasse and Nadim, 1996). Nevertheless, most geotechnical analyses adopt a deterministic approach based on single soil parameters applied to each distinct layer. Elkateb et al (2002) has applied the conventional tools for dealing with ground heterogeneity in the field of geotechnical engineering under the use of safety factors and by implementing local experience and engineering judgment. In the recent years, numerous studies have been undertaken to develop a slope stability analysis that deals with the

uncertainties of soil properties in a systematic manner (Alonso, 1976; Griffiths and Fenton, 2004).

Moreover, one of the important factors that induce instability in slopes is the effect of rainfall. Landslides often take place in mountainous areas after intense rainfall and pose a great threat to human lives and property. It is necessary to study the mechanisms of slope failure induced by intense rainfall. Both shallow and deep-seated landslides can be triggered by rainfall, with frequencies, both in time and space, and under the effects of different types of storms (Casagli et al. 2006). Generally, shallow landslides are the most common failure through which rainfall affects slope stability, as short, quick rainstorms are common. The rapid growth of pore-water pressure, a rise in ground water level, and a loss of the component of apparent cohesion have been well established to be caused by rainfall (Crosta and Frattini 2003; Qiu et al. 2007).

This study proposes a methodology in combining of the GIS-based 3D slope stability and hydrological model for assessing slope stability. First, the considering of homogeneous layer is used to predict the probability of slope failure under the variation of the cohesion (c) and internal friction angle (ϕ) values. Secondly, the effect of soil depth in the slope stability was presented. Thirdly, the 3D slope stability methods are then modified to reflect the effect of rainfall to slope stability. Finally, the safety factor corresponding to each rainfall moment and failure time can be calculated.

In this chapter, a methodology is presented which produces landslide hazard maps due to static or dynamic loading, implementing failure criteria. GIS were proved to be an indispensable tool for managing geological geotechnical, and climate information. Moreover, they offer the potential of a complete analysis, using tools of spatial analysis, as well as the implemented algorithms in order to produce landslide hazard assessment models. In terms of rainfall induced landslides the proposed model was used as a screening tool in order to detect landslide prone areas, and further analyze them applying sophisticated analytical and numerical tools.

4.2 GIS-based three dimensional method of limit equilibrium method

Generally, a GIS uses a raster data model for the storage, processing, display and analysis of spatial data. GIS raster data are composed of one or more equally spaced cells whose values usually record one property of a geographic phenomenon occurring over the patch of space it covers. Real-world features related to slope stability analysis are modeled by raster layers where each layer represents a certain type of information such as topography, stratum, or ground water. The superposed structure of the stratigraphy can be represented subsequently by the overlay of the multiple raster layers. The overlay extends the 2D raster layers to a third dimension. The structure of the overlay of raster layers is defined by same x, y coordinates and difference z coordinate. Each local position in the overlay can be imaged to a 3D grid-column that consists of several rater layers. The elevations of the ground surface and all the soil surfaces at the same x and y coordinates define the positions of the ground surface and the soil surfaces within a 3D grid-column.

Based on the Mohr-Coulomb criterion, the safety factor of a slope failure mass is evaluated by comparison of the magnitude of the available shear strength with the shear strength required just to maintain stability along with a potential failure surface. Using the function of GIS spatial analysis, all input data (such as elevation, inclination, slope, groundwater, strata, slip surface and mechanical parameters) for the 3D safety factor calculation can be available with respect to each grid pixel, while all slope related data are in the form of grid-based. By putting these data into a deterministic model of slope stability, a value of the safety factor can be calculated.

Without GIS, a 3D safety factor calculation based on this column-based model would be a tedious and time-consuming task, and the data renewal or a multi-case study would also be inconvenient. But in the GIS system, by using the GIS spatial analysis function, slope stability related data of the whole study area can be represented as GIS vector layers (point or line feature) as shown in Fig.4.2. For each vector layer, a grid-based layer can be obtained by using the GIS spatial analysis function and grid size (cell size) can be set with the requisite precision.

The slope failure has been evenly divided into columns and related to grid-based columns. For each column, with reference to the grid-based column in the Fig.4.2, the spatial data of surface, strata, underground water, fault and slip surface can be obtained from the grid-based layers. Because of so many slope

related data, it is not effective to manage all these grid-based datasets. Therefore, in this thesis, we use the 3DSLOPE GIS tool that has been developed by Xie et.al, 2003. All of the spatial analysis modules, including 3D slope stability analysis module, slip surface identification module, slope unit division module, infiltration module, and probability analysis module, have been incorporated into a standalone GIS system, called 3DSLOPE GIS tool, that is programmed by Visual Basic 6.0 using ArcObjects. In the system of 3DSLOPE GIS tool, a point dataset is used to store all these grid datasets. In this point data set, a feature table is used to relate all the slope related data. The point shape is set to be the central point of each grid column, other fields are respectively set to relate each slope related data.

4.2.1 Techniques for algorithms of GIS-based 3D model

In this study, there are three components in the techniques for algorithms of GIS-based 3D model, such as:

a. Coordinate conversion of ellipsoid

For searching the critical slip surface, the initial slip surface is assumed as the lower part of the ellipsoid, and the direction of inclination of the ellipsoid is set to be the same as the main inclination (dip) of the study area. The inclination angle of the ellipsoid is basically set as the main inclination angle of the study area with changes in certain fluctuations.

b. Identification of slip surface (Z Value)

The Z value (elevation) of point "B" of the slip surface is determined by the solution of equations of line AB and ellipsoid as in Equation (3-12) (Fig. 4.1) .

$$\left.\begin{array}{l} \dfrac{x-xo}{\sin(slope)}=\dfrac{Z-Zo}{\cos(slope)} \\ y=yo \\ \dfrac{x^2}{a^2}+\dfrac{y^2}{b^2}+\dfrac{Z^2}{c^2}=1 \end{array}\right\} \qquad (4.1)$$

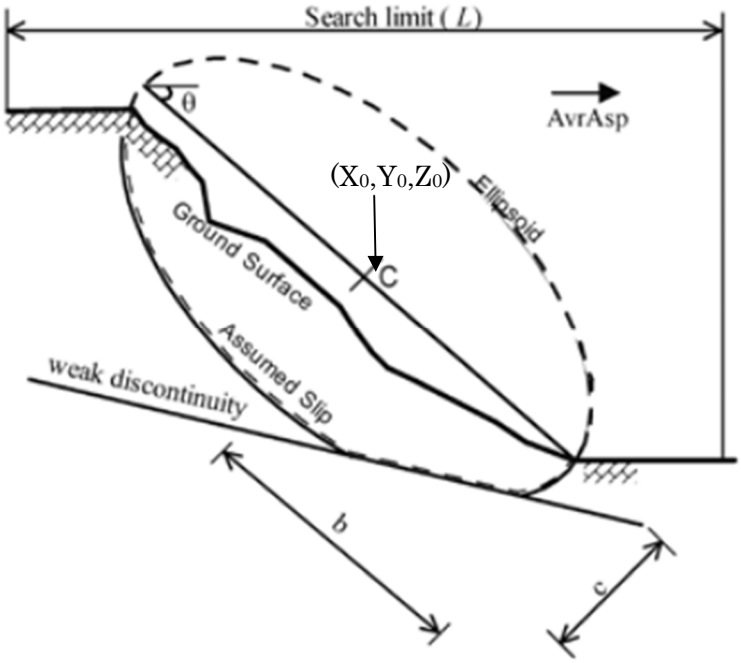

Fig. 4.1 Getting the Z value of slip surface

c. Computational processes

The whole study area (or the slope failure) range can be evenly divided into small rectangular meshes that are the same as the GIS based grids. For numerical calculation of this grid-based 3D slope stability analysis, all of the above calculation procedures are programmed by a Visual Basic (using GIS components)(Xie et all, 2003). The process for calculating the minimum 3D safety factor is illustrated in Fig.4.3. In this process, the function of data module is for obtaining all the slope related geological, geomorphologic and hydraulic data and the geomechanical parameters; the random variables production module is used for randomly selecting the trial slip surface by Monte Carlo simulating; the 3D factor of safety is calculated in the 3D slope stability module; finally the critical slip surface and its safety factor can be obtained by many trial calculating. From Fig.4.2, it can be seen that all modules are related to the GIS spatial analysis function that is implemented by a GIS component, just because a GIS component is implemented in this system of 3DSLOPE GIS tool, can the 3D safety factor problem be computed effectively. Using the slope related GIS data, at the same time, all the related data and results can be visualized in the system of 3DSLOPE GIS tool.

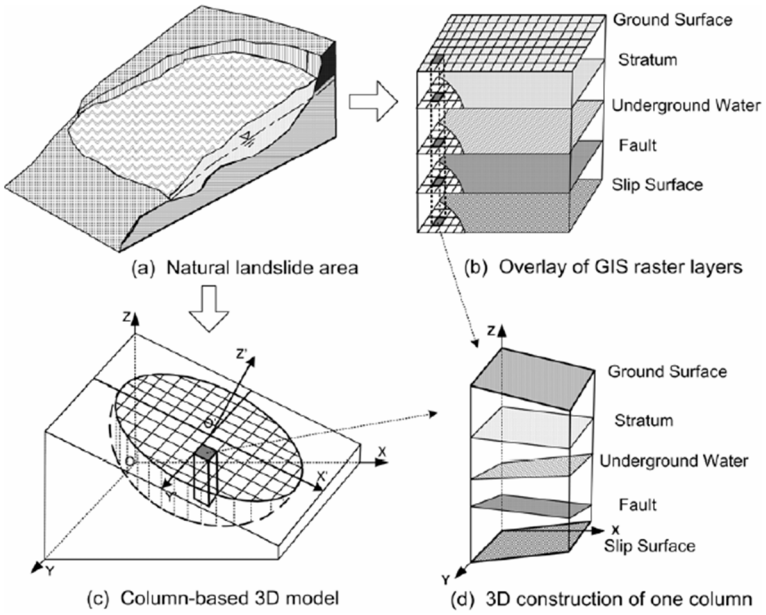

Figure 4.2 The mechanism of GIS raster-based 3D model

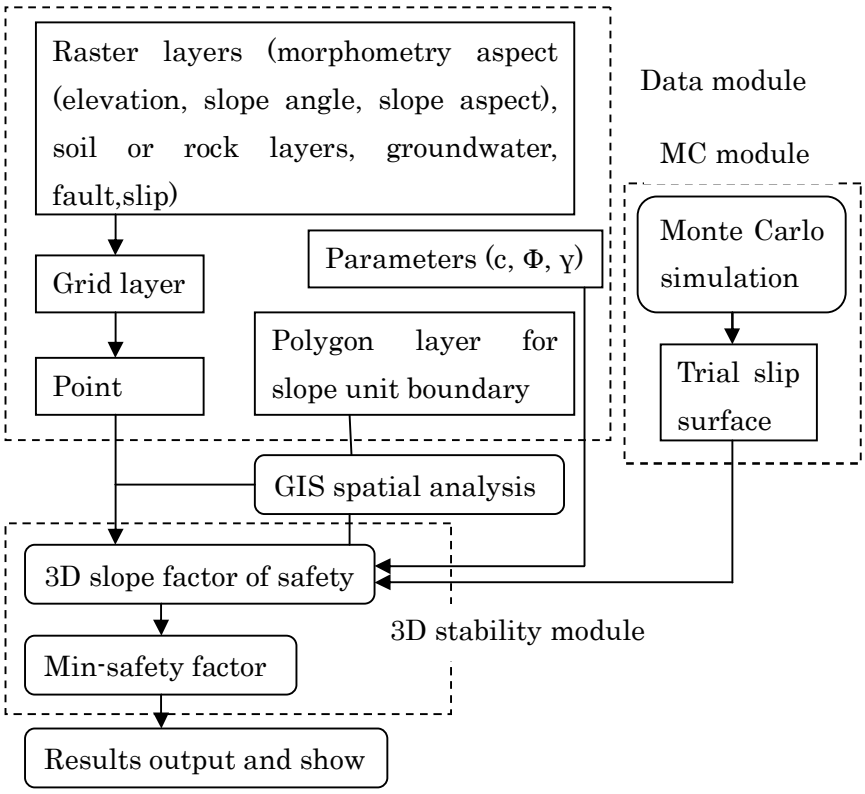

Fig.4.3 Computational processes for min-3D safety factor

4.2.2 Validation of GIS-based 3D model

In this study, the validation of results of GIS-based 3D model is important. Therefore, for verifying this GIS grid-based 3D stability analysis model, an example problem is calculated by this GIS grid-based 3D model (Xie et all. 2003). The example problem is a homogeneous, purely cohesive slope with a circular slip surface. From its results, three-dimensional safety factor was calculated to be 1.402 using the closed-form solution (Baligh and Azzouz, 1975); The safety factor was computed to be 1.422 using the CLERA model (Hungr 1987). Furthermore, the same problem was solved using the 3D-SLOPE model (Lam et al.1993), the computed 3D safety factor ranged from 1.386 to 1.472 depending on the number of columns used in discretizing the slope.

Using this GIS grid-based 3D stability analysis model and compared with the closed-form solution (the difference is about 1%), it is clear that this GIS grid-based model can be effectively used for the 3D slope stability evaluation.

4.3 Monte-Carlo simulation and evaluation of 3D stability

4.3.1 Method of Monte-Carlo simulation

The factor that will influence the safety factor of slope are the random variables that possess a certain random distribution, and then the safety factor K_s is a random variable too and its probability distribution is determined by the distributions of parameters. If the function of distribution of K_s can be obtained, then the failure probability P_{ks} is calculated by:

$$P_{ks}(K_s<[K_s])=\int_0^{[Ks]} f(Ks)d(Ks) \qquad (4.2)$$

In Equation (4-2), $[K_s]$ is the design of safety factor and P_{ks} is the probability that when K_s is the design safety factor (it is ordinarily set to 1.00).

In the practical use, because it is very hard to obtain the function of $f(Ks)$, it is always to use the Monte-Carlo simulation method to calculate the failure probability $P_{ks.}$ The method is that obtaining the random variables of the parameters based on the random distribution of parameters and then inputting into the formula of K_s, after many times calculating, the distribution function of $f(K_s)$ can be obtained, and then the failure probability of P_{ks} can be calculated.

Based on the uniform distribution on [0,1], the sample of the random variable which possesses a certain probability distribution can be calculated. Set z as a random variable and its distribution is $F(u)$:

$$P\{Z<u\}=Fu) \quad (4.3)$$

If $F(u)$ is continuous and strictly dull up, and then

$$X=F(Z) \quad (4.4)$$

is uniform distribution on [0,1], where is a random variable of uniform distribution on [0,1],

$$Z=F^{-1}(X) \quad (4.5)$$

Is random distribution that possesses the distribution of F(u), and where $F^{-1}(X)$ is the inverse function of $F(Z)$. If samples $X_k=\{X_1, X_2, \ldots\}$ of the uniform distribution on [0,1] can be calculated based on the function:

$$Z_k=F^{-1}(X_k), \text{ k=1,2.....} \quad (4.6)$$

The samples of distribution F(Z) can be calculated too. After normalized the function, its random sample is produced by the method of normal distribution. The law of large numbers states that the average of many independent random variables with common mean and finite variances tends to stabilize at their common mean; that is,

$$\mathrm{Lim}_{n\to\infty} Pm = P, \text{ with probability 1} \quad (4.7)$$

So, when the number of m is large enough, then the probability can be calculated by:

$$P_{ks}=\frac{1}{m}\{f(ks^{(1)})+f(ks^{(2)})+\ldots+f(ks^{(m)})\} \quad (4.8)$$

4.3.2 Random variables for identifying 3 critical slip surface

Locating the critical slip surface is an important part of analyzing slope stabilities, and a large number of approaches have been developed to automate as much of this process as possible (Cheng, 2003). When the potential failure surface is considered circular in shape, the safety factor may be obtained from widely used methods such as that proposed by Bishop (1955). The circular slip surface is simpler to treat, because it is described by three variables only: the coordinates of the center and the radius.

A simple circular slip surface method is sufficient for a slope in a homogenous soil layer, while for a heterogeneous multi-soil layers slope, a non-circular slip surface method should be considered as circular methods can over predict the safety factor. It has been widely recognized that slip surfaces should not be restricted to a circular shape for most real problems (Zhu, 2001). Determination of a general-shaped critical slip surface is much more complex than

that of a circular critical slip surface. Many investigators have developed strategies to solve this problem. Celestina and Duncan (1981) developed a method in which the safety factor is formulated as a multivariate function *F(x)* with the independent variables *x* describing the geometry of the slip surface. He employed the simplex method as the optimization technique. Nguyen (1985) used the same approach for non-circular slip surfaces, but used the alternating-variable optimization technique. Li and White (1987) proposed a more efficient 1D optimization technique to replace the quadratic interpolation method, which Celestino and Duncan (1981) used in the alternating-variable technique. Baker (1980) defined the slip surface by a number of nodal points connected by straight lines. The vertical coordinates of the nodal points were the variables in Baker's method and the dynamic programming technique was employed as the optimal method. Bardet and Kapuskar (1989) presented a simple method of optimization to search the critical slip surface using the downhill simplex algorithm. Bolton *et al.* (2003) defined a global optimization algorithm for finding the critical slip surface by nodal points connected by straight lines for any shape of the slip. A large number of computations are needed to find the critical slip surface, as an arbitrary nodal coordinate could be irrelevant among the rest of created nodal coordinate.

These methods are only efficient for simulating a 2D slope slip surface. However, any slope slip process a 3D geometry, so it is rational to manage the slope three-dimensional in locating the critical slip surface. In 2D analyses, a series of lines could represent a sliding surface. Naturally, a series of planes could constitute a surface in 3D analysis (Cheng *et al.*, 2005). For simple slopes, the use of a series of planes for a prescribed 3D slip surface can be adopted without much difficulty. To locate general critical 3D slip surface by series of planes will have great difficulties in global optimization as the number of planes or control variables will generally be greater. The solution time will be tremendous and unbelievably long. Therefore, adopting a relatively simple shape to simulate the shape of slip surface is beneficial for locating of critical slip surface.

Considering that many practical failure surfaces presented an ellipsoidal shape, in this study, the initial slip surface is assumed to be the lower portion of an ellipsoid and subsequently, each random produced slip surface is changed according to the different strata strengths and presence of weak discontinuities. If a randomly produced slip surface, based on the lower part of an ellipsoid, is lower

than a weak discontinuous surface or the confines of the hard stratum, the weak discontinuity or the confined surface of the hard stratum will be prioritized for selection as one part of the assumed slip surface.

4.3.3 Identifying 3D critical slip surface with a computational process

The whole study area can be evenly divided into small rectangular meshes that are the same as the GIS based grids. For the numerical calculation of this grid-based 3D slope stability analysis, all of the calculation procedures are programmed by a Visual Basic. In this process, the function of data module is for obtaining all the slope related geological, geomorphologic and hydraulic data and the geomechanical parameters; the random variables production module is used for randomly selecting the trial slip surface by Monte Carlo simulating; the 3D safety factor is calculated in the 3D slope stability module; finally the critical slip surface and its safety factor can be obtained by many trials calculating.

In 3D limit equilibrium analysis, the critical slip surface can be located by a series of planes. For simple slope, the use of a series of planes for a prescribed 3D slip surface can be adopted without much difficulty. To locate general critical 3D slip surface by series of planes will have great difficulties in global optimization as the number of planes or control variables will generally be greater. The solution time will be tremendous and unbelievably long. Therefore, adopting a relatively simple shape to simulate the shape of slip surface is beneficial for locating critical slip surface.

In this study, for each slope unit, the critical slip surface is located using a Monte-Carlo simulation. It assumes the slip surface to be the lower part of an ellipsoid (Fig. 4.1). If a randomly generated ellipsoid is lower than the bedrock or discontinuity layer, the slip surface will consist of part of ellipsoid and part of bedrock or discontinuity layer, which shows a non-ellipsoid shape.

Six parameters, namely: (1) the central point (C), (2) the inclination angle (θ), (3) inclination direction (Asp) of the ellipsoid, and three axial parameters, (4) semi- minor axis (a), (5) semi- major axis (b), and (6) height (c), are used to describe the size and location of the simulated ellipsoid. The central point is randomly chosen within a certain range in the slope unit.

The inclination direction is set to the same main inclination direction of the slope unit. The geometrical parameters (a, b, c) and the inclination angle (θ)

are assumed to follow uniform distribution and are randomly selected in a certain range.

4.4 Slope-unit based regional slope stability evaluation

For the landslide-hazard assessment of a large mountainous area with complex geometry and geological conditions, a key problem is how to extract the appropriate slope unit for potential sliding-surface identification and minimum 3D safety-factor calculation. Slope unit, namely, the portion of the land surface delimited by watershed divides and the channel has similar topographic and geological characteristics. The suitability of the slope units for landslide-hazard assessment and other landrated study has been recognized by several authors (Hansen, 1984; Xie. M et al., 2003; Dymond et al., 1995). To improve the results related to the distribution of slope unit, the eliminate tool have been used in the feature of GIS data.

A slope unit, here, is defined as one slope part, or the left/right part of a watershed. Topologically, the slope unit can be divided by the ridge line and valley lines. In this study, a hydraulic model tool is employed to draw dividing lines for forming slope units. By using the hydraulic model tool, the watershed can be obtained from digital elevation model (DEM) data. Topologically, the outline of the watershed polygon is the ridge line. To detect the valley line, reverse DEM data is used. By DEM grid analysis, high DEM values can be turned into low values, and low DEM values can be turned into high values, so the original valley line can be turned into a rudge line. By using this reverse DEM data, the valley line can also be obtained by watershed analysis.

As has been argued, by combined the watershed by DEM and watershed by reverse DEM, the slope unit can be obtained. Fig.4.4 illustrates the flow chart for determining the slope unit by DEM. Using a hydro model, firstly by filling the DEM data, secondly by getting the flow direction by this filled DEM, then by calculating the accumulation, the watershed can eventually be calculated by setting the minimum number of cells that flow to the calculating point (cell). It is certain that with the minimum number of cells is increasing, a bigger watershed can be obtained. With reference to Fig 4.4, the division of the slope unit will be changed when the minimum number is set to 100 for No.1, 200 for No.2, 500 for No.3 and 1000 for No.4. This implies that, by setting this minimum number, different size slope units can also be obtained, and then different size landslides

can also be studied. The valley line is calculated by the reverse DEM, this reverse DEM being obtained by the following formula:

$$R\text{-}DEM = DEM \times (-1) + DEM(Max) \quad (4.9)$$

Where R-DEM is the elevation of reverse DEM, and DEM (Max) is the maximum elevation of DEM.

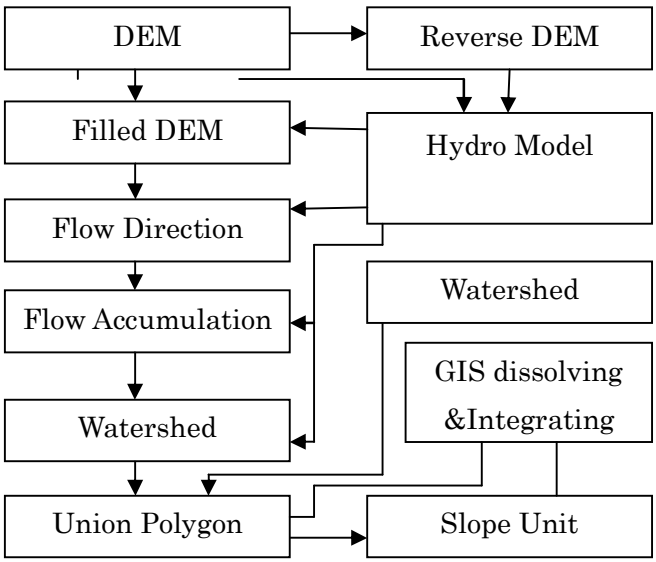

Fig.4.4 Flow chart for getting slope unit by DEM

After two watershed polygon classes are ready, using a GIS function, the union polygon can be obtained. This union polygon process may produce many spurious polygons and small or inharmonic polygon too, but after using "dissolving" and "integrating" GIS functions, the final result-slope unit polygon can be correctly determined. By using the slope unit polygon, the main inclination, slope angle and slope height of each slope unit can also be precisely calculated.

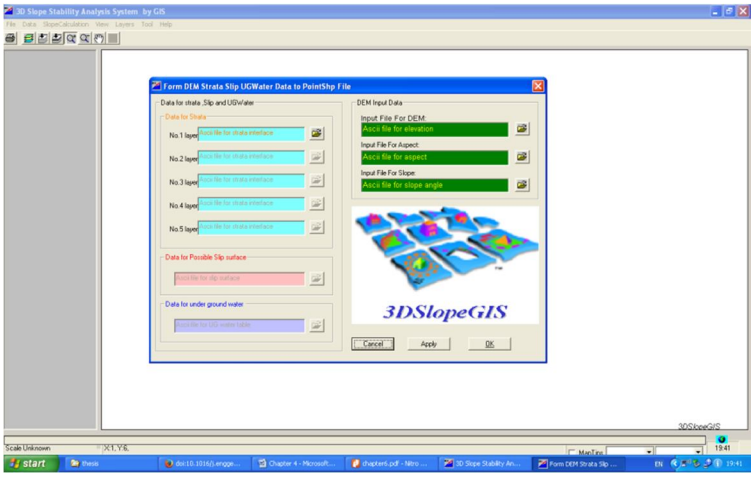

Fig.4.5. Interface of 3DSLOPE GIS tool for slope stability simulation (Xie, 2003)

4.5 Spatio-temporal estimation of shallow landslide hazard

4.4.1 Homogeneous layer

The interface of 3DSLOPE GIS for slope stability simulation is presented in Fig.4.5. Furthermore, the flowchart of GIS-based 3D deterministic landslide hazard assessment can be illustrated in Fig. 4.7. For each slope unit, stability evaluation includes using a Monte-Carlo simulation to locate possible slip surfaces and then applying one of three 3D limit equilibrium methods described in Section 3.2 to calculate the corresponding safety factors. After multiple runs of the calculation, the minimum safety factor is calculated and critical slip surface can be located in the corresponding slope unit. If all the slope units undergo this process, the distribution map of safety factors can be evaluated.

In this section, we consider the homogeneous layer of rock. To quantitatively assess the stability of a slope in engineering geology, a parameter F_{3D} known as factor of safety is introduced. A value F_{3D} >1 indicates stable, whereas F_{3D} ≤1 implies not stable. Thus, the transition between stability to collapse may be envisaged mathematically as a decrease in the factor of safety to values below unity.

4.4.2 Multi layer (consideration of weather layer)

The slope stability problem can be considered as a system with many potential failure surfaces. However, the determination of the exact system reliability of the slope stability problem is not possible. Therefore, the probability of the most critical slip surface is commonly used as the estimate of the system

failure probability. This approach assumes the probability of failure along different slip surfaces is highly correlated (Mostyn and Li, 1993; Chowdhury and Xu, 1995).

A common approach to a probabilistic analysis is to locate the critical deterministic surface and then calculate the probability of failure corresponding to this surface. However, the surface of the minimum factor of safety may not be the surface of the maximum probability of failure (Hassan and Wolff, 1999). Therefore, in this study, the three-dimensional safety factor of slope can be calculated based on the grid-based data from the following in the equation (4.10).

$$SF_{3D} = \frac{\sum_J \sum_I [c'A + (W\cos\theta - U)\tan\phi']\cos\theta_{Avr}}{\sum_J \sum_I W\sin\theta_{Avr}\cos\theta_{Avr}} \tag{4.1}$$

Where, SF_{3D}: the 3D slope safety factor; W: the weight of one column; A: the area of the slip surface; c: the cohesion; ϕ: the internal friction angle; θ: the normal angle of slip surface: and J,I: the amount of row and column of the pixel in the range of slope failure.

The principal source of variability in the 3D safety factor calculation will come from two geomechanical parameters, such as the cohesion (c) and the friction angle (ϕ)(Xie, et all, 2003). During heavy rains, water seeps into the ground and travels through unsaturated soils, as shown in Fig.4.6. The results of measurements at various field sites indicate that the unsaturated gradient is generally directed vertically downward during steady rainfall (Abramson *et al.*, 2002). This water may perch on lower permeability materials or a drainage barrier such as bedrock and a soil surface as rock weathering, creating a temporary, localized saturated zone.

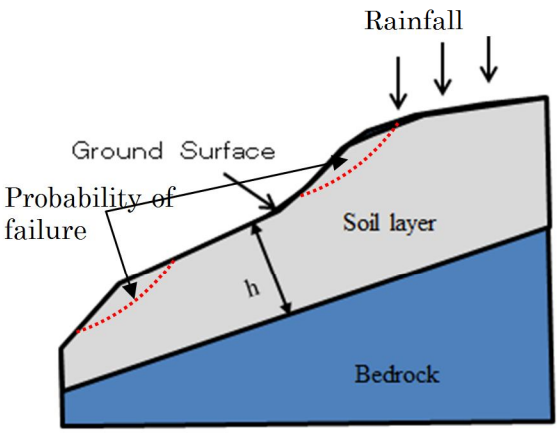

Fig.4.6 Diagrammatic representation of effects of soil depth (h) on slope

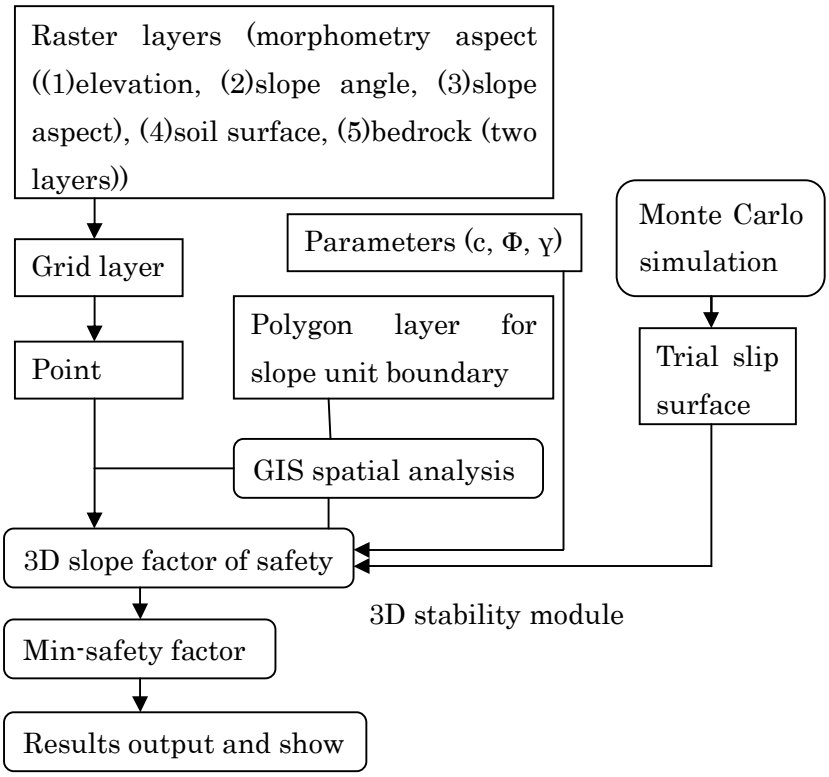

Fig.4.7 Computational processes for min-3D safety factor of soil depth effect in the slope stability analysis.

4.4.3 Effect of rainfall

One of the important factors that induce instability in slopes is the effect of rainfall. Landslides often take place in mountainous areas after intense rainfall and pose a great threat to human lives and property. It is necessary to study the mechanisms of slope failure induced by intense rainfall.

Rainfall-induced shallow landslides, also called “soil slips”, are becoming ever more frequent all over the world and are receiving a rising interest in consequence of the heavy damage they produce. Landslides often take place in mountainous area after intense rainfall and pose a great threat to human lives and property. It is necessary to study the mechanisms of slope failure induced by intense rainfall.

Both shallow and deep-seated landslides can be triggered by rainfall, with frequencies, both in time and space, and under the effect of different types of storm (Casagli et al. 2006). Generally, shallow landslides are the more common failure through which rainfall affect slope stability, as short, quick rainstorms are

common. The rapid growth of pore-water pressure, a rise groundwater level, and a loss of the component of apparent cohesion have been well established to be caused by rainfall (Crosta and Frattini 2003; Qiu et al. 2007).

Methods of analysis developed for saturated slopes of soil and rock can be extended to slopes comprising unsaturated soil zones as well. However, the relevant shear strength equation (different from that applicable to saturated soils) must be used. In unsaturated soils, rainfall triggered failures are a consequence of the elimination of negative pore-water pressures (soil suctions). Thus, it is necessary to estimate the distribution of suctions (negative pore pressures) within unsaturated soil zones.

Moreover, in many situations where shallow failures are concerned, studies have noted that the failure is attributed to the advance of a wetting front—the interface between wet soil and dry soil—into the slope instead of a rise in the groundwater level (Chou and Lee 2002; Kim et al. 2004; Ng et al. 2001). As the rainfall begins to infiltrate the slope from the surface, the wetting front advances into the soil and causes an increase of volumetric water content, which reduces soil suction. The loss of matric suction decreases the shear strength of the soil below the mobilized shear strength along the potential slip surface. Infiltration of rainfall into a residual soil slope may impair slope stability by changing the pore water pressure in the soil, which in turn controls the water content of the soil. Slope failures occur if the reduced shear strength becomes less than the resisting shear strength needed for equilibrium (Kim and Lee 2010). Several analyses have been proposed to simulate the infiltration process and its corresponding impact on slope stability (Chou and Lee 2002; Gasmo et al. 2000; Jia et al. 2009; Ng and Shi 1998). The integration of the rainfall infiltration model into slope stability analysis is advantageous in better understanding the extent of variation in the stability of a slope under rainfall. A simplified water-flow model allow to relate directly the safety factor of slope with rainfall amount and can thus be easily extended to a regional scale (Montrasio et al. 2008).

Rainfall Infiltration Model

Infiltration is the process through which ground surface water enters the soil. During a rainfall event, if the rainfall intensity is low and less than the infiltration capacity of the soil, all the rainfall will infiltrate the soil. If the rainfall intensity is heavy and exceeds the infiltration capacity, the soil surface will become ponded.

Thus, there are two distinct infiltration stages during a rainfall event: infiltration without surface ponding and infiltration with surface ponding.

Throughout the history, various infiltration models have been established to describe this process (Green and Ampt 1911; Philip 1957; Richards 1931; Smith et al. 1993; Montrasio and Valentino 2008). Among these, the Green and Ampt (GA) model is considered the preferred model in this study, although it is not the most accurate in predicting the wetting front of infiltration. The more accurate models contain parameters that are difficult to predict for geotechnical engineers or engineering geologists, while the variables in GA model are all predictable, since they have physical significance. For example, in the Richard model, the distribution of hydraulic conductivity with soil suction must be predicted, while in GA model, only the saturated hydraulic conductivity is needed. Furthermore, the GA model is easily programmed. Qi (2006) once did a study to compare the respective performances of the Richard, Philip, and GA models and concluded that GA model is acceptable if only the cumulative infiltration is concerned, which corresponds with the objective of this study to evaluate rainfall-induced slope stability. As a 1D model, the GA model cannot simulate the spatial distribution of infiltration process; however, this study focuses on individual landslides that cover a small range.

In the GA model, there are four assumptions: (1) the soil surface is continuously wet by water ponding; (2) as rain continues to fall and the water infiltrates, the wetting front advances at the same rate with depth, producing a well-defined wetting front; (3) the volumetric water contents remain constant above and below the wetting front as it advances; and (4) the soil-water suction immediately below the wetting front remains constant in both time and location as the wetting front advances.

Different GA model based approaches exist for modeling infiltration for a steady rainfall event and modeling infiltration for an unsteady rainfall event. In the case of steady rainfall, infiltration starts with an unponded surface that later changes into a stage with surface ponding, which lasts until the end of the rainfall event. A single ponding time, at most, occurs in a steady rainfall. In the case of an unsteady rainfall event, however, there may be several periods when the rainfall intensity exceeds the infiltration rate. The infiltration process may change from one stage to another and shift back to the original stage in a recurrent style (Chu

1978). Therefore, modeling rainfall infiltration separately according to the steady conditions of rainfall is reasonable.

As shown in Fig. 4.8, according to Darcy's law, the infiltration rate is given by

$$f=K_s\frac{\omega f+Zf}{Zf} \tag{4.11}$$

The depth of the wetting front can be related to the cumulative amount of infiltrating water by

$$F=Z_f(\theta_s-\theta_i) \tag{4.12}$$

Rearranging Equation (4−11) to solve for Z_f and applying it to Equation (4−12), the infiltration rate at any time t becomes

$$f(t)=K_s+K_s\frac{\psi f(\theta s-\theta i)}{F} \tag{4.13}$$

The expression of $F(t)$ can be stated as follows:

$$t=t_p+\frac{1}{Ks}[F-F_p+\psi_f(\theta_s-\theta_i)\ln(n)] \tag{4.14}$$

$$n=\frac{\psi f(\theta s-\theta i)+Fp}{\psi f(\theta s-\theta i)+F} \tag{4.15}$$

t_p and F_p can be calculated from the following equations:

$$t_p=\frac{Fp}{P} \tag{4.16}$$

$$F_p=\frac{\psi fKs(\theta s-\theta i)}{P-Ks} \tag{4.17}$$

Where f(t) is the infiltration rate (m/h) at time t (h); K_s is the soil saturated hydraulic conductivity (m/h); ψ_f is the matrix suction at the wetting front (m); Z_f is the depth of the wetting front (m); F is the cumulative amount of infiltrated water (m); θ_s is the soil saturated volumetric water content; θ_i is the initial soil volumetric water content; t_p is the time when water begins to pond on the soil surface (h); F_p is the amount of water that infiltrates before water begins to pond on the surface (m); and P is the rainfall rate (m/h).

It should be noted that a necessary condition for Equation (4-13) to (4-17) is that the rainfall rate must be greater than the soil hydraulic conductivity. If the rainfall

rate is not greater than the potential infiltration rate ($P \leq K$) or no surface ponding occurs ($t \leq t_p$), then all rainfall will infiltrate into the soil without runoff, and the actual infiltration rate is equal to the rainfall rate.

$$f(t)=P \tag{4.18}$$

$$F=Pt \tag{4.19}$$

Parameters of a typical soil used in the equations above can be obtained from a geotechnical test or from the literature (Ranwls *et al.*, 1983; Ogden and Saghafian, 1997).

Unfortunately, an iterative procedure is needed to calculate the infiltrated depth at a specific time because Equation (4-14) is not expressed explicitly as a function of time and the cumulative infiltration. Serrano (2003) proposed an approximate formula that can yield a solution very close to the exact solution under the condition that the rainfall rate is not very high relative to the soil saturated hydraulic conductivity.

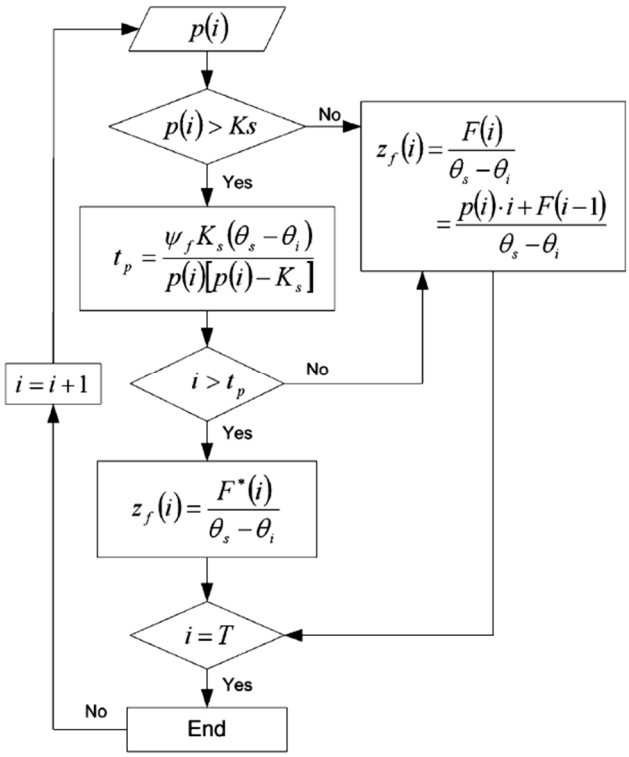

Fig.4.8 Flowchart of infiltrated depth calculating during duration T of rainfall

Integrating of the infiltration model with a cohesion model

Fig. 4.9 illustrates the computational procedures for estimation of rainfall induced slope stability. In the model, the integration of hydrological model is present. The cohesion value in the model, the considering of the effective cohesion (c') and the apparent cohesion (cψ) related to the matric suction is present. Montrasio et.all (2006) present the cohesion model by the following equation (4.20) :

$$c = c' + c\psi \tag{4.20}$$

where c' is the effective cohesion of soil; c_ψ represents the apparent cohesion related to the matric suction, which in turn, depends on the degree of saturation of the soil. We do follow the basis of the Mohr-Coulomb failure criteria. Mohr-Coulomb failure criteria for saturated soils are defined by the following equation (4.21):

$$\tau = (\sigma - u_w).\tan \Phi' + c' \tag{4.21}$$

where c' is the effective cohesion of soil and Φ' the shear strength angle. Fredlund and Rahardjo (1933) proposed equation (4.22) for unsaturated soils, such as :

$$\tau = c + (\sigma - u_a).\tan \Phi' + (u_a - u_w).\tan \Phi^b \tag{4.22}$$

where $(\sigma - u_a)$ is the net normal stress state on the failure plane at failure, u_a is the pore-air pressure on the failure plane at failure, $(u_a - u_w)$ is the matric suction and Φ^b is the angle indicating the rate of increase in shear strength relative to the matric suction $(u_a - u_w)$.

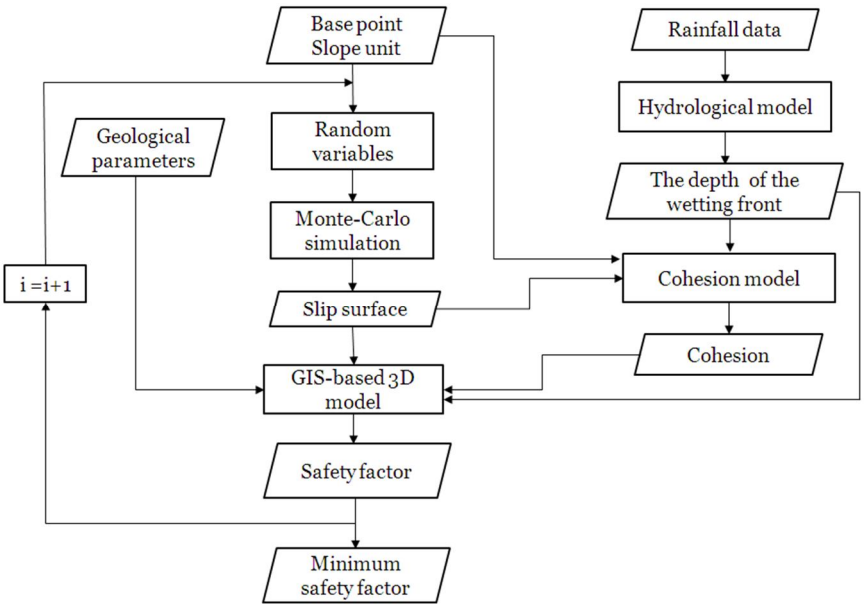

Fig.4.9 The computational procedures for estimation of rainfall induced slope stability

As reported by Montrasio et al (2008), Peterson (1988) proposed the following equation:

$$\tau = c' + (\sigma_n - u_a).\tan \Phi' + c_\psi \quad (4.23)$$

where c_ψ represents the apparent cohesion related to the matric suction, which in turn, depends on the degree of saturation of the soil. Regarding this, Fredlund et al (1996) presents the model of relationships a shear strength and degree of saturation for two soil samples (Fig 4.10). It was preferable to express the shear strength as a function of the degree of saturation, due to the relationship between the water content, the degree of saturation and the matric suction. In the experiment, $c_\psi - S_r$ trend can be fitted by a curve having a peak, whose value depends on the type of soil and corresponds to a degree of saturation approximately equal to 0.7.

Therefore, it can be reasonably approximated by curves having the following equation:

$$c_\psi = A.S_r.(1-S_r)^\lambda \quad (4.24)$$

where S_r is the degree of saturation; A is a parameter depending on the kind of soil and is linked to the peak shear stress at failure; λ is a numerical parameter which allows to translate the peak of the curve along the abscissa axis.

In this study, the groundwater table is consider to calculated the safety factor in the simulation. Moreover, the degree of saturation has been calculated by considering the depth of wetting front (H_w), the depth of the slip surface (Z), and the depth of the groundwater table (Z_w). However, if it does not consider groundwater, we need to estimate the ratio of the initial soil volumetric water content (θ_i) and the soil saturated volumetric water content (θ_s). The following is the equation of the saturation degree calculation:

$$S_{rAvr} = (H_w + (Z - H_w)S_{r1})/Z \quad (4.24)$$

Which $S_{r1} = \theta_1/\theta_s$,

If considering groundwater,

$$S_{rAvr} = (H_w + Z - Z_w + (Z - H_w)S_{r1})/Z \quad (4.25)$$

For a given rainfall intensity, the permeation depth at a specified time can be predicted by the infiltration model described above. At the same time, taking a cell of the raster dataset to be the central point of an ellipsoid, a trial slip surface can be formed using the Monte Carlo simulation model. A safety factor is calculated subsequently by the 3D slope stability model, depending on the relationship between the permeation depth and the location of the slip surface.

After many trials, the critical slip surface and the associated safety factor, which is the minimum of all the trial calculations, can be obtained. The safety factor is then saved to a point dataset as the safety factor of the raster cell. Also, if the safety factor is < 1, the information for the corresponding critical slip surface, such as location, shape, and volume, will be saved in the format of a polygon. In this way, the safety factor at a specified time can be calculated for all raster cells inside the slide mass range. As a result, the location of occurrence of a landslide can be predicted by means of the decrease of the safety factor along with the amount of rainfall.

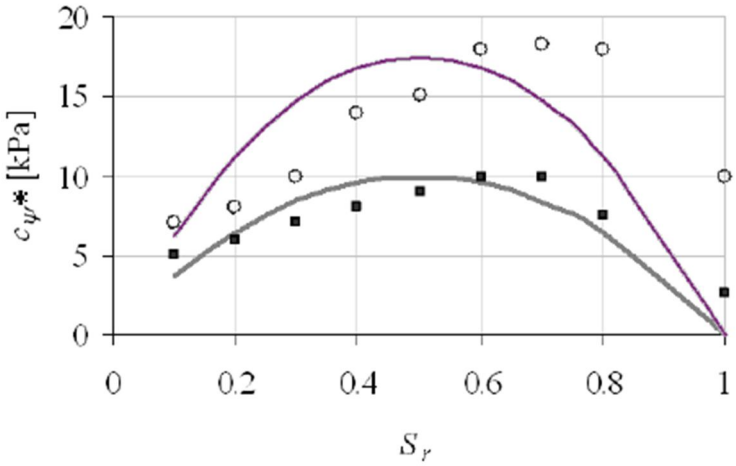

Fig.4.10. Relationships between shear strength versus degree of saturation for two soil samples (modified from Fredlund et al., 1996 in Montrasio et.al., 2008).

Combination of the infiltration model with the 3D slope stability model

Integrating Hovland' s (1977) 3D model and the GIS raster data format, a new GIS-based 3D model, in which the safety factor can be derived from the horizontal force equilibrium in the direction of sliding, will be proposed in the Chapter 5.

$$SF_{3D} = \frac{\sum_J \sum_I (cA + W \cos\theta \tan\phi) \cos\theta_{Avr}}{\sum_J \sum_I W \sin\theta_{Avr} \cos\theta_{Avr}} \tag{4.26}$$

Where SF_{3D} is the 3D safety factor of the slope; c is cohesion (kN/m^2); A is the area of the slip surface (m^2); W is the weight of one soil column (kN); ϕ is the friction angle (^{0}); θ_{Avr} is the angle between the direction of movement and the

horizontal plane (^{0}); and *J, I* are the numbers of rows and columns of the cell within the range of failure mass.

Fig.4.15 shows the interface of system 3D slope GIS combining with Hydrological model. It is widely known that rainfall causes a rise of groundwater level as well as an increase in pore water pressure that results in slope failure. However, in many situations where shallow failures are concerned, it has been noted that the failure was attributed to the advance of a wetting front into the slope instead of a rise in the groundwater level (Ng *et al.*, 2001; Cho and Lee, 2002; Kim *et al.*, 2004). The wetting front causes a reduction in soil suction (or negative pore pressure) and an increase in the weight of soil per unit volume. These results in a process in which soil resistant strength decreases while total stress increases, until failure occurs on the potential failure surface where equilibrium cannot be sustained.

Under these conditions, there are four possible situations regarding the slip surface that can be anticipated, and four models, based on the Equation (6-15), are thus proposed to calculate the corresponding safety factors.

1. The slip surface form in the unsaturated zone between the wetting front that is advancing from the ground surface and the groundwater table, as shown in Fig. 4.11. In this situation, the horizontal resistance force F_1 and the horizontal sliding force F_2 acting on the slip surface can be calculated using Equation (4-27) and Equation (4-28), respectively.

$$F_1=\{c_1'A'+[\gamma_1 Z+(\gamma_{sat}-\gamma_i)H_w]A\cos\theta\tan\Phi'\}\cos\theta_{Avr} \quad (4.27)$$

$$F_2=[\gamma_1 Z+(\gamma_{sat}-\gamma_i)H_w]A\sin\theta_{Avr}\cos\theta_{Avr} \quad (4.28)$$

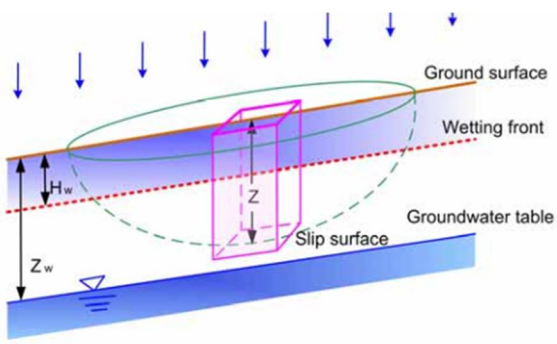

Fig 4.11 Model1: slip surface forms between the wetting front and the groundwater table

2. The slip surface forms in the saturated zone between the ground surface and the wetting front that is advancing from the ground surface, as shown in Fig.

4.12. In this situation, the horizontal resistance force and the horizontal sliding force can be calculated using Equation (4-29) and Equation (4-30), respectively.

$$F_1=[c'_wA'+(\gamma_{sat}z\cos\theta-u_w)A\tan\Phi'\}\cos\theta_{Avr} \quad (4.29)$$

$$F_2=\gamma satzA\sin\theta_{Avr}\cos\theta_{Avr} \quad (4.30)$$

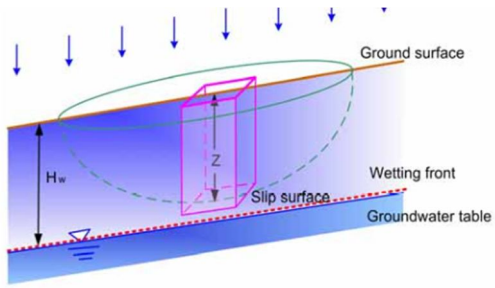

Fig. 4.12 Model2: slip surface forms between the ground surface and the wetting front

3. The slip surface forms in the saturated zone under the groundwater table and the unsaturated zone exists between the wetting front and the groundwater table, as shown in Fig. 4.13. In this situation, the horizontal resistance force and the horizontal sliding force can be calculated using Equation (4-31) and Equation (4-32), respectively.

$$F_1=\{c'_wA'+[\gamma_i(z_w-H_w)+\gamma_{sat}(H_w+z-z_w))\cos\theta-u_w]A\tan\Phi'\}\cos\theta_{Avr} \quad (4.31)$$

$$F_1=[\gamma_i(z_w-H_w)+\gamma_{sat}(H_w+z-z_w)]A\sin\theta_{Avr}\cos\theta_{Avr} \quad (4.32)$$

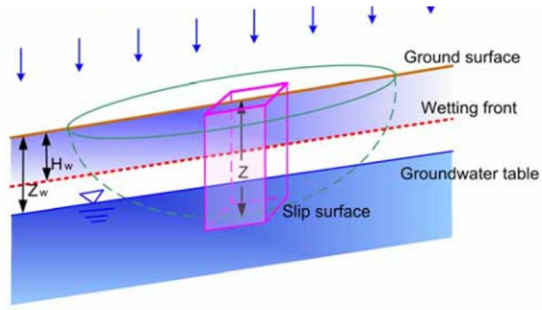

Fig.4.13 Model3: slip surface forms under the groundwater table and the unsaturated zone exists

4. The slip surface forms in the saturated zone under the groundwater table and the wetting front that has reached the groundwater table, as shown in Fig. 4.14.

The horizontal resistance force F_1 and the horizontal sliding force F_2 can be calculated using Equation (4-29) and Equation (4-30), respectively.

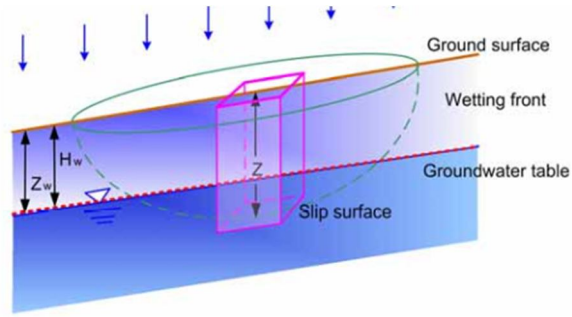

Fig. 4.14 Model4: slip surface forms under the groundwater table

where is the 3D safety factor of the slope; F_1 is the horizontal resistance force (kN); F_2 is the horizontal sliding force (kN); γ_{sat} is the saturated unit weight of soil (kN/m^3); γ_i is initial unit weight of soil (kN/m^3); c'_i is the initial effective cohesion of soil (kN/m^2); c'_w is the saturated effective cohesion of soil (kN/m^2); ϕ is the effective friction of soil (º); z_w is the depth of the wetting front (m); H_w is the depth of the groundwater table (m); z is the depth of the slip surface (m); u_w is the pore stress (kN/m^2); A is the area of the soil column (m^2); A' is the area of the slip surface of the soil column; θ is the inclination of the slip surface (º); θ_{Avr} is the dipangle of the main sliding direction (º); and J,I are the numbers of rows and columns of the cell in the range of failure mass.

The importance of uncertainties in geotechnical engineering and engineering geology is now widely understood. There are systematic uncertainties related to the estimation of geotechnical parameters because of the limits to the extent and quality of investigation and testing. It is also necessary to consider the natural variability of parameters, both spatial and temporal. For example, one frequently encounters spatial variability of shear strength parameters and pore-water pressures in natural slopes.

Consequently, there are limitations to the conventional deterministic methods of analysis and the calculated factor of safety, often designated by F, may not be a true reflection of the reliability of a slope. New approaches within the framework of statistics and probability have, therefore, been developed.

The components of 3DSlope GIS combined with an infiltration model are provided in the Table 4.1. The items of component consist of input data, data

processing, and output data. In the Table 4.1, the contribution of combining of 3DSlope GIS with infiltration model is clearly by points for each item.

4.5 Verification of results

Spatial effectiveness of the susceptibility map will be checked by the highest percentage of the actual slope failure by comparing the predicted unstable site.

The relationship between number of slope failure occurrence and number of slope unit by 3D slope stability analysis based on Factor of Safety (FS) criteria are the assumption that be used in the performance task. The frequency ratio is the ratio of the slope unit where slope failure occurred in the total slope unit in the study area, and also, is the ratio of probability of slope failure occurrence of a non-occurrence for a given factor's attribute.

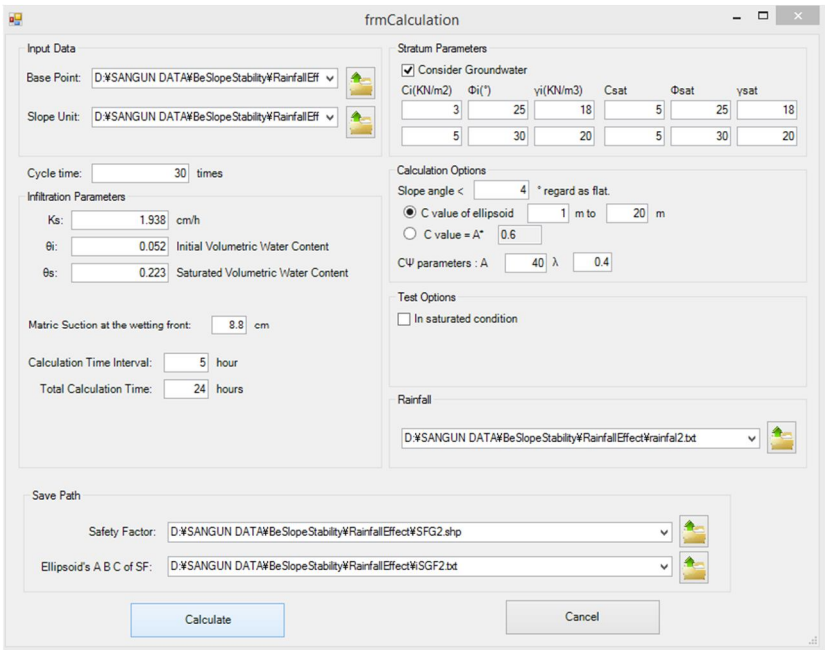

Fig.4.15 The interface of system 3D slope GIS combining with infiltration model

Table 4.1 The data components of system 3D slope GIS combined with infiltration model

Items	**3D Slope GIS**	**A 3D Slope GIS combines with Infiltration model**
Input data	− Elevation, slope angle, and slope aspect − Division of slope unit − Geotechnical data (cohesion, friction angle, and unit weight). − Soil distribution data	− Elevation, slope angle, and slope aspect − Division of slope unit − Geotechnical data (cohesion, friction angle, and unit weight). − Soil distribution data − Rainfall data − Infiltration parameters (saturated hydraulic conductivity, initial volumetric water content, saturated volumetric water content, matric suction) − An apparent cohesion related of soil type (λ and A) − Groundwater data
Data processing	−Monte Carlo simulation −Range of depth of failure (c)	− Monte Carlo simulation − Range of depth of failure (c) − Time interval of results related rainfall − Total of time calculation
Output data	−A map contains slope units and safety factor	− A map contains slope units and safety factor − A total number of maps depend of number of time intervals

4.6. Conclusion

The GIS-aided methodologies aiming at regional landslide hazard assessment, including the 3D slope stability analysis model and the infiltration model has been presented. The components of 3DSlope GIS combined with an infiltration model are provided in the Table 4.1. Items of component consist of input data, data processing, and output data. In the Table 4.1, the contribution of combining of 3DSlope GIS with infiltration model is clearly by points for each item. This model is effective of the large area with considering the rainfall effect and infiltration parameters.

References

Collison, A., Wade, S., Griffiths, J. & Dehn, M. 2000. Modelling the impact of predicted climate change on landslide frequency and magnitude in SE England. Engineering Geology 55: 205–218.

Dehn, M., Bürger, G., Buma, J. & Gasparetto, P. 2000. Impact of climate change on slope stability. Engineering Geology 55: 193–204.

Popescu, M., (1994) "A suggested method for reporting Landslide causes", Bull of Int. Assoc. Engineering Geology, 50, 71-74.

Wu W, Sidle RC (1995) A distributed slope stability model for steep forested basins. Water Resour Res 31(8):2097–2110

Crosta, G. B., and Frattini, P. (2003). "Distributed modelling of shallow landslides triggered by intense rainfall." *Natural Hazards and Earth System Science*, 3(1-2), 81-93.

Casagli, N., Dapporto, S., Ibsen, M. L., Tofani, V., and Vannocci, P. (2006). "Analysis of the landslide triggering mechanism during the storm of 20th-21st November 2000, in Northern Tuscany." *Landslides*, 3(1), 13-21.

Qiu, C., Esaki, T., Xie, M., Mitani, Y., and Wang, C. (2007). "Spatio-temporal estimation of shallow landslide hazard triggered by rainfall using a three-dimensional model." *Environmental Geology*, 52(8), 1569-79.

Cho, S. E., and Lee, S. R. (2002). "Evaluation of surficial stability for homogeneous slopes considering rainfall characteristics." *Journal of Geotechnical and Geoenvironmental Engineering*, 128(9), 756-763.

Gasmo, J. M., Rahardjo, H., and Leong, E. C. (2000). "Infiltration effects on stability of a residual soil slope." *Computers and Geotechnics*, 26(2), 145-165.

Jia, G. W., Zhan, T. L. T., Chen, Y. M., and Fredlund, D. G. (2009). "Performance of a large-scale slope model subjected to rising and lowering water levels." *Engineering Geology*, 106(1-2), 92-103.

Ng, C. W. W., Wang, B., and Tung, Y. K. (2001). "Three-dimensional numerical investigations of groundwater responses in an unsaturated slope subjected to various rainfall patterns." *Canadian Geotechnical Journal*, 38(5), 1049-1062.

Cheng, Y.M., 2003. Locations of critical failure surface and some further studies on slope stability analysis. Computers and Geotechnics 30, 255–267.

Chowdhury, R.N., Xu, D.W., 1995. Geotechnical system reliability of slopes. Reliability Engineering and Systems Safety 47, 141–151.

Christian, J.T., Ladd, C.C., Baecher, G.B., 1994. Reliability applied to slope stability analysis. Journal of the Geotechnical Engineering Division, ASCE 120, 2180 –2207.

D'Andrea, R., 2001. Discussion of "Search algorithm for minimum reliability index of earth slopes " by Hassan and Wolff. Journal of Geotechnical and Geoenvironmental Engineering, ASCE 127 (2), 195–197.

Elkateb, T., Chalaturnyk, R., Robertson, P.K., 2002. An overview ofsoil heterogeneity: quantification and implications on geotechnical field problems. Canadian Geotechnical Journal 40, 1–15.

Richards, R. A. (1931). "Capillary conduction of liquid through porous media." *Physics*, 1, 318-333.

Philip, J. R. (1957). "The theory of infiltration: 1. The infiltration equation and its solution." *Soil Sci*, 83, 345-357.

Green, W. H., and Ampt, G. A. (1911). "Studies on soil physics Part I - The flow of air and water through soils." *Journal of Agricultural Science*, 4, 1-24.

Serrano, S. E. (2003). "Improved decomposition solution to green and ampt equation." *Journal of Hydrologic Engineering*, 8(3), 158-160.

Smith, R. E., Corradini, C., and Melone, F. (1993). "Modeling Infiltration for Multistorm Runoff Events." *Water Resources Research*, 29(1), 133-144.

Kim, J.Y., Lee, S.R., 1997. An improved search strategy for the critical slip surface using finite element stress fields. Computers and Geotechnics 21 (4), 295–313

CHAPTER 5

GIS-BASED SLOPE FAILURE HAZARD ANALYSIS AND PREDICTION IN SANGUN MOUNTAINOUS, FUKUOKA PREFECTURE, JAPAN

5.1 Introduction

On July, 2003, following a short duration of heavy rainfall, a slope failure disaster occurred in the Sangun Mountain area, Fukuoka Prefecture, Japan. This disaster was triggered by a landslide. In order to assess the slope failure hazard potential in the future, the study of probability of slope failure is critical. The prediction of the location, intensity and time or periodicity of landslides is the primary goal of the landslide hazard assessment (Ondrasik. R.,2002). The prediction of localities with landslides potential or probability is the simplest case. Analyze the relationship between landslides and the various factors causing landslides not only provides an insight to understand landslide mechanisms, but also can form a basis for predicting future landslides and assessing the landslide hazard. Chunxiang.W.et.al (2005), summarized that in areas with the similar geotechnical conditions, researchers generally make two fundamental assumptions. Such as, the one hand, landslides will occur in the same geological, geomorphological, hydrogeological and climatic conditions as in the past. On the other hand, the properties and types of landslides will also be the same. Therefore, the study of the mechanisms and properties of past landslide is a valuable reference for assessing the future landslide hazard in its adjacent or geotechnically similar area.

Here, we demonstrated the implementation of the 3D slope stability modelling to assess the factor of safety (FS) of the whole slope units based on sub catchment and produce a reasonable cohesion values. The critical 3D slope stability simulation gave the results about the relationship on between morphological aspect and Geotechnical parameters. The Factor of Safety (FS) values has become important to explain the susceptibility of landslide. In this analysis is a concern for two parts of FS value ranges, such as FS≤1.0, and FS>1.

In this study, we have considered the homogeneous layer, soil depth effect and rainfall effect. However, there was no information about an influence on the type of soils on the occurrence. Moreover, in the slope stability analysis, soil

thickness is an important input parameter. Shallow landsliding in soil-mantled landscapes can generate debris flows which scour low order channels, and deposit large quantities of sediment in higher order channels (Costa et al, 1987). At the catchment scale, an active geomorphologic process is dominant, such as soil erosion and landsliding (Catani et al, 2010). Moreover, this variability is considered by the deterministic approach that explicitly incorporates the influences of rainfall to the water content and shear strength of soil. Therefore, it is suggested to study rainfall-induced slope stability with deterministic approach. In this study, a combining the 3D slope stability model with rainfall infiltration model was developed to predict the failure into a slope due to rainfall and its effect on soil slope behavior.

Furthermore, the observation of relationships between the distribution of slope failures in the past and probability of the occurrence slope failure based on 3D slope stability analysis is carried out by determining the best-fit model for each geotechnical parameter value. In this study, the frequency ratio (FR) model is used, furthermore, the reasonable value obtained. Moreover, the effect of soil depth and rainfall was analyzed to obtain more knowledge about hydrology control in slope failure susceptibility.

5.2 Study area and slope failure historical

The catchment is located in the mountain region in northern Kyushu, Japan, the Sangun mountain massif (Fig.5.1). The geology consists mainly of Mesozoic granitic rock. Paleozoic and Mesozoic metamorphic rocks can be also observed on some valley slopes as roof pendants, but they are limited. The mountainous catchment, especially in the Sangun region is hazardous areas for sediment disasters. On July 18-19, 2003, a short duration, high-intensity rainfall event impacted the city of Sangun area in Fukuoka Prefecture, Japan (Fig.5.3). The rainfall triggered many landslides and debris flows (Hanamura et.al., 2004). The slope failure and resultant debris flow in a Sangun area in Fukuoka was the largest and most damaging of these disasters. A moderate-size, 1-8 m deep debris avalanche triggered the debris flow about 0.5 km at the upslope of where the casualties occurred. The rainfall intensity that plunging into the village of Sangun area was estimated about 315 mm /day, and the density of slope failure were estimated about 48 points/km^2. Based on the aerial map and field investigation, the number of slope failure in the study area was about 55 points.

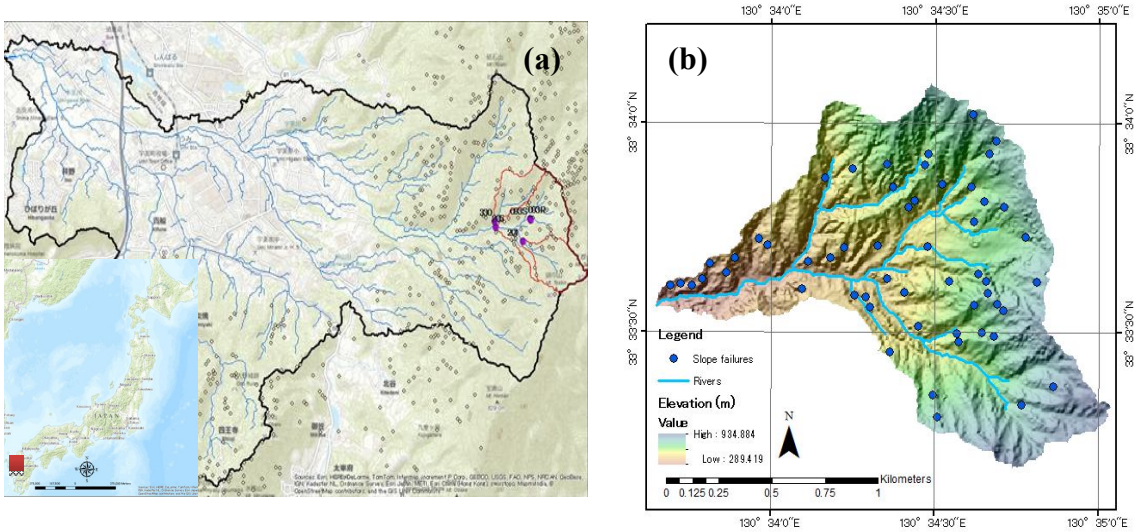

Fig.5.1 Sangun basin boundary (a) and small studied catchment in the upstream part (b) which have been selected for the study area.

5.3 Data preparation

5.3.1 GIS data creation

The following Geo-spatial data were prepared for the slope stability analysis: (1) geology map, scale 1: 200,000 obtained from the Geological Survey of Japan, AIST 2005 and (2) airborne laser survey data (LiDAR data), provided by local government in Japan. The LiDAR data were a point cloud with only attributes of x, y and z values. In this study, minimum-z-values in each 5 m-grid were assumed as ground elevations to create a DTM. For obtaining an elevation, aspect, slope angle information, a DEM data for ground surface with 5m mesh size were utilized by using the Spatial Analyst tool of Arc GIS 10.2 (a GIS software by ESRI, USA), as show in Fig. 5.2.

Geotechnical data, including cohesion, friction angle, and unit weight of soil surface and bedrock of granite rock were derived from the laboratory test of previous studies conducted in the area and literature review (Table 5.1). In this study, slope failures location map is prepared based on the previous researches conducted in the area and aerial photographs. The instability factors were chosen based on the above-mentioned studies which were carried out from literatures and field investigations.

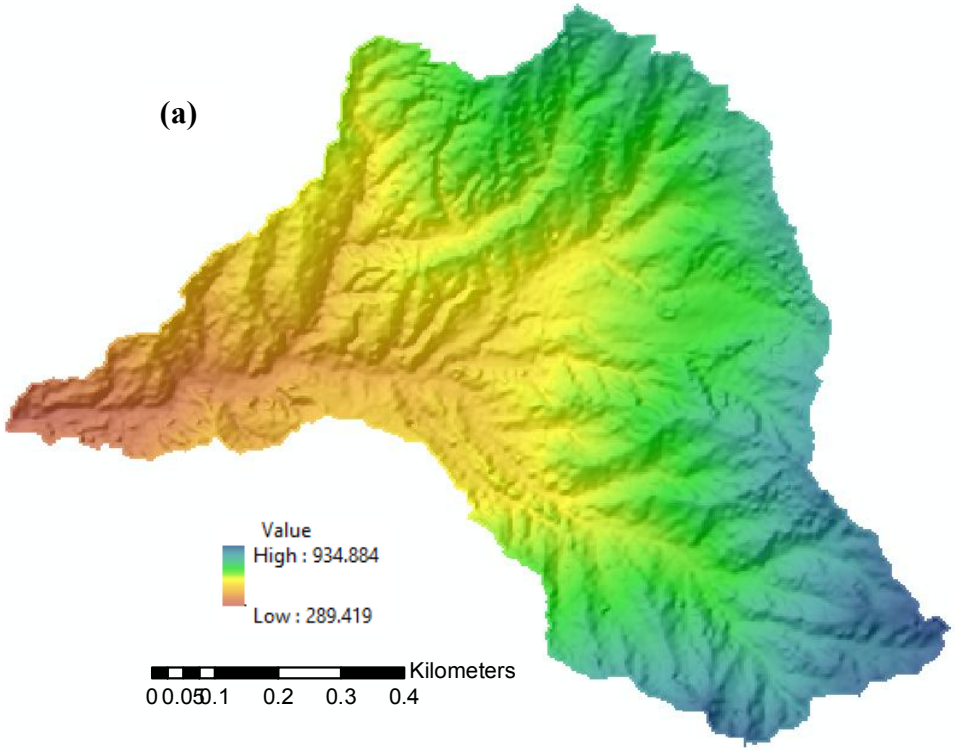
(a)
Value
High : 934.884
Low : 289.419
Kilometers
0 0.05 0.1 0.2 0.3 0.4

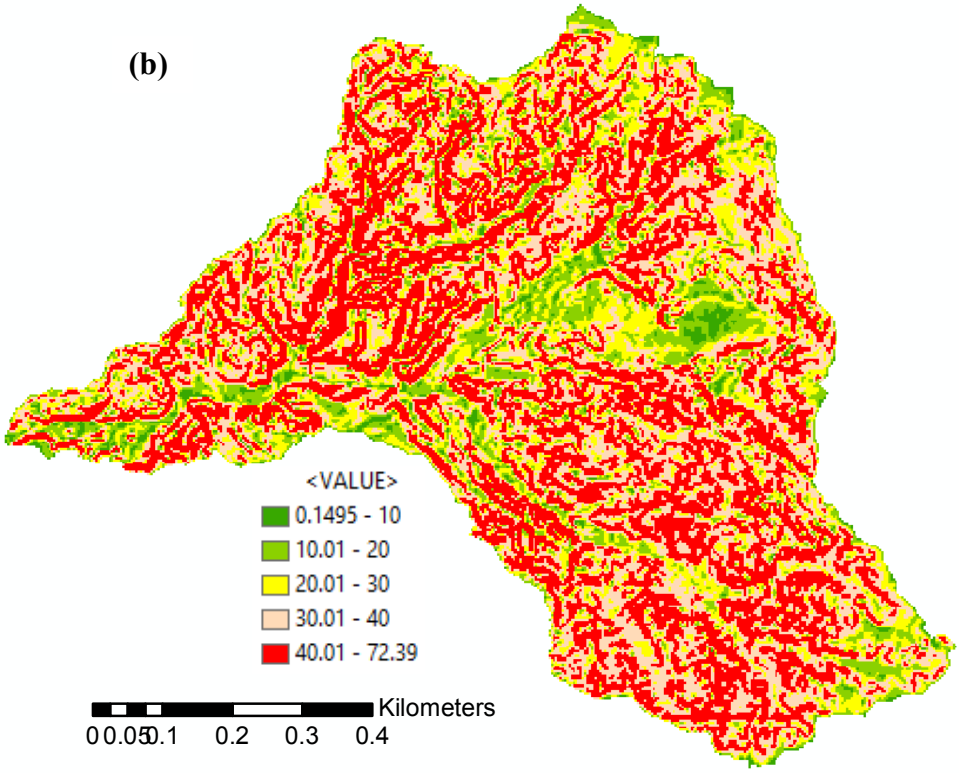
(b)
<VALUE>
0.1495 - 10
10.01 - 20
20.01 - 30
30.01 - 40
40.01 - 72.39
Kilometers
0 0.05 0.1 0.2 0.3 0.4

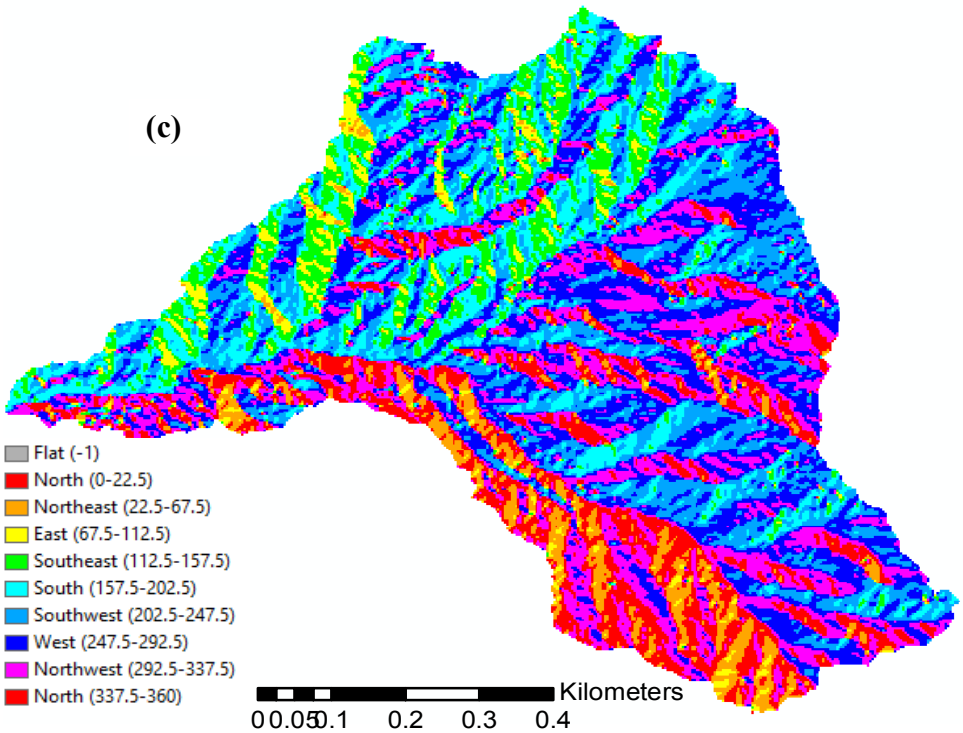

Fig. 5.2. Morphology aspect in the 3D Slope stability analysis. (a) Elevation data (m); (b) Slope angle (º); and (c) Slope aspect

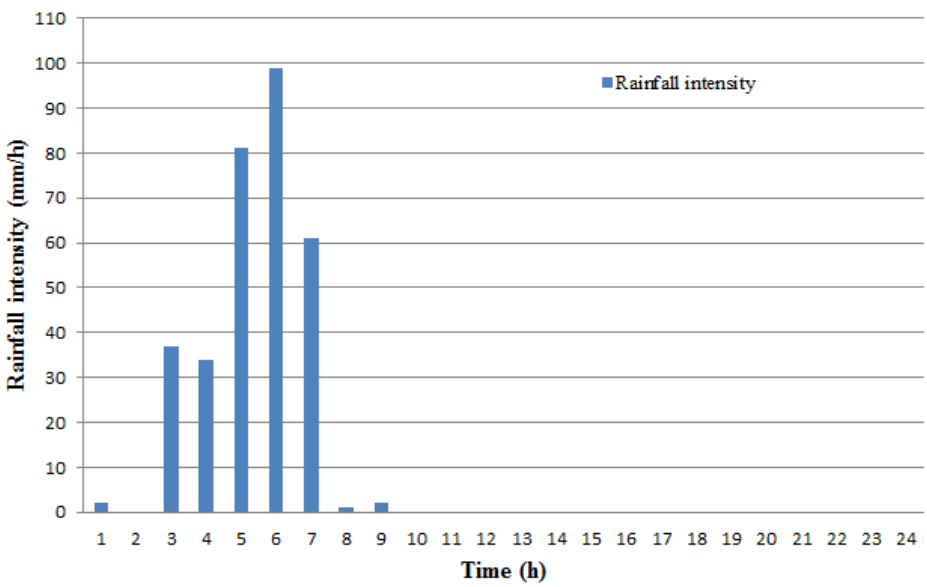

Fig. 5.3 Rainfall intensity in the Sangun Catchment area.

Using the simulation method described in Chapter 3, the estimation of depth

of soil distribution was done. The raster data of soil depth with 5m mesh size was then created from the simulation of soil depth through a process based model. The mean value of the resultant soil depth data is 74cm while the minimum value is 0cm and the maximal value is 255cm. The bedrock surface was then abstracted as a GIS raster dataset by subtraction of the surface elevation and the soil depth.

5.3.2 Rainfall data

The hourly rainfall variation of Sangun mountain on July 19, 2003 is shown in Fig. 5.3. The maximum rainfall was found throughout 3 to 7 am during the rainy season of the area. The minimum rainfall was found between 8 am to 9 am and very little or no rainfall occurred during 10 am to 11 pm.

5.3.3 Slope Units

For the landslide-hazard assessment of a large mountainous area with complex geometry and geological conditions, a key problem is how to extract the appropriate slope unit for potential sliding-surface identification and minimum 3D safety-factor calculation. Slope unit, namely, the portion of the land surface delimited by watershed divides and the channel has similar topographic and geological characteristics. The suitability of the slope units for landslide-hazard assessment and other land rated study has been recognized by several authors (Hansen, 1984; Xie. M et al., 2003; Dymond et al., 1995). To improve the results related to the distribution of slope unit, the eliminate tool have been used in the future of GIS data. Fig. 5.4 presents the distribution of slope units in the study area. The total number of slope unit is 64 units.

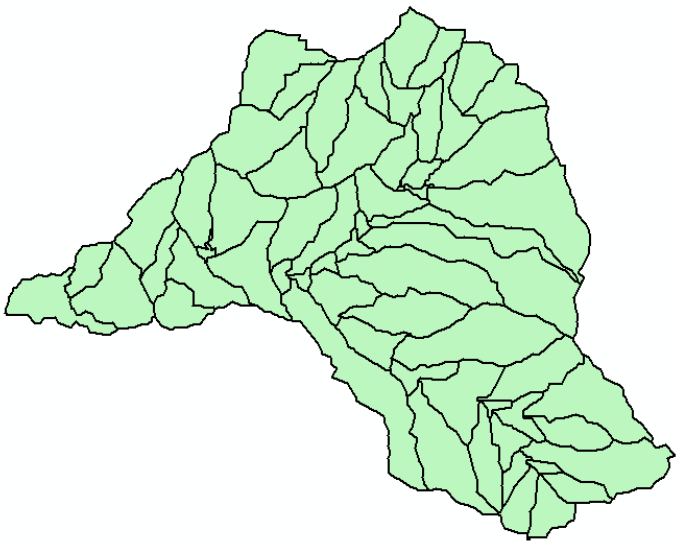

Fig. 5.4 Distribution of Slope units in the study area.

5.3.4 Geotechnical and infiltration parameters

In this study, we assume the flat area is the slope value at less than 4^0. Based on the field slope failure survey in July, 2013, the depth of slope failure was described, such as 1 to 10 meters. The geological map was described that the Sangun mountainous is most of granite rock. Geotechnical data of cohesion, internal friction angle, and unit weight, were derived from the laboratory test of previous studies conducted in the area and literature review. In the paper, each soil type was assigned soil cohesion, internal friction angle, and unit weight adapted from Jia. N (2011). Table 5.1 shows the initial value of mechanical parameters in the study area. Table 5.2 shows the parameter λ and A for different types of soil. The parameters were obtained from a number of experimental tests (Montrasio, and Valentino, 2008). Infiltration parameter data for soil properties is presented in the Table 5.3.

Table 5.1. Geotechnical properties of soil in study area

Soil type	Cohesion (*c*) (kN/m^2)	Friction angle (°)	Unit weight (kN/m^3)
Weathered granite	3.2	25	18
Bedrock	5	30	20

Table 5.2. Parameters λ and A for different types of soil

Soil type	Linked to the peak shear stress at failure (*A*)	A numeric parameter which allows to translate the peak of the curve along the abscissa axis (λ)
Mud	80	0.4
Sandy mud	80	0.4
Loose sand	40	0.4
Medium sand	40	0.4
Dense sand	40	0.4

Table 5.3. Changes in Soil properties by considering the organic materials in the surface (Tatsuro Sato, 2013).

Textural classification	Effective porosity (θ_s)	Wilting point water content (θi)	Saturated hydraulic conductivity (Ks) (mm/min)	Soil suction in wetting front (ψf) (mm)
Weathered Granitic rock	0.223	0.052	0.323	88
Weathered Granitic rock+organic materials (10%)	0.247	0.047	0.669	235
Weathered Granitic rock+orgnic materials (20%)	0.243	0.045	0.980	113
Weathered Granitic rock+organic materials (30%)	0.285	0.039	2.796	60

5.4 Simulation process

As the adjacent region has similar engineering geological conditions, we assume that the slope failure in this region has the same mechanism with the past landslide, that is to say, the potential failure surface would develop along the interface between map units granite rock under heavy rainfall. In this study, we assume three points to get the best performance of the possible slope failure. The following are the point (1) homogeneous layer by considering to change of cohesion and internal friction angle value; (2) multi layer (consideration of weather layer) for two layers and considering to change of cohesion and internal friction angle value; and (3) multi layer with rainfall effect. To detect the 3D critical slip surface of each slope unit, a search is performed by Monte Carlo simulation (Xie et al., 2003). The initial slip surface is assumed to be the lower part of an ellipsoid and changes according to multiple layer strengths and the conditions of the discontinuous surface. The five parameters that describe an ellipsoid are selected as random variables with uniform distribution: three axial parameters “a, b, c”, the central point “C”, and the inclination angle “θ” of the

ellipsoid (Fig. 4.9). The central point of the ellipsoid is first to set as the central point of a slope unit, and then randomly chosen within a certain range. The critical slip surface is fulfilled by searching the parameter space of the 3D safety factor.

In this study, a 3DSLOPE GIS and the combining of the 3DSLOPE GIS with hydrological model were applied. A detailed description of the method can be found in Chapter 4. The 3DSLOPE GIS is applied to simulate the slope failure probability by considering the homogeneous layer and multi layers. In the simulation, the calculating parameter of 3D shape searching has been set up about Monte Carlo calculating times 50, slope angle <= 4 is taken as flat, the assume of a depth of slope failure (c) is 1 – 5 m.

Furthermore, the effect of rainfall has been simulated by considering the infiltration parameters, groundwater level, the degree of saturation, and matric suction at wetting front. Those parameters obtained from the laboratory test which located around the study area in the Fukuoka (Table 5.3). During simulation, the calculating parameter of 3D shape searching has been set up about Monte Carlo calculating times 50, slope angle <= 4 is taken as flat, the assume of a depth of slope failure (c) is 1 – 5 m. To investigate the effect of rainfall with the times in 24 hours, the calculating time interval is 5 hours and calculating total time 24 hours.

5.5 Results

5.5.1 Homogeneous layer

To investigate the effect of geotechnical aspect on the slope stability, two different parameters of standard geotechnical (cohesion and friction angle) were adopted. The rock layer was also assumed to be homogeneous. An initial of representative rock parameters for homogeneous of cohesion and friction angle is listed in Table 5.1. In the Table 5.1, the bedrock of granite was used in the simulation. The elevation, slope angle, and slope aspect were analyzed by GIS tool for DEM data. In the simulation, the range values of cohesion are 1 to 10 kN/m^2 and internal friction angle are 15 to 35^0. The safety factor results have been divided in two categories, such as SF≤1.0 and SF>1.0. Fig. 5.5 and Fig. 5.6 present the results of 3D Slope GIS simulation in the spatial distribution on the variability of cohesion and internal friction angle value. Moreover, Table 5.4 shows the number of slope unit which safety factor <=1.0 based on cohesion (c) and internal friction angle (Φ) values for homogeneous layer.

Table 5.4. Number of slope unit which safety factor <=1.0 based on cohesion (c) and friction angle (Φ) values for homogeneous layer.

No	Layer type	Geotechnical parameters		Number of slope unit which safety factor <=1.0 (%)
		cohesion (c)	Friction angle(φ)	
1	Homogeneous	1	30	34.38
2		3.2	30	18.75
3		5	30	18.75
4		7	30	12.50
5		10	30	9.38
6		1	15	98.44
7		1	20	89.06
8		1	25	65.63
9		1	30	34.38
10		1	35	0

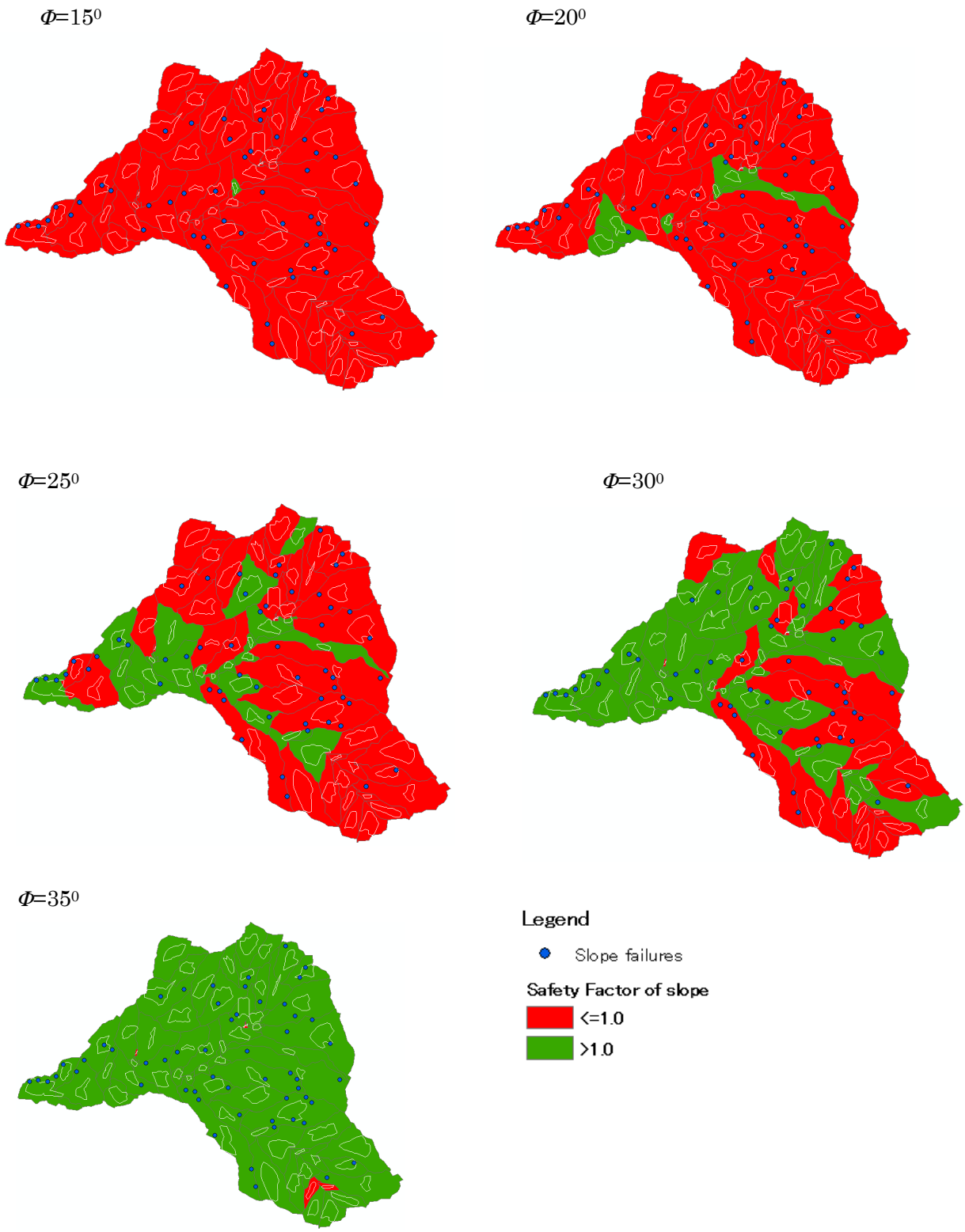

Fig. 5.5 Distribution of Safety factor values of the homogeneous layer based on friction angle (Φ) values.

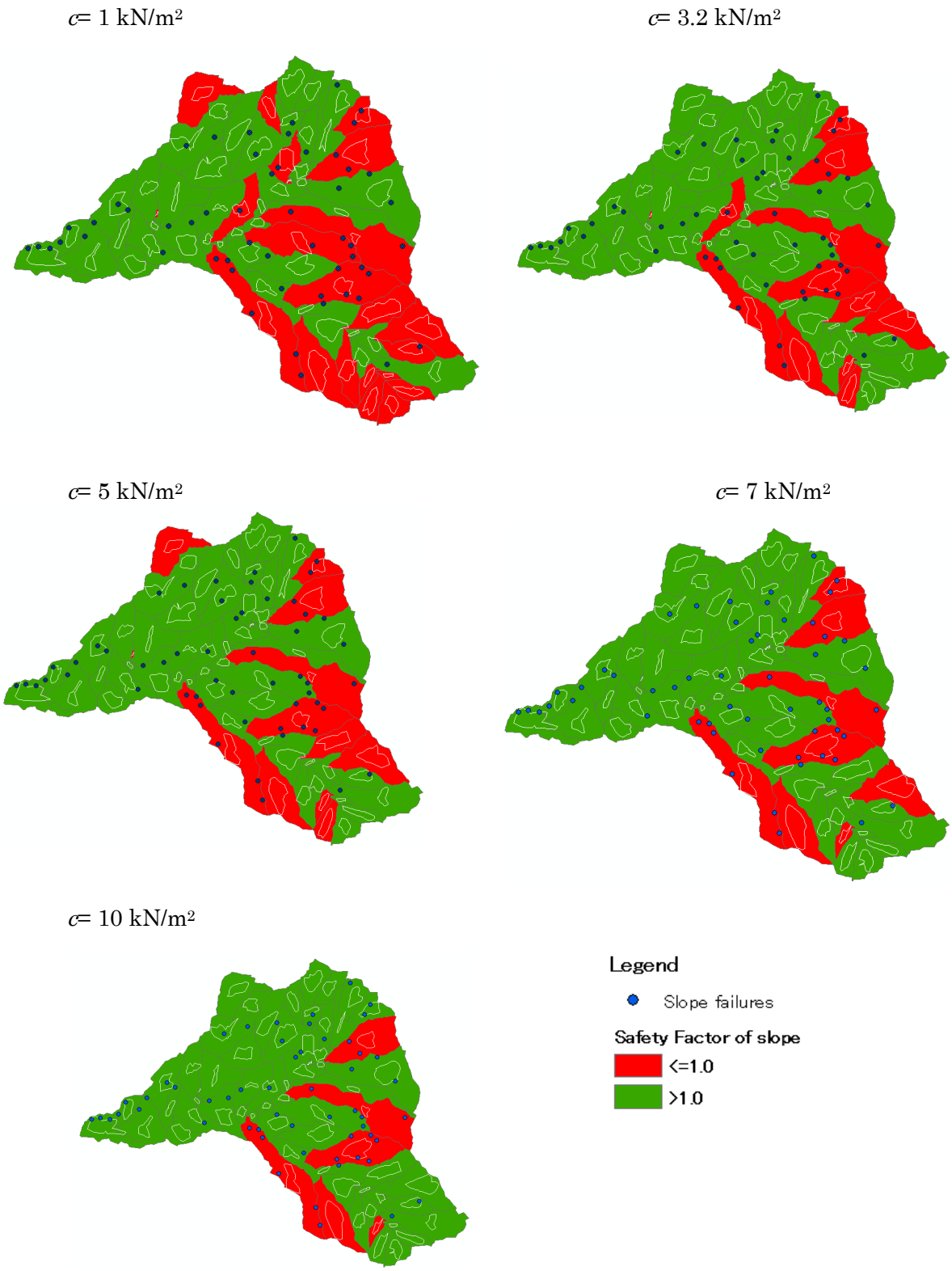

Fig. 5.6 Distribution of Safety factor values of the homogeneous layer based on cohesion (c) values.

5.5.2 Multi layer

In this part, the rock layer was assumed to be multi layer. The influence of soil depth as soil production from the granite weathered. An initial of representative rock parameters for heterogeneous of cohesion and friction angle is listed in Table 5.1. The bedrock of the study area is represented by granites, which is hard in a fresh state, but often heavily weathered to form deep residual deposits. The soil cover in the area, with an average depth of about 0.75m, is composed mainly of colluviums and residual deposits formed by weathering of granites and accumulation of slope failures as results of landslide activity.

To investigate the effect of geotechnical aspect on the slope stability, two different parameters of standard geotechnical (cohesion and internal friction angle) were adopted. The elevation, slope angle, and slope aspect were analyzed by GIS tool for DEM data. In the simulation, the range values of cohesion are 1 to 10 kN/m^2 and friction angle are 10 to 30^0. The safety factor results have been divided in two categories, such as SF≤1.0 and SF>1.0. Fig. 5.7 and Fig. 5.8 present the results of 3D Slope GIS simulation in the spatial distribution on the variability of cohesion and internal friction angle values. Moreover, Table 5.5 shows the number of slope unit which safety factor ≤1.0 based on cohesion (c) and friction angle (Φ) values for homogeneous layer.

Table 5.5. Number of slope unit which safety factor ≤1.0 based on cohesion (c) and internal friction angle (Φ) values for multi layer (soil depth effect).

No	Layer type	Geotechnical parameters		Number of slope unit which safety factor <=1.0 (%)
		Cohesion (c)	Internal friction angle (Φ)	
1	Two layers (soil of granite weathering+ bedrock)	1	26	60.94
2		3.2	26	51.56
3		5	26	50.00
4		7	26	42.19
5		10	26	35.94
6		1	10	100
7		1	15	96.88
8		1	20	86.15
9		1	25	65.63
10		1	30	34.38

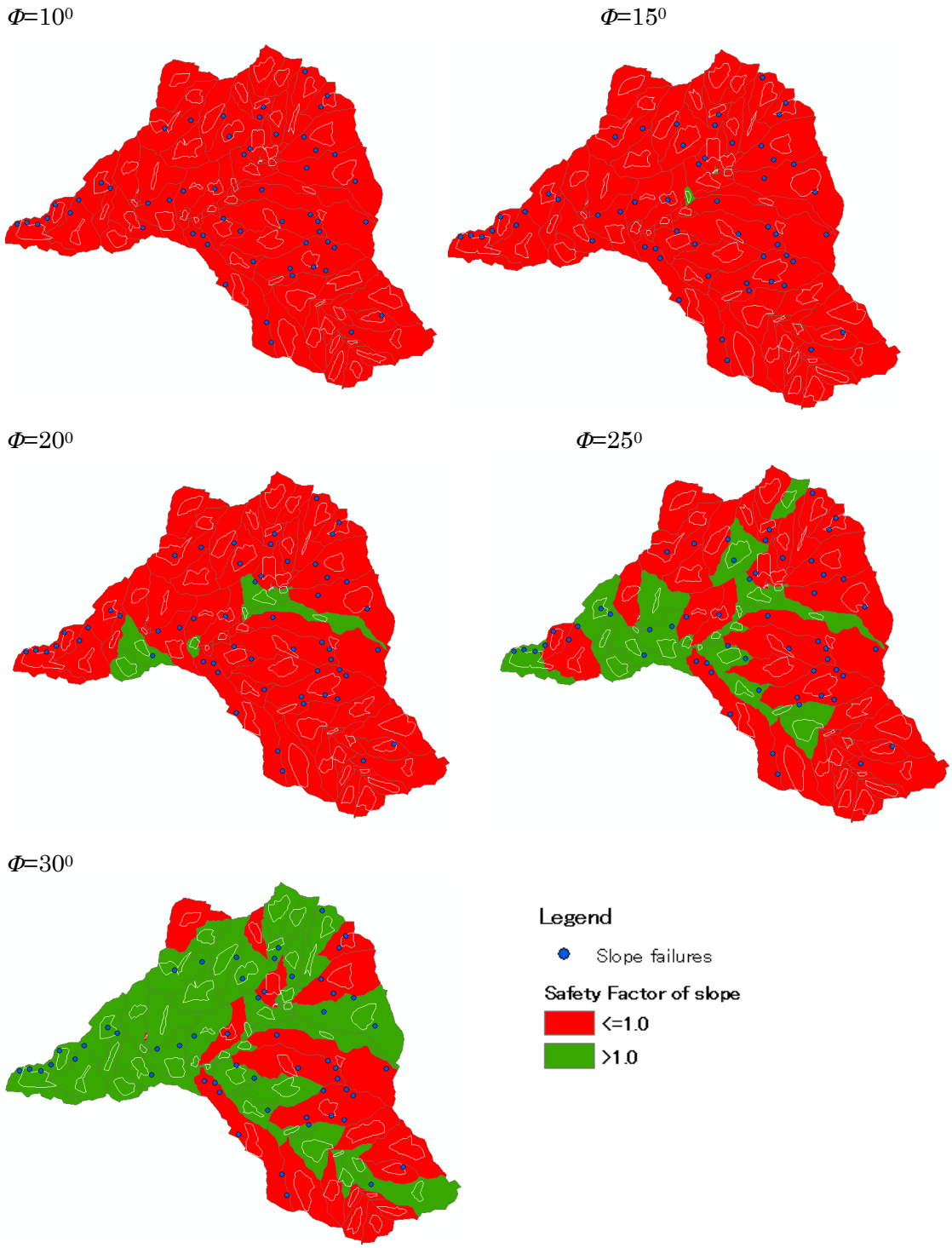

Fig. 5.7 Distribution of Safety factor values of the multi layer based on friction angle (Φ) values.

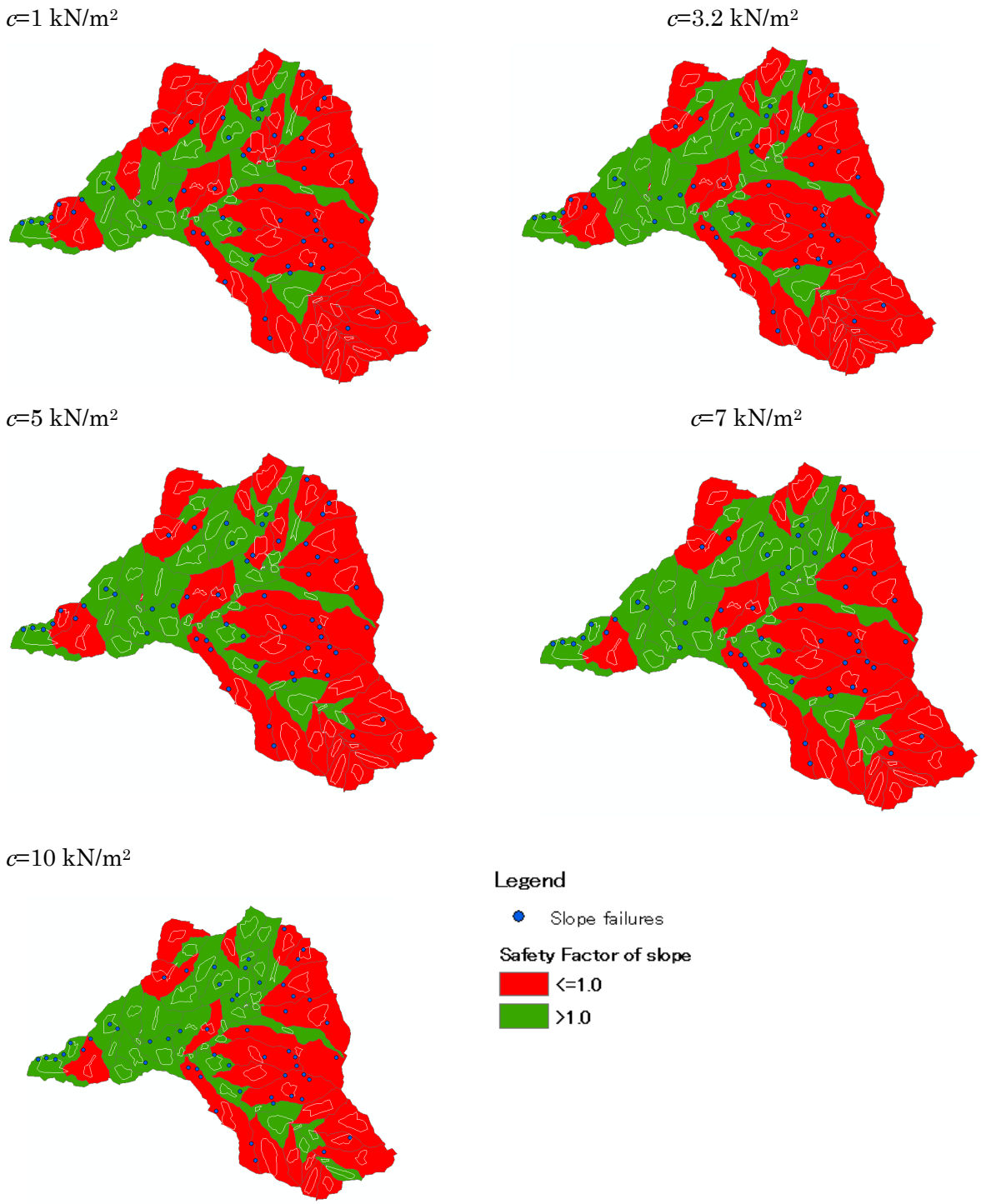

Fig. 5.8 Distribution of Safety factor values of the multi layer based on cohesion (*c*) values.

5.7.3 Rainfall effect

The proposed the combining of an infiltration model with an improved Colum-based 3D slope stability analysis model, an integrating of hydrological and GIS-based 3D model has been developed for evaluating the variety of surficial slope stability during rainfall events. The Sangun mountainous is located in the Fukuoka city, where slope disasters have happened frequently. To forecast slope failure and to provide support for deciding on suitable countermeasures, the system described here was used for landsliding mapping.

In this study, the infiltration parameter has been considered the textural of soil classification (Table 3). There are four of infiltration parameters will be used in this study, such as saturated hydraulic conductivity (*Ks*); Effective porosity (θ_s); Wilting point water content (θ_i); and Soil suction at wetting front (ψ_f). Furthermore, the effect of rainfall, there are five cases; (1) infiltration parameter for soil as weathered granitic rock and the occurrence of groundwater level (5m) (Fig. 5.9); (2) infiltration parameter for soil as weathered granitic rock and groundwater level (0m) (Fig. 5.11); (3) infiltration parameter for soil as weathered granitic rock +organic materials (10%) and groundwater level (0m) (Fig. 5.13); (4) infiltration parameter for soil as weathered granitic rock + organic materials (20%) and groundwater level (0m) (Fig. 5.15); and (5) infiltration parameter for soil as weathered granitic rock + organic materials (30%) and groundwater level (0m) (Fig. 5.17)

For study area, a variation of rainfall event with duration of 24 h and a maximum intensity of 9.9 cm (Fig. 5.3) was applied. Geotechnical and hydraulic properties of this soil in that area were extensively studied by several authors by laboratory measurements. Furthermore, to investigate the influence of rainfall, the cohesion (c') value of 1 kN/m^2 has been used in the simulation. A parameter depending on the kind of soil and is linked to the peak shear stress at failure (A) and numerical parameter which allows to translate the peak of the curve (λ) are 40 and 0.4.

Fig. 5.10, Fig. 5.12, Fig. 5.14, Fig. 5.16, and Fig 5.18 present the results of 3D Slope GIS simulation in the spatial distribution on the variability of infiltration parameter's values.

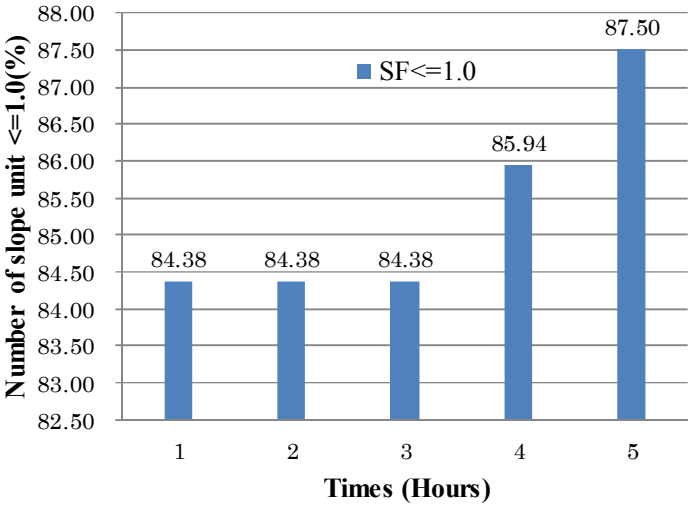

Fig. 5.9 Relationships between the number of slope unit <= 1.0 and a time of rainfall intensity based on cohesion (c) value =1 kN/m^2; groundwater table =5m and; K_s=0.323 mm/min, θ_i=0.052, θ_s=0.223, ψ_f = 8.8 cm (Case 1).

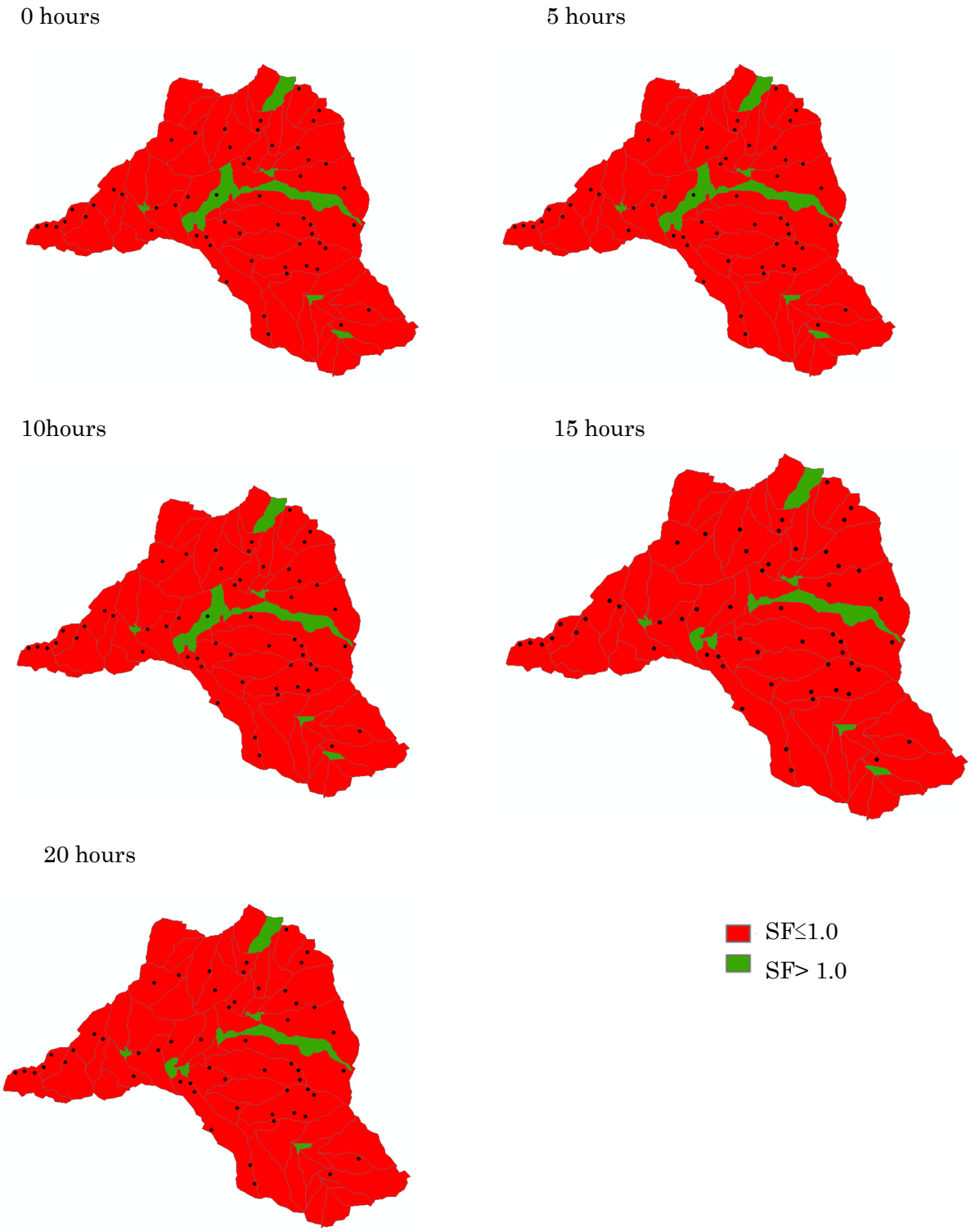

Fig. 5.10 Distribution of Safety factor values of the multi layer with rainfall effect and cohesion values (c) = 1 kN/m^2; K_s=0.323 mm/min, θ_i=0.052, θ_s=0.223, ψ_f=8.8 cm (Case 1).

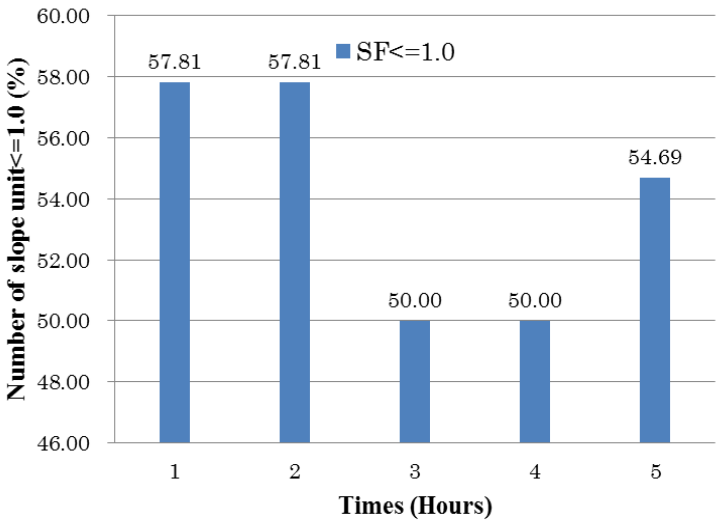

Fig. 5.11 Relationships between the number of slope unit <= 1.0 and a time of rainfall intensity based on cohesion (c) value=1 kN/m^2; groundwater level (0m) and; K_s=0.323 mm/min, θ_i=0.052, θ_s=0.223, ψ_f = 8.8 cm (Case 2).

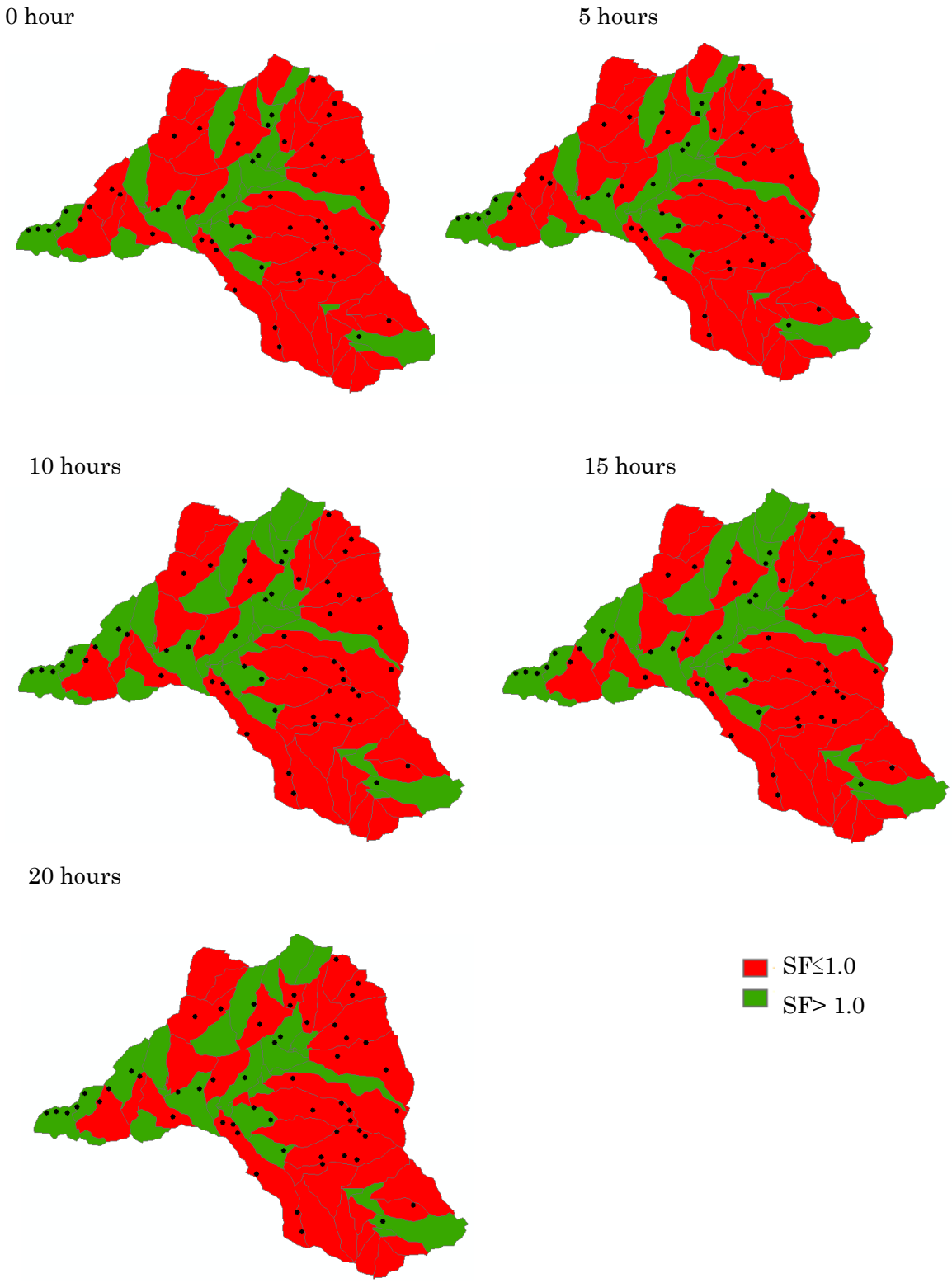

Fig. 5.12 Distribution of Safety factor values of the multi layer with rainfall effect and cohesion values (c) = 1 kN/m^2 ; K_s=0.323 mm/min, θ_i=0.052, θ_s=0.223, ψ_f =8.8m (Case 2).

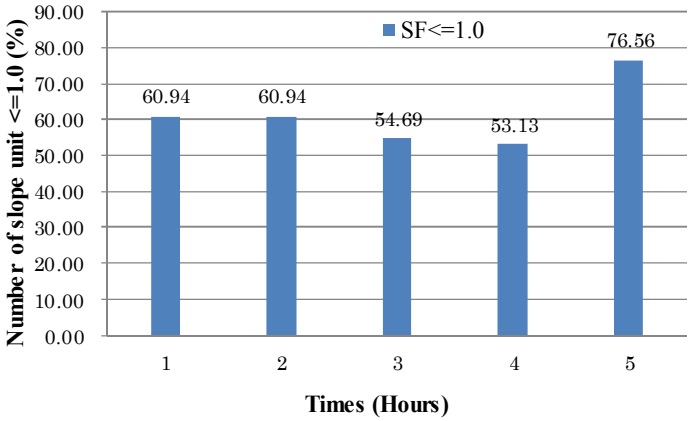

Fig. 5.13 Relationships between the number of slope unit <= 1.0 and a time of rainfall intensity based on cohesion (c) value=1 kN/m^2; groundwater level (0m) and; K_s=0.669 mm/min, θ_i=0.047, θ_s=0.247, ψ_f = 23.5 cm (Case 3).

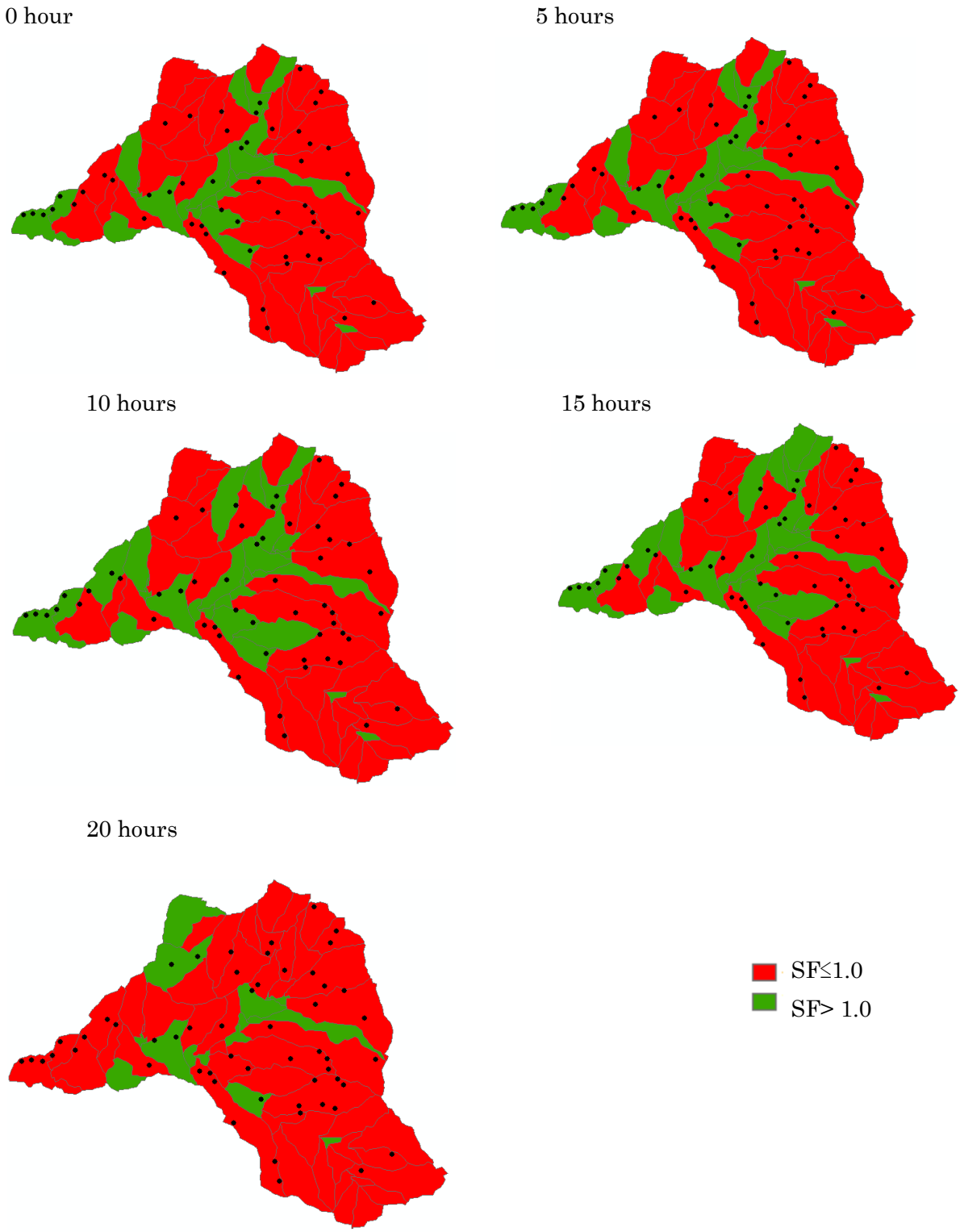

Fig. 5.14 Distribution of Safety factor values of the multi layer with rainfall effect and cohesion values (c) = 1 kN/m^2 ; K_s=0.669 mm/min, θ_i=0.047, θ_s=0.247, ψ_f=23.5m (Case 3).

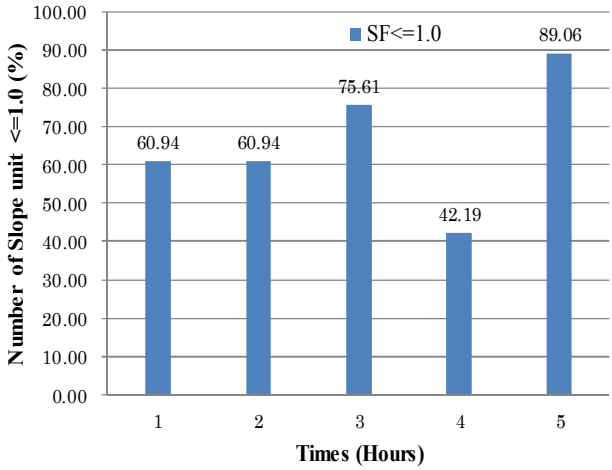

Fig. 5.15 Relationships between the number of slope unit <= 1.0 and a time of rainfall intensity based on cohesion (c) value=1 kN/m^2; groundwater level (0m) and ; K_s=0.980 mm/min, θ_i=0.045, θ_s=0.243, ψ_f = 11.3 cm (Case 4).

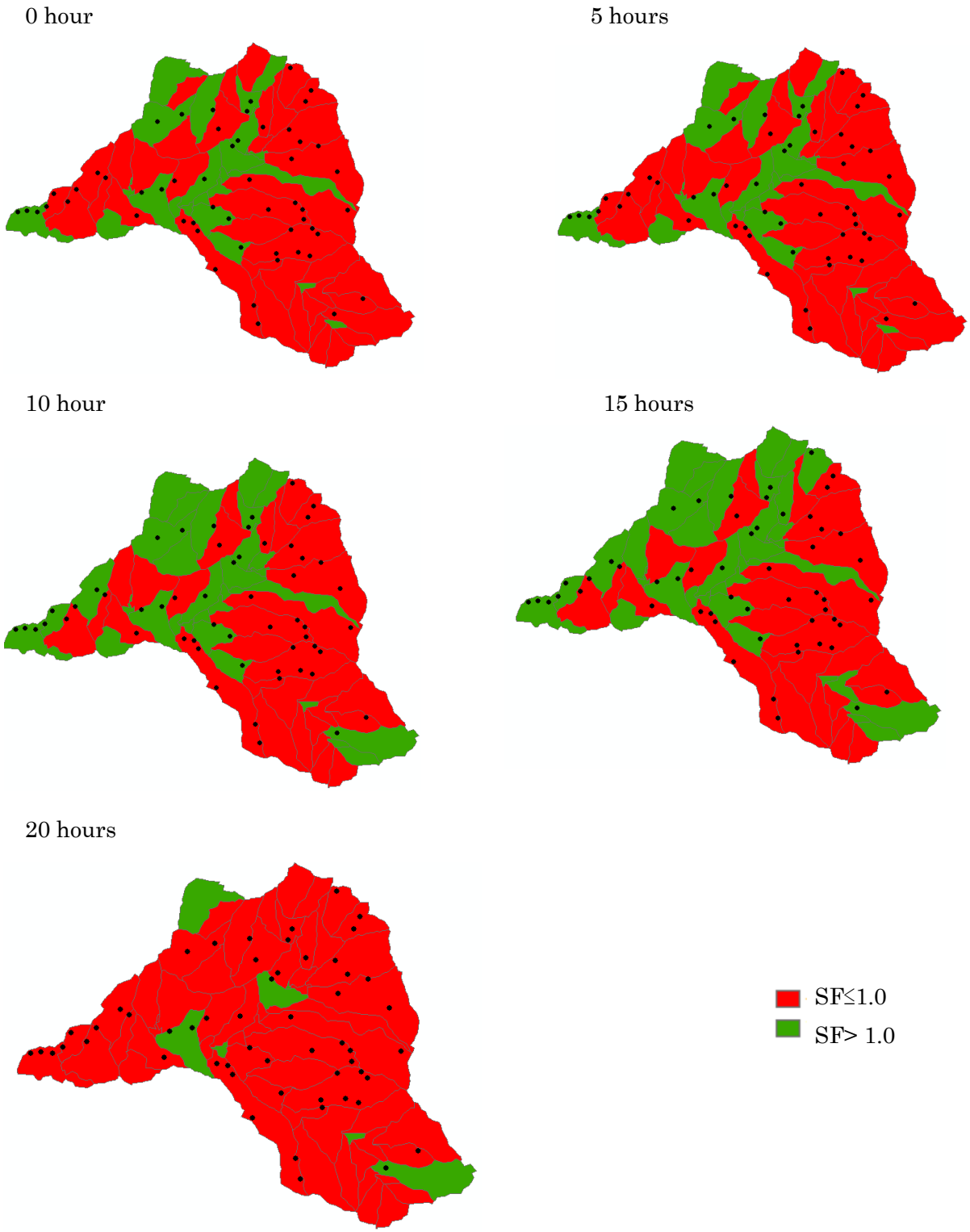

Fig. 5.16 Distribution of Safety factor values of the multi layer with rainfall effect and cohesion values (c) = 1 kN/m^2 ; K_s=0.980 mm/min, θ_i=0.045, θ_s=0.243, ψ_f =11.3m (Case 4).

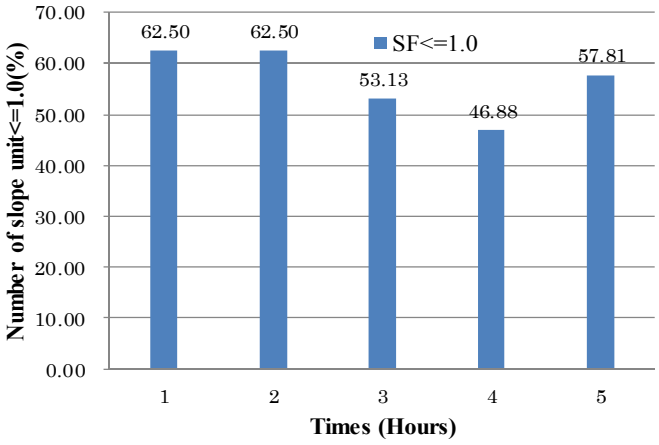

Fig. 5.17 Relationships between the number of slope unit <= 1.0 and a time of rainfall intensity based on cohesion (c) value=1 kN/m^2; groundwater level (0m) and ; K_s=2.796 mm/min, θ_i=0.039, θ_s=0.285, ψ_f = 6.0 cm (Case 5).

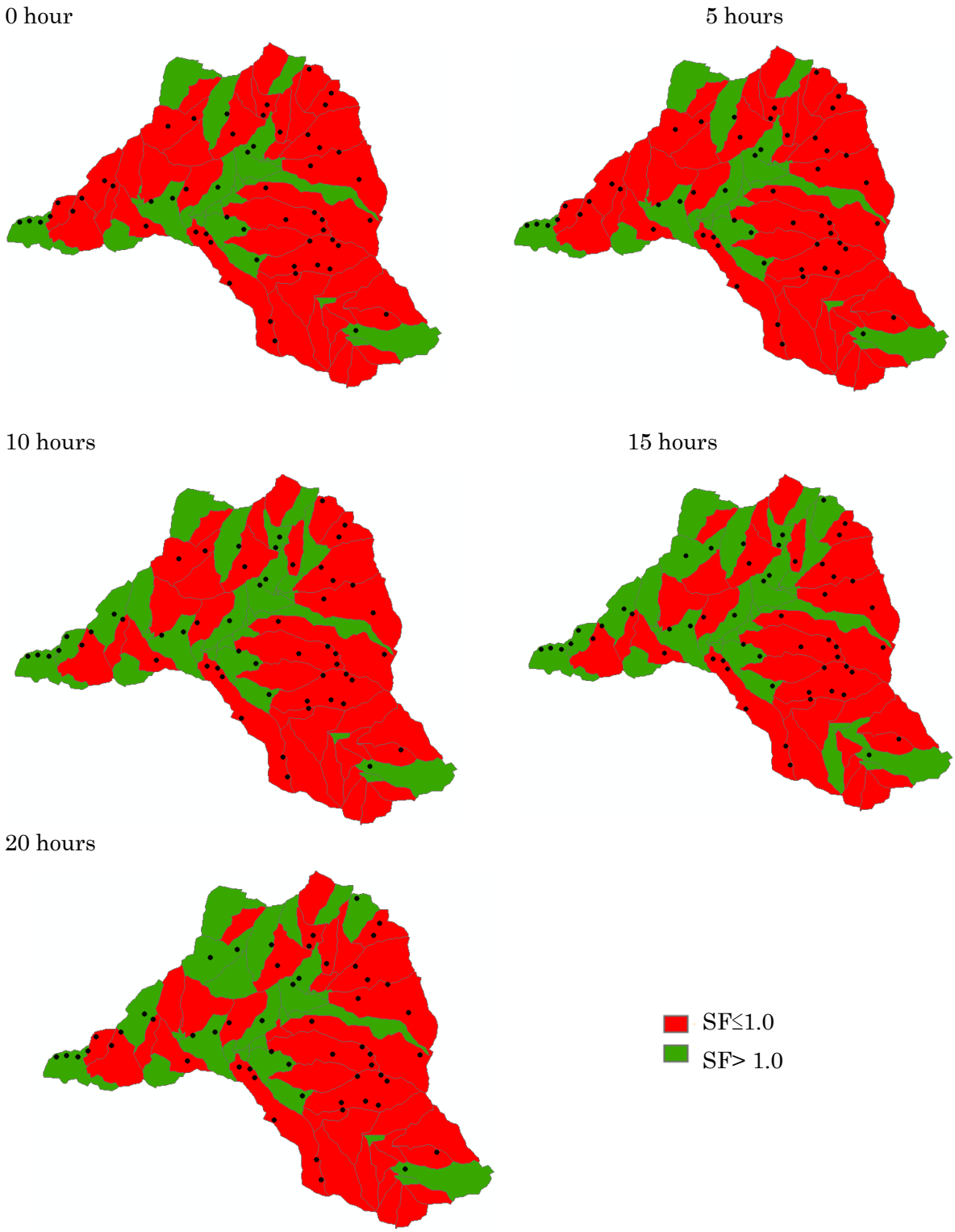

Fig. 5.18 Distribution of Safety factor values of the multi layer with rainfall effect and cohesion values (c) = 1 kN/m^2 ; K_s=2.796 mm/min, θ_i=0.039, θ_s=0.285, ψ_f=6.0m (Case 5).

5.6 Discussions

5.6.1 Slope failures characteristic in the catchment

A slope failure inventory map shows the location, morphology characteristic of slope failures (Fig. 5.1). However, no detailed slope failure inventory map existed in the study area. The locations of landslide scars are determined and mapped by a field survey in 2003. The relationships between morphology aspect and slope failure distribution is presented in this study (Fig. 5.21). The distributions of slope failure are used in this analysis. The morphology aspect are elevation, slope angle, and slope aspect.

Elevation is classified into five categories such as., <150 m, 150-300 m, 300-450 m, 450-600 m, and >600 m. It is found that the majority of the area failures in the category of 300-450 m followed by 150-300 m, >600 m, 150 -300 m, and <150 m. From the calculation of frequency ratio, class interval of 300-450 m is the highest with 92 slope failures each out of 278 failures which are 33.09 %.

Slope angle is classified into five categories such as, <100, 10-200, 20-300, 30-400, and >400. Majority of slope failures (172 units) in the area have been occurring within a slope angle of 30 - 400 followed by <400, 20-300, <100, and 10-200. The amount of slope failure shows increase with the increasing of slope angle values in the range 10 -400 (Fig.5.21b).

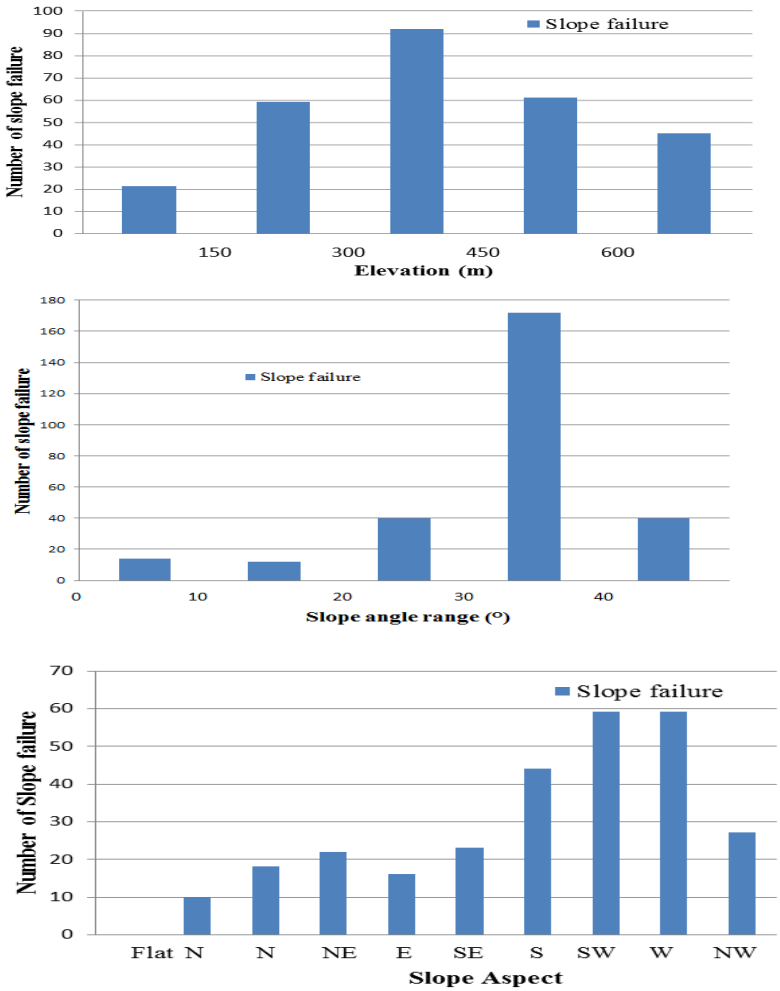

Fig. 5.19 Slope failure characteristic in the Sangun basin

Slope aspect is classified into eight categories such as., North (0-22.50, 337.5-3600), Northeast (22.5-67.50), East (67.5-112.50), Southeast (112.5-157.50), South (157.5-202.50), Southwest (202.5- 247.50), West (247.5-292.50), and Northwest (292.5-337.50). Majority of slopefailure in the area have been occurring within the slope aspect of the Southwest and West which are 59 units. In the Figure 5.19c, the graph shows the direction of slope aspect which N=North, NE=Northeast, E=East, SE=Southeast, S=South, SW=Southwest, W=West, and NW=Northwest. Figure 5.19c shows the slope failure increase with the direction of slope aspect of East to West.

5.6.2 Slope failure probability analysis by using a 3D Slope stability tool on Sangun mountainous

The stability model was applied two times by considering homogeneous and multi layer (using the soil thickness map) on a slope unit basis in the cohesion value ranges, a safety factor map was produced with a 5 m spatial resolution. For each simulation, a summarizing Safety Factor map of the event was produced assigning to every slope unit the lowest SF value assumed during the analyzed periods. Slope unit with SF values higher and lower than 1 (limit equilibrium) were interpreted as stable and unstable (respectively).

Given the uncertainty about the parameters in Table 5.1, we have performed a number of sensitivity analysis by using the range of *c* and φ values. Table 5.4 and Table 5.5 summarize some of results of slope stability simulation. This shows the number of ranges of *c* and φvalues that are the number of slope unit which of safety factor <=1.0.

Firstly, the homogeneous layer is using the geotechnical value of bedrock as a containing granite rock in the study area (Table 5.4). The range of cohesion values are 1, 3.2, 5, 7, and 10 kN/m^2 and friction angle value is 30^0. Furthermore, the range of friction angle values are 15, 20, 25, 30, and 35^0, and cohesion value is 1 kN/m^2. For safety factor <= 1.0 show the variety of percentage of the number of slope unit. Number of slope unit by 3D slope stability calculation is decreased when the cohesion value increases about between 34.38 to 9.38% for *c*=1 kN/m^2 to *c*= 10 kN/m^2. For the variance of friction angle values, the number of slope unit shows decrease when the friction angle value increases. Number of slope unit by 3D slope stability calculation is decreased when the friction angle value increases about between 98.44 to 0% for Φ=15 ^{0} to Φ= 35^0.

Secondly, 3D slope stability simulation was performed by considering the distribution of soil depth. With increasing thickness, the area of predicted instability in the study area. The soil depth model, systematically and correctly predicts thin soil on the ridges and thick in the valley, which has the effect when combined with the influence of cohesion and friction angle values. In the simulation, the initial parameter in Table 5.5 was used and the making of varied value will describe the variety of probability of number slope unit is less than 1.0. The range of cohesion values are 1, 3.2, 5, 7, and 10 kN/m^2 and friction angle value is 30^0. Furthermore, the range of friction angle values are 15, 20, 25, 30, and

35^0, and cohesion value is 1 kN/m^2. For safety factor <= 1.0 show the variety of percentage of the number of slope unit. Number of slope unit by 3D slope stability calculation is decreased when the cohesion value increases about between 60.94 to 35.94% for c=1 kN/m^2 to c= 10 kN/m^2. For the variance of internal friction angle values, the number of slope unit shows decrease when the friction angle value increases. Number of slope unit by 3D slope stability calculation is decreased when the internal friction angle value increases about between 100 to 34.38% for Φ=15 ^{0} to Φ= 35^0.

Thirdly, the effect of rainfall has been simulated by considering the infiltration parameter, and the occurrence of groundwater level. The safety factor determine with the slope stability analysis using the rainfall-infiltration model is shown in Fig. 5.9, Fig.5.11, Fig.5.13, Fig.5.15 and Fig.5.17. Fig. 5.9 and Fig.5.13 presents the safety factor change with the occurrence of the fix of groundwater level (5m) and do not consider of groundwater during rainfall on the 24 hours. Based on the rainfall data, the intensity of rainfall is linear the number slope failure from 0 to 10 hours. After 10 hours, the safety factor <= 1.0 is increasing. From this figure, the relationship between matric suction and the safety factor indicate a linear increase. The relationship between effective degree of saturation and the safety factor indicates a linear decrease, and the shear strength decrease as the water content increases (Yeh et al, 2008). Furthermore, to obtain the effect of infiltration parameters (Ks, θ_i, θ_s, and matric suction) have been changed (Fig. 5.19). The number of slope unit <=1 of case 1 (Ks= 0.323 mm/min) shows lower than the case 2 (Ks=0.699 mm/min). Moreover, the number of slope unit<=1.0 is almost to 100%. Therefore, the author assumes the considering of the groundwater level. Because in this study, the groundwater level data were obtained from the investigation and decide 5m is initial groundwater level data. Furthermore, the groundwater data were changed to 0m that is meant no groundwater level in this study area. Fig. 5.20 presents the effect of groundwater level occurrence during rainfall occur to obtain the slope failure probability by simulated with combining the 3D Slope Stability and hydrological model. In this analysis, the data of the fifth cases for infiltration parameter, and the groundwater level data 0 and 5m were used. As results, the number of slope unit<=1of groundwater level 5m is higher than the groundwater level 0m about more than 90% on 20h. Furthermore, to get the best performance, the validation of the results will be conducted by comparing the slope failure inventory map in the past.

5.6.3 Validation of Slope failure probability

Application of the developed slope stability model was performed for a range of soil depth conditions. The three wet scenarios identified based on the amount of layer, the range of soil depth, and cohesion and friction angle values of each soil depth condition, are typical of the conditions and susceptibility that might be expected in this region. For Sangun mountain area the largest uncertainty is the geotechnical parameters, since these are not measures in-situ. It is also a limited availability of representative literature data and knowledge of the actual slope conditions. Therefore the input parameters are assumed to have as good quality as possible. The input parameters are based on literature, this does clearly introducing some uncertainty. For all the figures that have been modeled in the 3D slope stability analysis has been measured with the influence of cohesion and friction angle parameter.

Spatial effectiveness of the susceptibility map will be checked by the highest percentage of the actual slope failure by comparing the predicted unstable site. The rate graph will be created for variance of geotechnical values, and their percentage will be calculated. The rate explains how well the model and controlling factors predict the landslide.

The model with the highest percentage is considered to be the best. Figure 4 shows a representative the evaluation of slope failure predicted that produced by 3D slope stability analysis of variance of geotechnical values for safety factor less than 1.0.

In fact, the number of slope failures (%) is increasing with the cohesion and friction angle values decreases for homogeneous and heterogeneous layers. Furthermore, Fig. 5.20a and 5.20c present the number of slope failures (%) that influenced by cohesion (*c*) values for homogeneous and heterogeneous layers. In order, the graph of Fig. 5.20c shows more higher of the actual slope failure occurred than Figure 5.20a. Moreover, Fig. 5.20b and 5.20d show the total number of slope failure (%) that influenced by friction angle (Φ) values. The both of graph 5.20b and 5.20d present the same number of slope failure for each friction angle values. Due to the *c* values gave the similar values in homogeneous and heterogeneous layers, therefore the cohesion value equal 1 kN/m^2 gave a very reasonable performance compare to similar *c* values performed by other cohesion values. However, for the friction angle value, we need to compare the number of slope unit probability in the safety factor $\leq$ 1.0 (Table 2) and number of slope

failure (%) for each friction angle value. Furthermore, the friction value of 25^0 is a reasonable performance in the both homogeneous and heterogeneous layers about 76.36%.

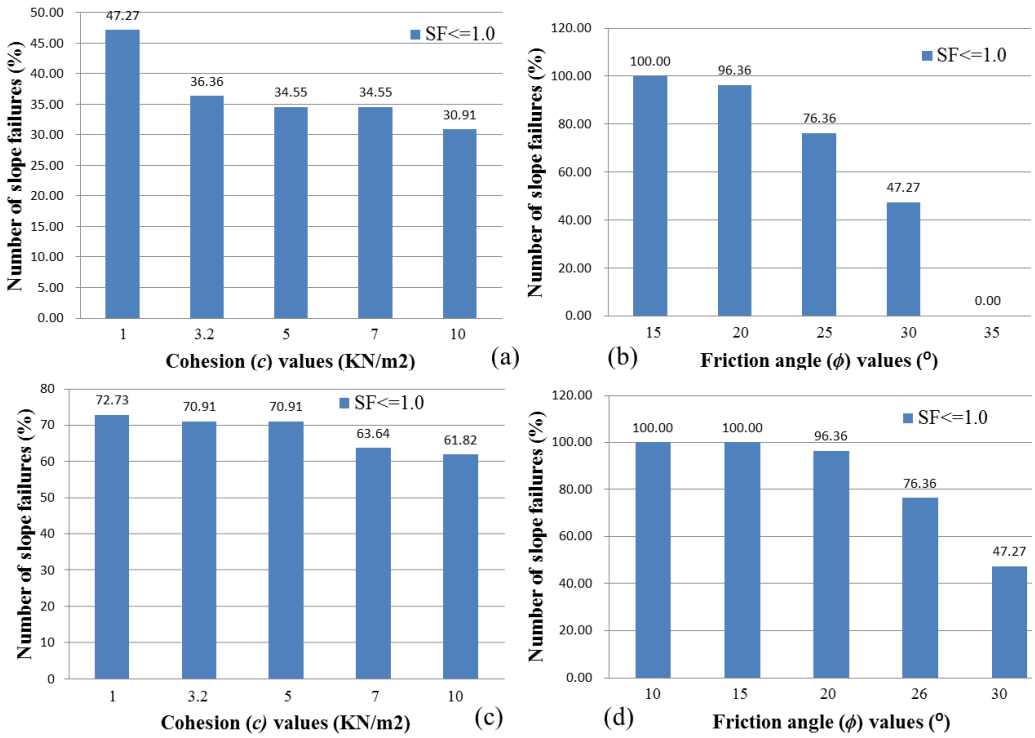

Fig 5.20 Relationships of cohesion (*c*), friction angle (*Φ*) values and number of slope failures (%) based on the factor of safety (FS) of the slope stability simulation. (a) homogeneous layer with cohesion (*c*) values; (b) homogeneous layer with friction angle (*Φ*) values; (c) multi layer with cohesion values; (d) multi layer with friction angle (*Φ*) values.

Fig. 5.21 show the slope failure probability map obtained with 3D Slope stability simulation that consider the soil layer and geotechnical parameters. Fig. 5.21a presents the homogeneous layer with cohesion value 1 kN/m^2 that represent the better performance than other cohesion values with comparing the number of slope failure in the past. Distributions of slope unit that probability will failure in the upstream part about 34.38%. Moreover, Fig. 5.21b presents the homogeneous layer with influenced the friction angle value with 25^0. This map is represent the better performance than other friction angle values, which the distribution of slope unit will failure about 65.63%. Furthermore, Fig.5.21c and 5.21d show the multi layers by influencing the variability of cohesion and internal friction angle values.

Fig. 5.21c represent the better performance of cohesion value that the distribution of slope unit will failure about 60.94% and the number of slope failure about 72.73%. And, Fig. 5.21d represent the best performance of friction angle value that the distribution of slope unit will failure about 65.65% and the number of slope failure about 76.36%.

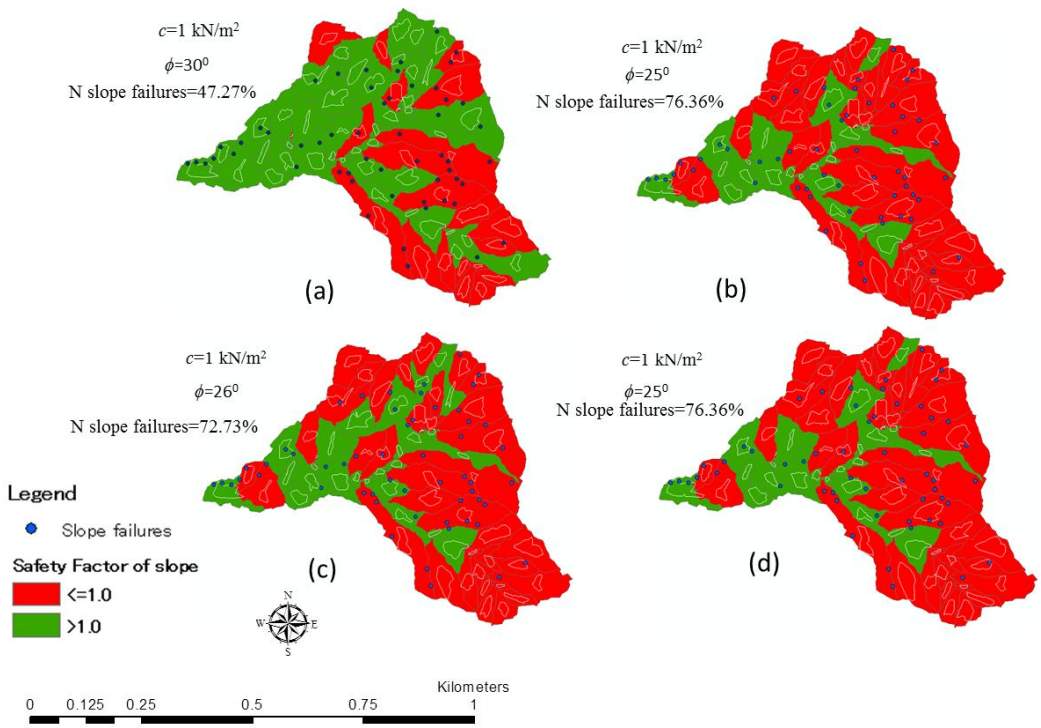

Fig. 5.21 Distribution of Safety factor values based on the type of layer. (a) homogeneous layer with cohesion (c) values; (b) homogeneous layer with friction angle (Φ) values; (c) multi layer with cohesion values; (d) multi layer with friction angle (Φ) values.

Fig 5.22 presents the validation of the results of simulation on the rainfall effect. The y axis is the number slope failure (%) in the past. It obtained by comparing the distribution of slope failure in the past and the number of slope unit ≤1.0 which matching number is needed. The x axis is the number of times (hours) in July 19, 2003. The trend of number of slope failure from 0 to 20h is increasing for all cases. For each of the graph, the number of slope failure in the case 1 is the highest number of slope failure which show 100% in the 20 hours. And this

validation is suggested not good performance because the number of slope unit ≤ 1.0 (%) from simulation show the high numbers. The occurrence of groundwater level data is constant may be the reason of these results.

Therefore, the assume of occurrence of groundwater level will be changed to 0m. In this simulation, case 2, case 3, case 4, and case 5 presents the infiltration model without of considering the groundwater level. Furthermore, the number slope failure (%) during rainfall until 20 hour is increasing, and the best performance is reasonable for this analysis about 89.09% in case 3. It considers the mean of number slope failure from 0 to 20 hours about 76% for case 3. From this result, the distribution of groundwater level is important to assess the slope stability during rainfall in the Sangun mountainous area.

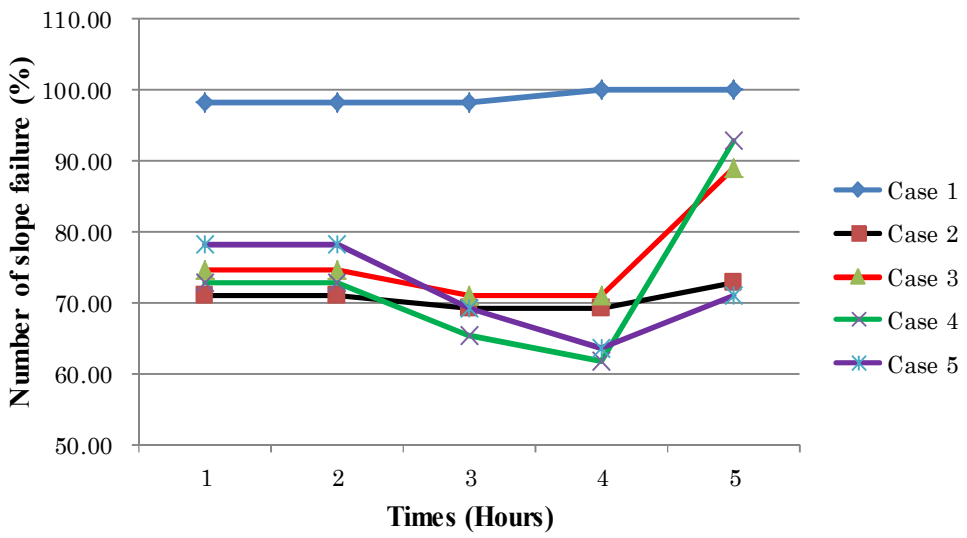

Fig 5.22. Relationships between number of slope failure (%) that compared the slope failure probability with the number of rainfall time (hours) based on the infiltration parameters, the occurrence of groundwater level during on 3D slope stability simulation.

5.7 Conclusions

In Chapter 5, aiming to apply 3D deterministic model with combining of hydrological model to a wide natural area for predicting the location of slope failure with soil depth and rainfall, a slope-unit-based evaluation method is given. The 3D Slope Stability Analysis for homogeneous and multi layers based on verification of the results will be conducted by considering the inventory slope

failure in the past. As results, due to the cohesion (*c*) values gave the similar values in homogeneous and multi layers, therefore the cohesion value equal 1 kN/m2 gave a very reasonable performance compare to similar cohesion values performed by other cohesion values (47.27% for homogeneous layer and 72.73% for multi layer). Furthermore, the friction value of 25^0 is a reasonable performance in the both homogeneous and multi layers about 76.36%. Furthermore, the effect of rainfall, there are five cases; (1) infiltration parameter for soil as weathered granitic rock and the occurrence of groundwater level (5m); (2) infiltration parameter for soil as weathered granitic rock and groundwater level (0m); (3) infiltration parameter for soil as weathered granitic rock +organic materials (10%) and groundwater level (0m); (4) infiltration parameter for soil as weathered granitic rock + organic materials (20%) and groundwater level (0m); and (5) infiltration parameter for soil as weathered granitic rock + organic materials (30%) and groundwater level (0m)

As results, the validation has been conducted in all cases. Therefore, the assuming of the groundwater level is 0m have been changed (case 2 to case 5). Furthermore, the result shows 89.09% the number of slope failure after 20h is good performance in the case 3.

For rainfall-induced slope analysis, the evaporation and distribution of groundwater level were not considered in the current analysis. Evaporation cannot be ignored if the rainfall lasts days, and the influence of antecedent rainfall depends on the duration. Groundwater level prior to the major rainfall event can significantly decrease the safety factor even if the rainfall is minimal in comparison to the major rainfall. These two factors should be considered in future study.

References

Dietrich, W.E., Dunne.T. (1978): Sediment budget for a small catchment in mountainous terrain. Zeitschrift fur Geomorpologie, Supplementband 29, 191-206.

Hanamura,et.al. (2004). Heavy rain Disaster in Kyushu Area on July 2003, J*apan Society of Engineering Geology,*No.25, ISSN 0917-2289, pp.30-31.

Mezughi, T.H. Akhir,J.M. Rafek,A. and Abdullah, I.(2011): Landslide assessment using frequency ratio model applied to an area the E-W highway (Gerik-Jeli), *Am. J. Environ. Sci*, (7)1, pp. 43-50.

Montrasio, L and Valentino,R. (2008). A model for triggering mechanisms of shallow landslides. Nat.Hazards Earth syst.Sci., 8, 1149-1159.

Ondrasik,R. (2002): Landslides in the West Carpathians, Proceding of The European Conference on Landslides, Prague, Czech Republic. A.A.Balkema Publisher, ISBN 90-5809-393, pp.45-58.

Sato.T.(2013). Development of water retention permeability soil improvement technique. Kyushu Construction Technology Management Association, Japan.

Wang,C. Esaki,T and Qiu,Q. (2006): Landslides and debris-flow hazard analysis and prediction using GIS in Minamata-Hougawachi area, Japan, Environmental Geology, No.51, pp.91-102, DOI 10.1007/s00254-006-0307-0

Xie, M. Esaki,T. Qiu,T. Wang,C. Wang, Z. (2009): Deterministic Landslide Risk Assessment at a Past Landslide Site, *Geotech Geology Engineering*, 27: 355-364.

Xie, M. Esaki, T. Zhou,G and Mitani,Y.(2003): Geographic Information System-Based Three-Dimensional Critical Slope Stability Analysis and Landslide Hazard Assessment, *Journal of Geotechnical and Geoenvironmental Engineering*, ASCE, (**129**)12, 1109-1118.

CHAPTER 6

CONCLUSSIONS

6.1 Conclusions

In this thesis, a set of GIS integrated models is proposed to systematically evaluate slope failure hazard at regional scale. It considers the influences of soil depth and rainfall infiltration, and is applied to assess stabilities of a natural slope in Sangun mountainous area. Moreover, to evaluate the consequence and the risk of slope failure hazard to human society, a slope failure inventory in the past is also used to evaluate the probability triggered by landslides. The research process involves dividing slope units, integrating three 3D limit equilibrium methods within a GIS environment, searching for the critical slip surface, simulating soil depths of the large scale area, studying the influence of rainfall on slope stability and simulating inundation area of slope failure triggered by rainfall. The contents, results and conclusion of each chapter are as follows:

In Chapter 1 describes some background knowledge about landslide hazard. Finally, the objective of this thesis is proposed. Chapter 2 reviews three widely used landslide hazard assessment approaches: Landslide inventory based probabilistic approach, statistical approach and deterministic approach. All these approaches are considered valid in certain contexts. Deterministic approach is used in this study because it provides the best quantitative information for landslide hazard assessment. Most of deterministic models are based on the limit equilibrium approach for a one-, two-, or three-dimensional model. For natural slopes, 3D model is preferred because it considers the spatial distributions of slip body, stratum, and groundwater table. Moreover, the effect of rainfall in the slope stability analysis was considered.

Chapter 3 introduces a proses based model analysis to simulate soil depths of mountainous area. The methods of simulating the distribution of soil depth by spatial. Soil depth is one of the most important parameters for controlling landslides. The easiest and most accurate way to measure soil depth is through field measurements. For large-scale areas, especially in mountainous areas, this method is not cost effective or practical as some places are not accessible. To overcome this difficulty, a process based model analysis is used to evaluate soil depths. All the terrain attributes that control soil depth are selected as influential factors. The effectiveness of this method has been tested by applying it to Sangun Mountainous of Japan. The result shows a consistency between

predicted soil depths and samples from field investigation. In the simulation, the third of soil production rate (*Po*) values, such as 0.019, 0.022, and 0.025 cm/yr had been used. Results from the simulation analysis indicated that topographic variables, soil production rate (*Po*), and a soil production time (year) provide the reasonable model for distribution of soil depth. Therefore, the soil depth ranged from 0.51 to 1m has the largest area of soil distribution.

Chapter 4 provides the methodology of GIS-based 3D analysis of rainfall-induced slope stability. Firstly, the homogeneous layer is considering to assume that the variance of the uncertainty of geotechnical parameter is important in the slope stability to get the best performance. Furthermore, we are concerned in the soil depth and rainfall effect in the analysis. In this study, the analysis of effect of infiltration parameter for the soil textural and the occurrence of groundwater has been conducted. Therefore, the combining of GIS-based 3D model and hydrological model are presented. Such as, saturation degree and matric suction of the soil texture were being used in the hydrological model. Furthermore, this model provides the effect of rainfall intensity on the slope failure probability.

In Chapter 5, aiming to apply 3D deterministic model with combining of hydrological model to a wide natural area for predicting the location of slope failure with soil depth and rainfall, a slope-unit-based evaluation method is given. The 3D Slope Stability Analysis for homogeneous and multi layers based on verification of the results will be conducted by considering the inventory slope failure in the past. As results, due to the cohesion (*c*) values gave the similar values in homogeneous and multi layers, therefore the cohesion value equal 1 kN/m2 gave a very reasonable performance compare to similar cohesion values performed by other cohesion values (47.27% for homogeneous layer and 72.73% for multi layer). Furthermore, the friction value of 25^0 is a reasonable performance in the both homogeneous and multi layers about 76.36%. Furthermore, the effect of rainfall, there are five cases; (1) infiltration parameter for soil as weathered granitic rock and the occurrence of groundwater level (5m); (2) infiltration parameter for soil as weathered granitic rock and groundwater level (0m); (3) infiltration parameter for soil as weathered granitic rock +organic materials (10%) and groundwater level (0m); (4) infiltration parameter for soil as weathered granitic rock + organic materials (20%) and groundwater level (0m); and (5) infiltration parameter for soil as weathered granitic rock + organic materials (30%) and groundwater level (0m)

As results, the validation has been conducted in all cases. Therefore, the assuming of the groundwater level is 0m have been changed (case 2 to case 5). Furthermore, the result shows 89.09% the number of slope failure after 20h is good performance in the

case 3.

And, finally, conclusions of this thesis are given in Chapter 6.

6.2 Future work

For rainfall-induced slope analysis, the evaporation and distribution of groundwater level were not considered in the current analysis. Evaporation cannot be ignored if the rainfall lasts days, and the influence of antecedent rainfall depends on the duration. Groundwater level prior to the major rainfall event can significantly decrease the safety factor even if the rainfall is minimal in comparison to the major rainfall. These two factors should be considered in future study.